University of Alberta

The Genesis of the Gayna River Carbonate-Hosted Zn-Pb Deposit

by

Sara Rose Bronwen Wallace

A thesis submitted to the Faculty of Graduate Studies and Research
in partial fulfillment of the requirements for the degree of

Master of Science

Department of Earth and Atmospheric Sciences

Fall 2009
Edmonton, Alberta

Examining Committee

Dr. Sarah Gleeson, Earth and Atmospheric Sciences

Dr. Jeremy Richards, Earth and Atmospheric Sciences

Dr. John Duke, SLOWPOKE Nuclear Reactor Facility, Pharmacy and Pharmaceutical Sciences

ABSTRACT

Geochemical analyses on samples from the Mississippi Valley Type Gayna River deposit, Northwest Territories, Canada, have resulted in the definition of three ore stages and a deposit genesis model. Pb/Pb and Re/Os isotopic analyses indicate that the mineralization at Gayna River was emplaced during the Cretaceous – Tertiary. The sphalerites at Gayna River contain at least 21 trace elements including abnormally high Ga concentrations. Trace elements and $^{87}Sr/^{86}Sr$ ratios, ranging up to 0.7219 in the ore stage, indicate that underlying shales were the source of metals. The main stage of mineralization resulted from a hot saline brine probably derived from evaporated seawater. Stable isotopes suggest that thermochemical sulphate reduction (TSR) of local gypsum was the source of main and late stage sulphide. Fluids circulating through shale units, by tectonically driven flow, reacted with local gypsum causing TSR and resulting in the deposition of Pb and Zn sulphides at Gayna River.

ACKNOWLEDGEMENTS

The field support for this thesis and funding for analyses were generously provided by Eagle Plains Resources of Cranbrook, BC. Additional financial support for this project was provided by the Natural Sciences and Engineering Research Council (NSERC) of Canada through Discovery operating grants to Sarah Gleeson (University of Alberta) and through a CGSM scholarship and extension.

I would like to thank Sarah Gleeson for continual support, guidance, and willingness to read numerous drafts. I would also like to thank Sarah Gleeson and Jeremy Richards for access to the petrography and fluid inclusion laboratories, Karlis Muehlenbachs for access to the stable isotope laboratory, Tony Simonetti for help with running the Pb and Sr isotope analyses and their interpretation, Rob Creaser for running all the Re/Os analyses and doing the lead separation from sphalerite, Sergei Matveev for help with the electron microprobe analyses, Don Resultay for preparing thin sections, and Andrew Locock for information on crystallography. In addition, some of the C and O isotope analyses were done at the University of Waterloo by Robert Drimmie and the S isotope analyses were done at the University of Calgary by Stephen Taylor. The oxygen isotope analyses of quartz were done at the Laboratory for Stable Isotope Science, University of Western Ontario. Special thanks to Duane Petts for the quartz isotope results and methods, and for originally encouraging me to take on this project and go to grad school.

Thanks to Melissa, Cuppy, and Margot for collecting samples in the field and making our rainy camp fun and to Liz Turner for an introduction to the stratigraphy. Special thanks to Bob Sharp for all the ideas and help throughout this project. Also thanks to Keith Dewing and Bob Sharp for their help with cross-section making and the discussion which grew out of that.

To all the good friends I've made while in Edmonton - I wouldn't have made it without you. Finally, I would like to thank my family for their support throughout my whole school career and for always believing in me.

TABLE OF CONTENTS

SECTION **PAGE**

CHAPTER 1 - INTRODUCTION

CHAPTER 2 - SAMPLING AND ANALYTICAL METHODS

CHAPTER 3 - RESULTS

CHAPTER 4 - DISCUSSION

SECTION **PAGE**

CHAPTER 5 - CONCLUSION

APPENDICES

LIST OF TABLES

LIST OF FIGURES

Chapter 1
Introduction

1.1 Location and access to Gayna River

The Gayna River Zn-Pb deposit is located in the Mackenzie Mountains, Northwest Territories, Canada. The deposit is centered at 64°58’N latitude and 130°41’ W longitude, corresponding to UTM Zone 9 419641E /7203425N. The property can be accessed by helicopter from Norman Wells, NWT, which is ~180 km to the east and is located 80 km west of the proposed Mackenzie Valley pipeline route. If this pipeline project is completed it could supply access and power to any future mine development at Gayna River.

The Gayna River area is generally snow-free from mid-June to mid-September. It is above the alpine tree line and shrubs and grasses are the dominant vegetation. The property extends from the bottom of a broad valley with elevations of ~1100 m over the side of a rugged mountain with a peak elevation of 2239 m. The steep topography makes some areas inaccessible. Most of the outcrops at Gayna River are exposed within stream cuts, or on slopes, and there is limited exposure in flat areas. The deposit was initially staked by Cordilleran Engineering Limited on behalf of Rio Tinto Canadian Exploration Limited in 1974. Property and regional reconnaissance, geological mapping, geochemical sampling, diamond drilling, and geophysical surveys were performed by Rio Tinto between 1975 and 1979. These data are published in assessment reports 080567 and 080724, which are available from the Northwest Territories Geoscience Office. There was no further activity on the property until 1999 when 49 claims were staked by Eagle Plains Resources. Some geological mapping, sampling, and core relogging followed in 2000, 2003, 2004, and 2006. These data are published in assessment report 084410 and two unreleased reports due out in 2009 and 2011.

The numerous Zn-Pb showings are predominantly hosted in the Neoproterozoic Little Dal group with some mineralization extending into the overlying Cambrian Franklin Mountain formation. The Gayna River Zn-Pb deposit occurs at the border of two National Topographic System (NTS) map sheets, 106G and 106B. The Upper Ramparts River map sheet, 106G, was mapped by Aitken and Cook (1975) and covers the northern extent of the deposit. The Bonnet Plume map sheet, 106B, was partially mapped by Aitken (1974) but is incomplete for the Gayna River area. The most complete geologic mapping available for this area is from Welcome North exploration internal reports which were digitized by the Yukon Geologic Survey.

1.2 Rationale for the study

The Gayna River deposit is potentially one of the world's largest undeveloped carbonate hosted Zn-Pb deposits. The deposit is hosted by the Neoproterozic aged Little Dal Group in the Mackenzie Mountains, Northwest Territories (Figure 1) and as a result previous workers have suggested that the deposit may be a rare example of an undeformed, Proterozoic Mississippi Valley Type deposit (MVT) (Hardy, 1979; Kesler and Reich, 2006).

A historical size estimate of greater than 50 millions tonnes with over 5% combined Zn-Pb (Hewton, 1982) has been published several times in the literature. However, this estimate is non NI 43-101 compliant and was determined using broad assumptions and limited drilling data. The Gayna River Zn-Pb deposit is more accurately described in current terminology as an estimated exploration target of 1 to 1.5 million tonnes with 3 to 6% combined Zn-Pb (based on Hewton and Wilson, 1977). While the potential for a large resource does exist, it is not presently well defined.

Despite the importance of the deposit, there have been few studies carried out on the Zn-Pb mineralization at Gayna River. A thesis by Hardy (1979) outlined the stratigraphy, and carried out a paragenetic and cathodoluminescence study and breccia classification of the units at Gayna River. Hewton (1982) summarized the geology and exploration work done on the Gayna property. Hardy (1979) and Carrière and Sangster (1999) carried out microprobe analyses on the sphalerites at Gayna, and showed them to contain significant trace element abundances including Se, Cd, Cu, Co, Ni, As, Ga, Fe, Ag, and Mn.

Hardy (1979) carried out a preliminary fluid inclusion study and this was followed up by work by Carrière and Sangster (1992), Carrière and Sangster (1999) and Gleeson (2006). Hardy (1979) and Carrière and Sangster (1999) concluded that primary and pseudosecondary fluid inclusion homogenization temperatures in sphalerite had means of 186°C and 169°C respectively, and quartz-hosted fluid inclusions had homogenization temperatures with means of 192° and 176°C respectively. Salinities are reported ranging from 13.9 to 26.5wt% NaCl equivalent. Fluid inclusion work undertaken in 2005 (Gleeson, 2006) found data comparable with those reported in Carrière and Sangster (1999).

This study was undertaken to delineate the nature of mineralization and the origin of the mineralizing fluids at Gayna River with an ultimate goal of determining the main controls on mineralization. A petrographic study was carried out on samples from the deposit. Following this, microprobe analyses, fluid inclusion microthermometry and stable isotope (C, O, Sr, and S) data sets from sulphides and carbonate gangue minerals were collected. Finally, radiogenic isotope data (Pb/Pb and Re/Os) were used to provide age constraints on the mineralization at Gayna River. The integrated data set is compared to other MVT deposits and a fluid history is proposed for Gayna River. The controls on mineralization for this deposit and the additional perspectives that the Gayna River data sets provide on Cordilleran mineralization are discussed.

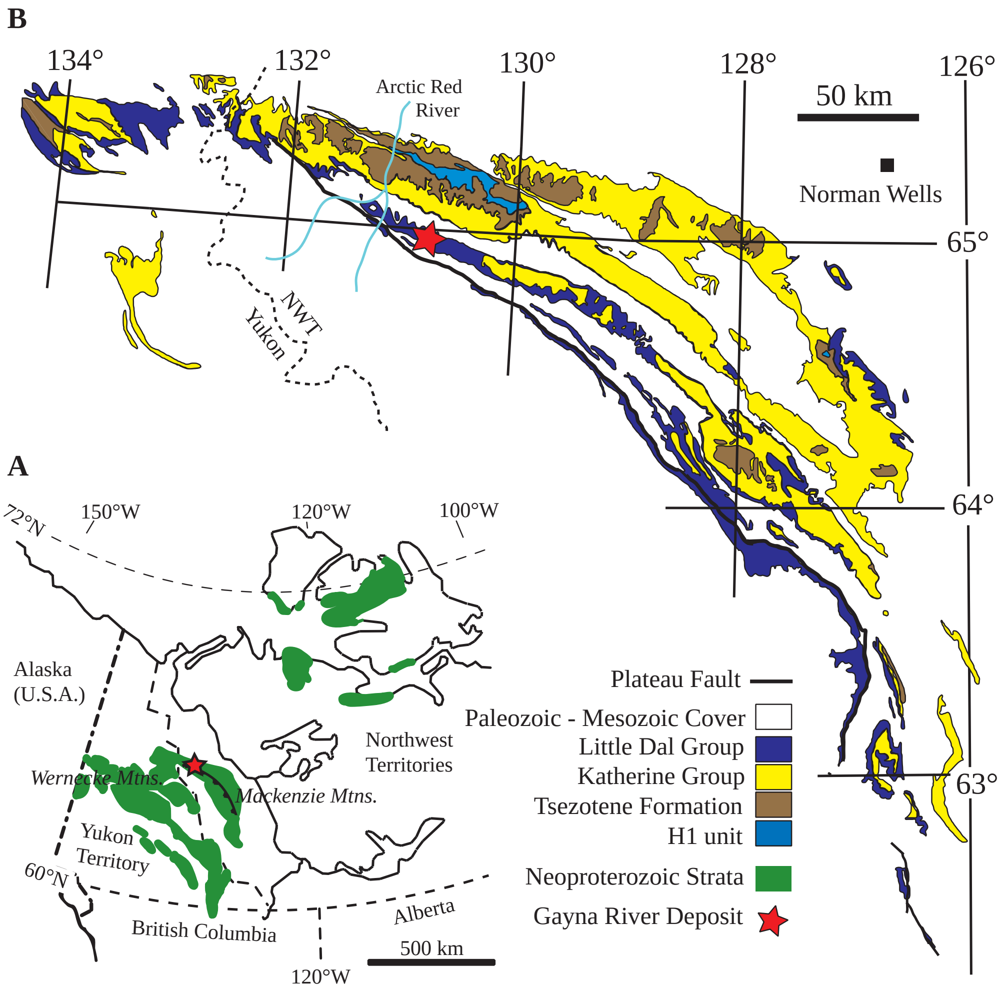

Figure 1. (A) The location of the Gayna River deposit, which is marked with a red star, and the distribution of Neoproterozoic strata in northwestern Canada, which is shown in green (map modified from Narbonne and Aitken, 1995). (B) The geology of the exposed Mackenzie Mountain Supergroup (MMSG) in the deposit region, with the Gayna River deposit marked by a red star (map modified from Turner and Long, 2008).

1.3 Geologic Setting

Regional Geology

The Gayna River deposit is located on the eastern margin of the Canadian Cordillera in the Foreland Belt. In this region, the Proterozoic Windermere and Mackenzie Mountains Supergroups are both exposed over hundreds of kilometers (Gabrielse and Campbell, 1991). The Mackenzie Mountains Supergroup includes from bottom to top; Map-unit HI, the Tsezotene Formation, the Katherine Group, and the Little Dal Group (Figure 1). The Mackenzie Mountains Supergroup formed as a regional platform extending westwards from the Canadian Shield and is a succession of mainly shallow-water siliciclastic and carbonate strata (Narbonne and Aitken, 1995). Regionally there are thick sequences of Paleozoic rocks overlying the Proterozoic strata. The youngest rocks which occur in the vicinity of the Gayna River property are the Upper Cambrian Franklin Mountain and the Upper Ordovician Mount Kindle Formations (Hardy, 1979). Stratigraphically above these are the Delorme, Arnica, Landry, and Hume Formations which are grouped here as Upper Paleozoic Strata (Figure 2) for simplicity and because they are not directly relevant to the Gayna River deposit.

Large-scale folds and strike-slip and thrust faults dominate the regional structure to the east of the Plateau Fault. There are three broad anticlines over the 125 km distance between the Plateau Fault and the mountain front (Cook, 1991). There has been little geological work done in the region to the southwest of the Gayna River area and, here, the exact nature of the Plateau Fault in this area is unknown but has been interpreted (Figure 3) following the model used further southeast (MacNaughton et al., 2008).

Local Geology

At the Gayna River property the oldest outcropping rocks are the Katherine Group Quartzites which underlie the Little Dal Group (Figure 4). The Katherine Group consists of thick beds of quartz arenite separated by thin beds of fine grained black shale. Near the top of the group are poorly sorted quartzites, siliceous dolostones, and fine grained shales (Hardy, 1979; Hewton, 1982). Aitken (1981) grouped the Little Dal into lower and upper sections. The lower Little Dal includes the Mudcracked formation, Platformal and Basinal assemblages, and the Grainstone formation. The upper Little Dal contains the Gypsum formation, the Rusty Shale formation, and the Upper Carbonate formation (Figure 5). Calcimicrobial reefs with dimensions of up to 6.5 by 1.6 km wide and up to 500 m high are present throughout the lower part Little Dal Group. These reefs are unusual in that they combine features of both Proterozoic and Paleozoic reef ecosystems (Turner et al., 2000). Further descriptions of the Little Dal Group geology and Neoproterozoic reefs can be found in Aitken (1982), Batten et al. (2004) and Turner et al. (1997; 2000).

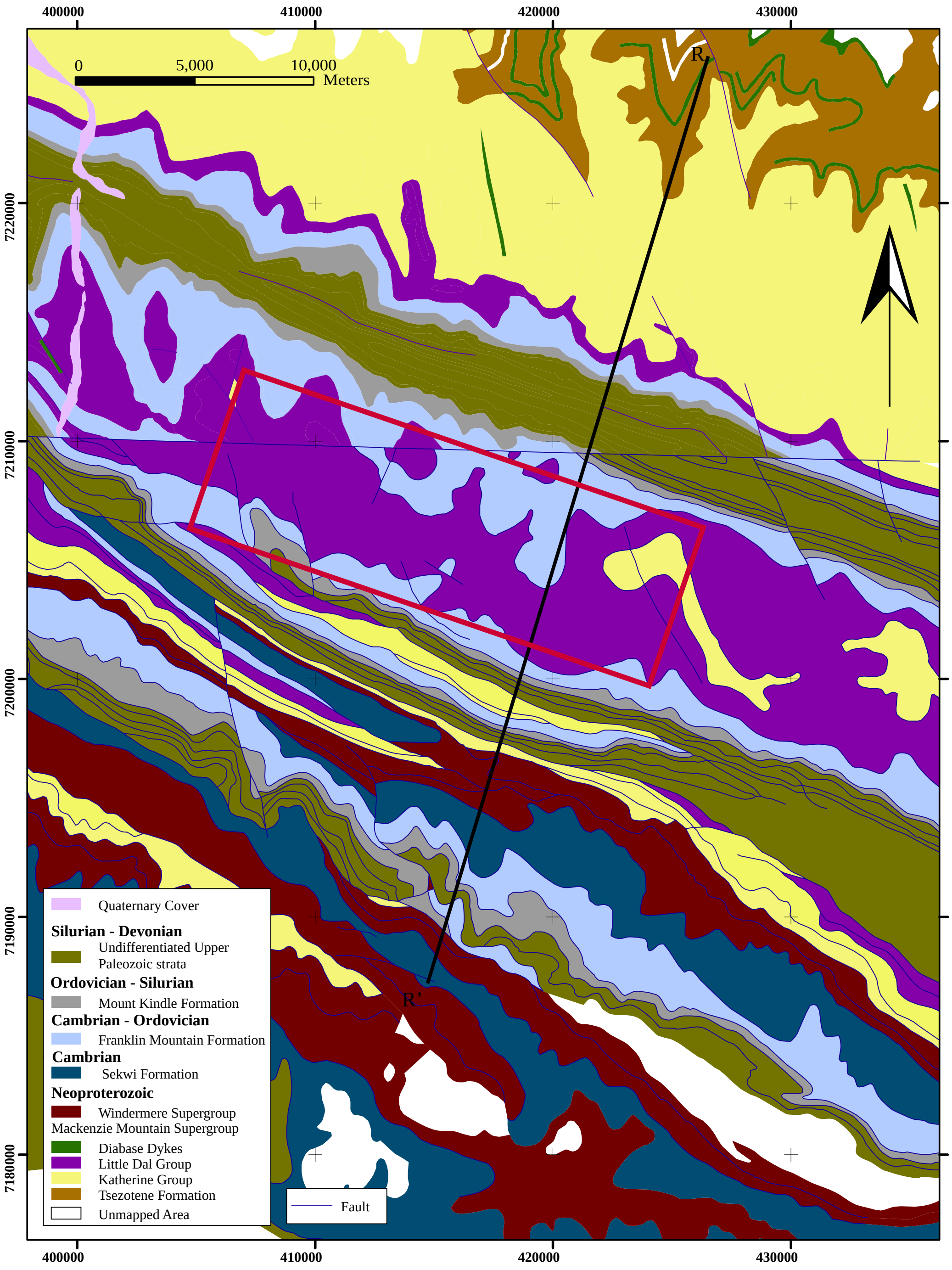

Figure 2. A regional geology map of the Gayna River area. The southern portion of the map is compiled from Welcome North internal reports. The northern portion of the map is based on Aitken and Cook (1975). Line R-R' marks the section shown in Figure 3. The Gayna River deposit area is roughly contained within the red box. The undifferentiated Upper Paleozoic strata include the Delorme, Arnica, Landry, and Hume Formations. Projection is NAD 83 UTM Zone 9N.

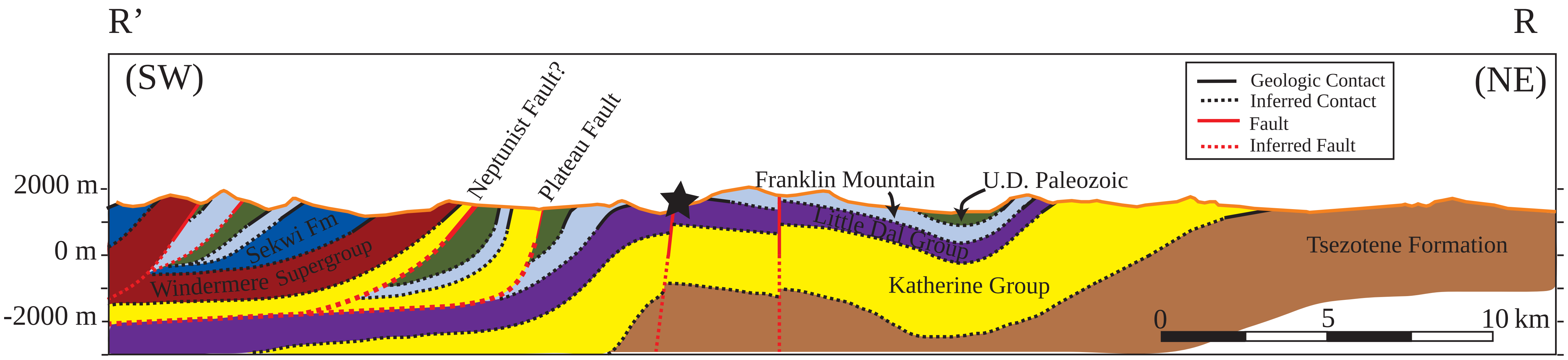

Figure 3. A regional cross-section through the Gayna River Zn-Pb deposit. The 'A' showing location is marked by a black star. See Figure 2 for the location of the section. U.D. Paleozoic = undifferentiated Paleozoic rocks including; Mount Kindle, Delorme, Arnica, Landry, and Hume Formations.

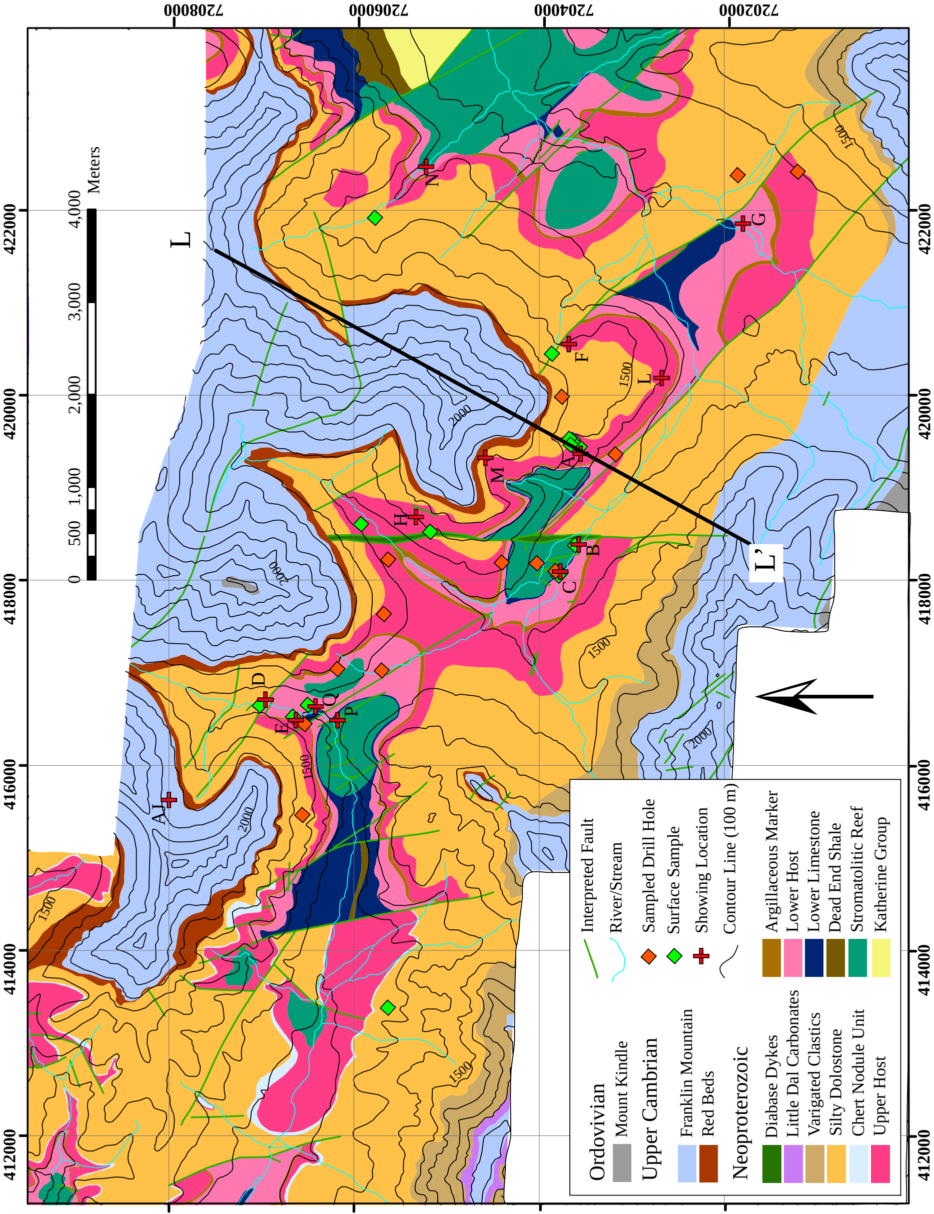

Figure 4. The geology of the Gayna River property (based on Rio Tinto mapping in Hewton and Wilson, 1977). The projection is NAD 83 UTM Zone 9N. The locations of samples collected for this study are shown by orange and green diamonds. Line L-L' marks the cross-section shown in Figure 6.

The property was originally mapped by Rio Tinto geologists and they used a different terminology for the units in the property, based largely on drill core observation. The terminology used for the sequence from bottom to top was; Dead End Shales, Lower Limestone, Lower Host, Argillaceous Marker, Upper Host, Silty Dolostone, Variegated Clastics, Little Dal Carbonates (Figure 5). In this study, we have used the Rio Tinto property maps and drill logs and, thus, we use the Rio Tinto terminology throughout. However, the descriptions by Aitken (1981) of the Little Dal Group are currently accepted by the Geological Survey of Canada (GSC) (Turner et al., 1997).

The following unit descriptions are based on Hardy (1979) and Hewton (1982), in which more detailed descriptions can be found. The Dead End Shales conformably overlie the Katherine Quartzite and consist of 180 m of thinly bedded shale with minor interbedded limestone. Above the Dead End Shales is the Lower Limestone which is often indistinguishable to the lower unit; thus, both are often referred to as the Lower Limestone. The Lower Limestone is a 150 m sequence of interbedded black limestones and shales. Notable features in this unit include well developed molar tooth structures and a sedimentary breccia with lathlike fragments known as the sharpstone breccia. The Lower Limestone grades into the Lower Host, which consists of 65 m of medium bedded dolostone. Shallow water features such as abundant oolites, ripple marks, sedimentary breccia, and stromatolites are seen in this unit. The Argillaceous Marker separates the Lower and Upper Host units. This 15 m thick unit consists of thinly and evenly bedded black argillaceous limestone and commonly has interbeds of graphitic and argillaceous shale. The Upper Host is similar to the Lower Host, medium bedded dolostone, and is 80 m thick. The Upper Host contains fewer sedimentary breccias and more stromatolite beds than the Lower Host. Chert nodules are seen at the top of the Upper Host. Conformably overlying the Upper Host is the Silty Dolotone unit which can be greater than 350 m thick. The Silty Dolostone is shallow-water dolostone with minor limestone and contains ripple marks, desiccation cracks, stromatolites, oolites, and sedimentary breccias. At Gayna River the Silty Dolostone was mapped as containing evaporites with thicknesses of more than 250 m. Elsewhere these evaporites occur as a distinct formation, the Gypsum formation, consisting of white to pale grey gypsum with minor red, grey, or green gypsiferous siltstone and dolostone which can be greater than 550 m thick. The Variegated Clastics overlying the Silty Dolostone are interbedded red, green, yellow, and white shale and quartzite. The Little Dal Carbonates are up to 305 m thick at Gayna River and consist of dolostone with minor interbeds of siltstone and mudstone in the lower 9 m. The Little Dal Group is truncated by an Upper Cambrian unconformity which intersects the succession anywhere from the Upper Host unit to the Katherine Quartzites. Above the unconformity lies the Cambrian Franklin Mountain Formation which consists of interbedded red, orange, and green clastic sedimentary rocks and thick beds of grey carbonates.

The Gayna River area has undergone only minor deformation. The major structure at Gayna River is a large box anticline which spans the entire length of the property (Figure 6). North trending strike-slip faults and northwest trending block faults have been interpreted as two phases of Racklan orogeny related deformation at Gayna River (Hardy, 1979). In addition both folding and faulting occurred during the Laramide orogeny, producing steep synclines and northwest trending normal and reverse faults (Hardy, 1979).

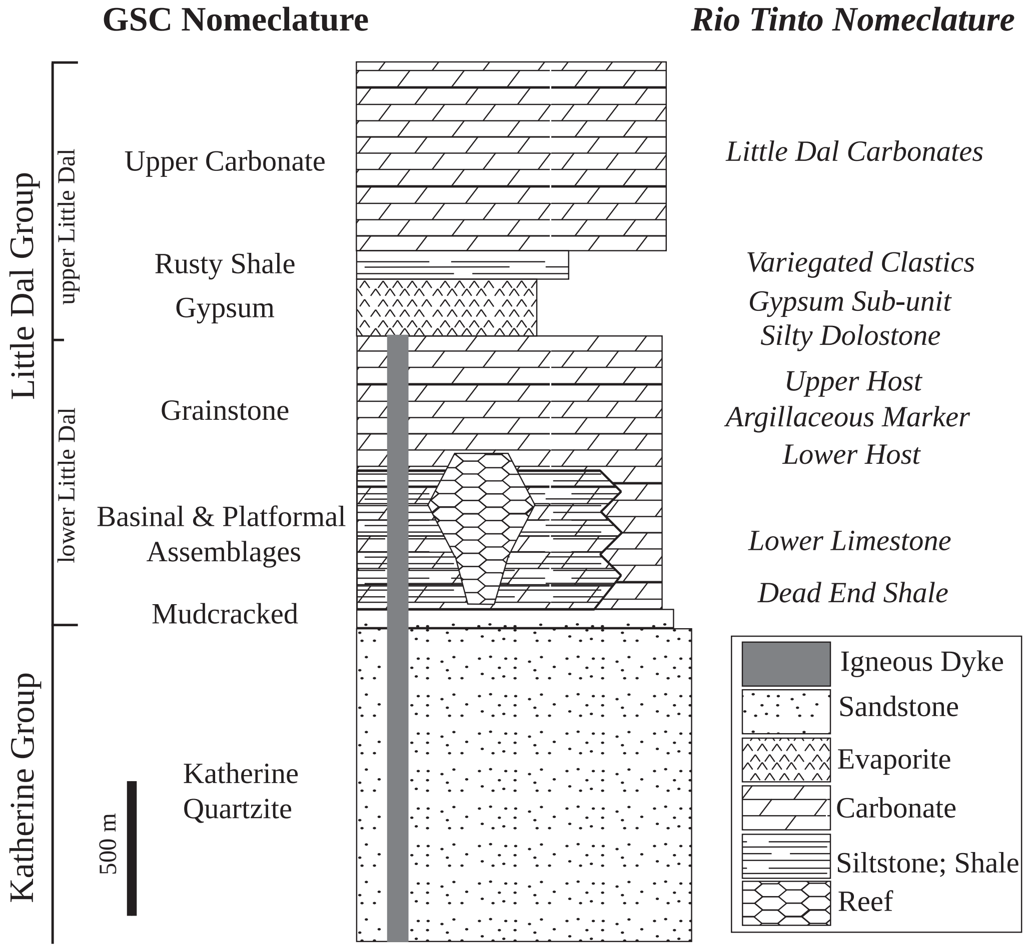

Figure 5. A stratigraphic section (modified from Turner et al., 1997) representing the Gayna River area with a comparison of GSC (from Aitken, 1981) and Rio Tinto nomenclature (from Hewton, 1982).

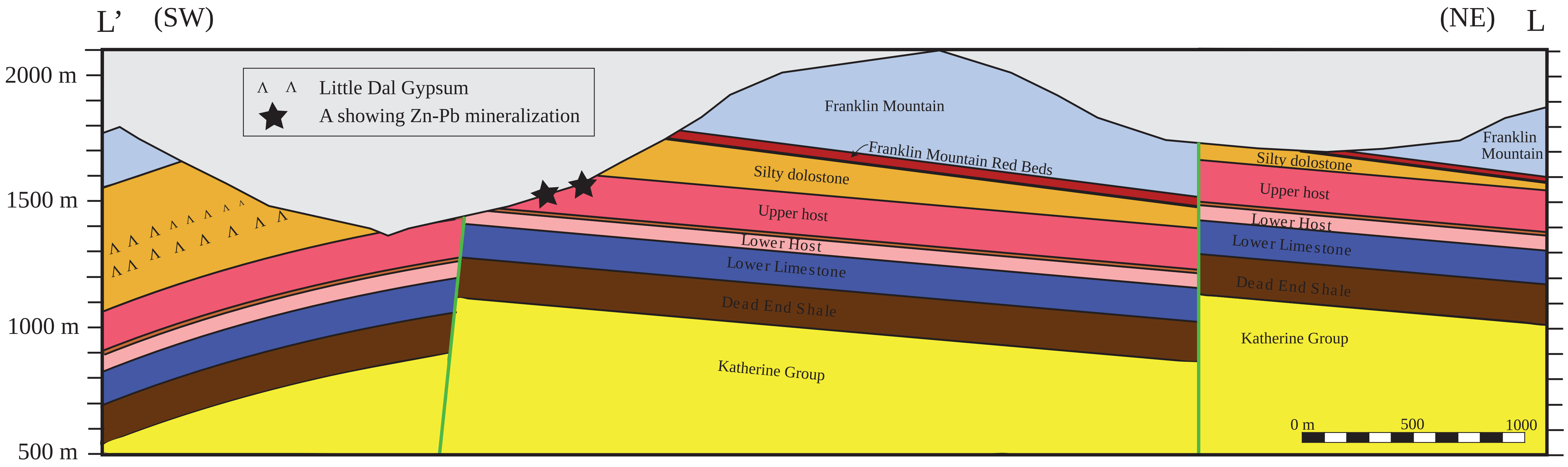

Figure 6. A cross-section through the 'A' showing of the Gayna River deposit. See Figure 4 for the location of the section and legend.

Chapter 2
Sampling and Analytical Methods

Samples were collected from old drill core, part of ~ 27,000 m of diamond drilling done by Rio Tinto Canadian Exploration Ltd. between 1975 and 1979, and surface outcrops at the Gayna River property (see description and location in Appendix 1). As part of the study, 7 of the sampled drill holes were re-logged. These core logs are included as Appendix 2.

2.1 Lead isotopes

The Pb isotope analyses were done at the Radiogenic Isotope Facility at the University of Alberta. Single galena grains samples were hand picked, crushed and then ~ 10 mg of each was dissolved in HCl. A 2% HNO_3 solution spiked with the NIST SRM 997 Tl standard was used to dilute the HCl and dissolved Pb solution to a concentration of ~50 ppb Pb. Single sphalerite grains were processed following the method of Kesler et al. (1994). The samples were digested in hot HCl with HNO_3 added. After the sphalerite had dissolved the solution was evaporated to dryness. The Pb was taken up in HBr and separated using an AG 1X-8 anion exchange column in the HBr form. The Pb was further purified by an addition run through the column in HCl form. These samples were then treated to the same processes as the dissolved galena samples.

The Pb isotope compositions of both galena and sphalerite were measured using a NuPlasma™ multicollector-inductively coupled plasma-mass spectrometer (MC-ICP-MS). The samples were aspirated into the ICP source using an ARIDUS microconcentric nebulizer following the method of Simonetti et al. (2004). The added Tl standard was used to correct for the instrumental mass bias by comparing the measured $^{205}Tl/^{203}Tl$ ratio to the accepted value of 2.3887. A 50 ppb solution of the NIST SRM 981 Pb standard spiked with the NIST SRM 997 Tl standard was analyzed before running each sample group and yielded ratios (error at 2σ) of $^{208}Pb/^{204}Pb = 36.692 \pm 0.044$, $^{207}Pb/^{204}Pb = 15.490 \pm 0.018$, and $^{206}Pb/^{204}Pb = 16.935 \pm 0.016$ which compare well with the accepted values of 36.7006, 15.4894, and 16.9356, respectively.

2.2 Rhenium and osmium isotopes

The Re-Os isotope analyses on hand picked pyrobitumen samples were conducted at the Radiogenic Isotope Facility at the University of Alberta. Approximately 200 mg of pyrobitumen was picked from each of 8 samples. One sample was lost during analyses. Re and Os concentrations and isotopic compositions were determined by isotope dilution negative thermal ionization mass spectrometry (ID-NTIMS) following the method described in Selby et al. (2005). The bitumen samples were dissolved in inverse aqua regia by Carius-tube at 240°C for 48 h (Creaser et al., 2002) and equilibrated with a mixed tracer containing a known amount of ^{185}Re and ^{190}Os. The Os was then separated using solvent extraction and the Re was separated using anion chromatography techniques (Selby and Creaser, 2001). Isotopic analyses were done on a Micromass Sector 54 mass spectrometer with the purified Os and Re loaded on Pt and Ni filaments, respectively. Uncertainties in Re and Os mass spectrometer measurements, blank abundances and isotopic compositions, spike calibrations, standard Re and Os isotopic values, and typical weighing uncertainties are all used in the error propagation to determine uncertainties for Re–Os isotopic data and abundances.

2.3 Electron Microprobe

Electron microprobe analyses were performed on polished standard petrographic thin sections using a JEOL 8900 microprobe equipped with five wavelength dispersive spectrometers at the University of Alberta. Calibration was carried out using mineral and metal standards. The beam was operated at an accelerating voltage of 20.0kV and a diameter of 1 μm. Detailed qualitative maps were obtained for 4 single sphalerite crystals using a time of 65 ms per spot analysis giving a total analysis time of 20 to 21 hours per map. Backscattered electron images were captured to note the relationship of crystal deformities to trace element concentrations. Mineral transects were performed with a step size of 5 to 30 μm between points.

2.4 Microthermometry

The microthermometric study was performed on a THMSG600 Linkam heating-freezing stage at the University of Alberta. This stage was calibrated using synthetic fluid inclusion standards manufactured by Syn Flinc. The reproducibility of the measurements was ±0.2°C below 0°C and ±2°C for heating to 300°C. For calcite and dolomite samples the homogenization temperatures (Th) were always determined in the first run to minimize the effects of fluid inclusion stretching.

The eutectic temperatures seen in fluid inclusions from the Gayna River deposit indicate that NaCl cannot be the only salt present in the system (see section 3.4). With only final ice melting temperature data, the salinity of a system with multiple salts cannot be calculated. For this reason NaCl equivalent salinity has been used. The NaCl equivalent salinity was calculated using the equation from Bodnar (1993). The Th values have not been corrected for pressure.

2.5 Sulphur isotopes

Hand picked grains of pyrite, sphalerite, and galena were analyzed for their S isotope composition at the University of Calgary Isotope Science Laboratory. Pure sulphide samples were heated in high purity tin cups to 1020°C releasing SO_2 gas which was then separated from other produced gases. The SO_2 was analyzed using Continuous Flow-Isotope Ratio Mass Spectrometry (CF-EA-IRMS) with a Carlo Erba *NA 1500* elemental analyzer coupled to a VG Prism II mass spectrometer (Glesemann et al. 1994). Precision for the sphalerite and galena samples was better than ±0.3‰. Several of the pyrite analyses had poor reproducibility so accuracy for pyrite should be taken as ±1‰. The isotope ratios were calculated using the IAEA S1, IAEA S2, and IAEA S3 standards with $\delta^{34}S$ values of -0.3 (by definition), 22.7 ± 0.2, and -32.6 ± 0.2‰, respectively. All $\delta^{34}S$ values are reported in per mil relative to the Canyon Diablo Troilite (CDT) standard.

2.6 Carbon and oxygen isotopes in carbonates

Host rock dolostone, main ore stage dolomite, and late ore stage calcite samples were analyzed for C and O isotopes compositions at the University of Alberta and the University of Waterloo. CO_2 was extracted following the method of McCrea (1950). The samples were ground into a fine powder and then ~20 or 30 mg of each calcite or dolomite sample, respectively, was reacted with 3 mL of phosphoric acid in a sealed and evacuated reaction tube. The calcite samples were reacted for 2 hours at 25°C and the dolomite samples were reacted for 1 day at 50°C. At the University of Alberta the collected CO_2 was analyzed using a Finnigan Mat 252 mass spectrometer. Semi-automated CO_2 production was employed at the University of Waterloo Environmental Isotope Laboratory and the samples were analyzed using a VG PRISM mass spectrometer. Replicate analyses of samples performed at each location were equivalent within error. Reproducibility of the analyses for both C and O was better than ± 0.1‰. All values are reported in per mil with the $\delta^{18}O$ compositions relative to Vienna Standard Mean Ocean Water (VSMOW) and the $\delta^{13}C$ compositions relative to Vienna Peedee Belemnite (VPDB).

2.7 Oxygen isotopes in quartz

The quartz samples were analyzed for O isotope composition at the University of Western Ontario. Oxygen extraction from the mineral samples followed the conventional method of Clayton and Mayeda (1963), as modified by Borthwick and Harmon (1982) for use with ClF_3. Approximately 8 to 10 mg of each sample was dried under vacuum overnight at 150°C and then for 2 hours at 300°C. The dried samples were then reacted with ClF_3 at 580°C in sealed Ni reaction vessels overnight to liberate the O. The released O gas was then converted to CO_2 over a red-hot carbon rod and yields were measured to determine if the conversion had been completed. The O isotopic ratios were measured using a dual-inlet VG Optima mass spectrometer. The measured $\delta^{18}O$ values of ORX (internal laboratory standard quartz) and NBS-30 (biotite) were 11.6 ± 0.2‰ and 5.0 ± 0.1‰ respectively, which compare well with their accepted $\delta^{18}O$ values of 11.5‰ and 5.1‰. Reproducibility of the $\delta^{18}O$ values for standards and samples was generally better than ±0.2‰. All quartz isotope values are reported in per mil relative to Vienna Standard Mean Ocean Water (VSMOW).

2.8 Strontium isotopes

Strontium isotopes were analyzed by laser-ablation at the Radiogenic Isotope Facility of the University of Alberta. The Sr isotope compositions were determined by *in* *situ* ablation of 1-inch epoxy mounts using a New Wave Research laser ablation system coupled with a Nu Plasma LA-MC-ICP-MS, following the methods of Schmidberger et al. (2003) and Bizzarro et al. (2003). A 320 x 320 µm raster pattern with a spot size of 160 µm and a repetition rate of 20 Hz was used for each laser ablation analysis. Multiple analyses were preformed on each epoxy mount to establish the relationships between the different carbonate paragenetic phases. The corrections applied to the raw data for each analysis include; a baseline correction, a ^{87}Rb correction based on the ^{85}Rb ion signal intensity, a correction for doubly charged middle to heavy REE isobaric interferences, and an instrumental mass bias correction. The Sr ion signal intensity, in volts, was measured for each spot and is interpreted as a qualitative proxy for Sr concentration.

Chapter 3

Results

3.1 Field and Sample Descriptions

3.1.1 Outcrop Mineralization

During the summer of 2006 approximately 25 outcrops were studied at the Gayna River deposit. The field work was focused on previously discovered showings to facilitate sampling of mineralization.

The Upper and Lower Host units are, most commonly, comprised of well bedded dolomitized oolitic or intraclastic grainstones and packstones. Oolitic and intraclastic wackestones and mudstones are less common. Fresh surfaces of the Upper and Lower Host rocks are medium to dark grey in colour and weather grey. Most of the Host unit is dolomitized with some irregular centimeter to meter sized areas of limestone, however, dolostone/limestone boundaries are often indistinguishable by eye. Original carbonate depositional features such as ooids, aggregate grains, and microbial and stromatolitic fragments are usually preserved in the dolomites.

The reefs are also commonly dolomitized with areas of limestone located in reef cores. Stromatolites and laminations are the dominant features of reef outcrops. Detailed investigation into reef framework facies is not attempted in this study but can be found in Turner et al. (2000). Most mineralization occurs within the Lower and Upper Host units with some mineralization in the reefs. Core re-logging confirms that mineralization is most commonly associated with complete dolomitization of the host rocks and extensive brecciation and veining.

The mineral showings at Gayna River are meters to tens of meters in scale in outcrop (Figure 7A). Most outcrops have some degree of veining that displays sharp margins and crosscuts the carbonate fabric. Veins ranges from sparse millimeter size calcite or dolomite veins to meter size calcite or dolomite veins. The vein density can increase until the rocks develop crackle, mosaic, then rubble type breccias (as defined by Hardy, 1979). In the breccias, clasts can range from millimeters to several centimeters in size and are sub-rounded to angular fragments of host unit grainstones and packstones. The matrix is composed of fine to coarse grained dolomite and/or sphalerite (Figure 7B). Vein/host rock contacts and clast/matrix contacts show evidence of dissolution in many areas and can include partially recrystallized margins and stylolites.

The highest grade mineralization occurs in areas of intense hydrothermal alteration as interstitial cements in secondary breccias. Such high grade zones generally do not exceed tens of centimeters in size. Sulphides can also be disseminated in breccia clasts or replacing host rock along structural features. In all cases the sphalerite can range in colour from red, yellow, orange, green to brown in hand specimen.

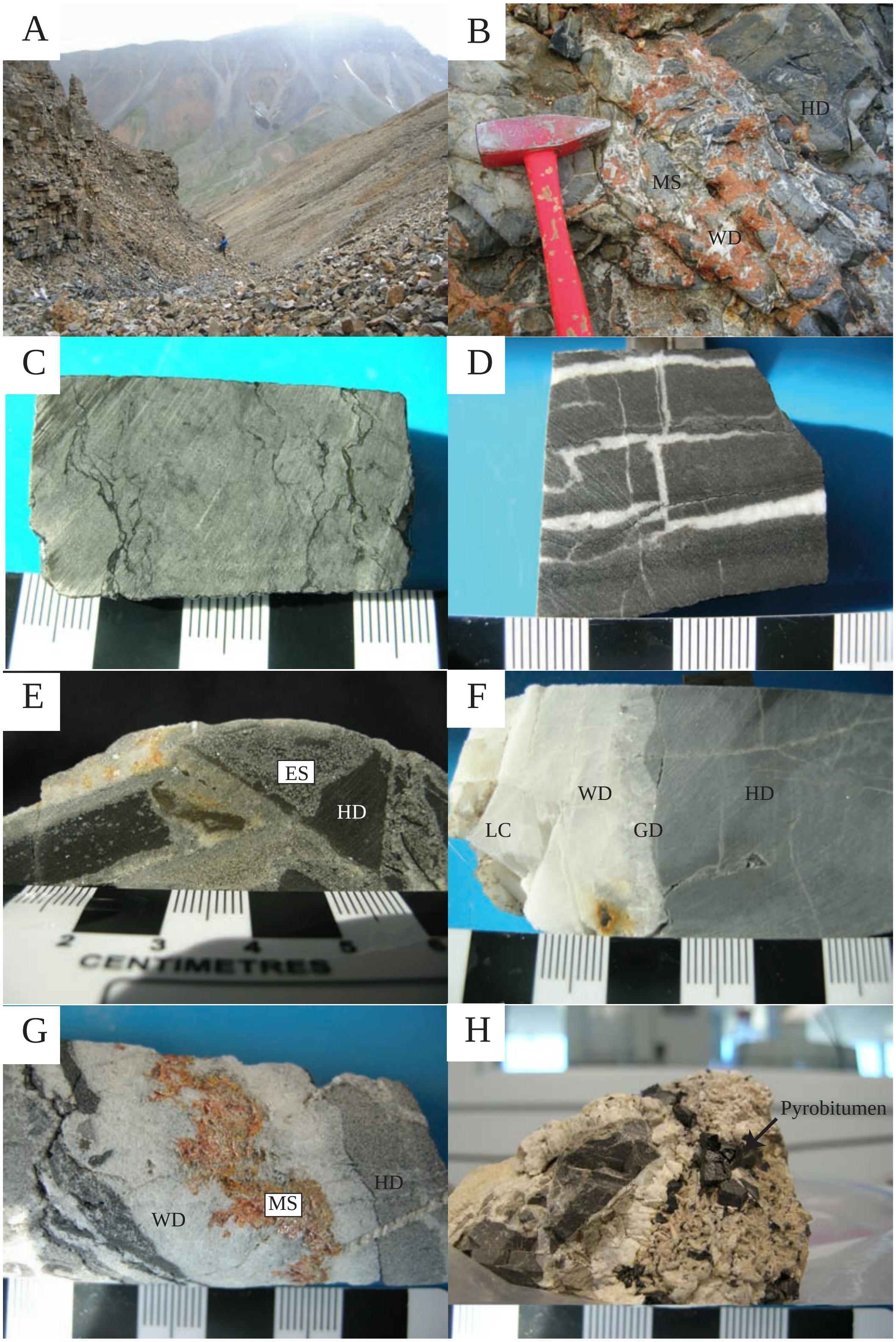
A
B
HD
MS
WD
C
D
E
ES
HD
2
3
4
5
6
CENTIMETRES
F
WD
HD
LC
GD
G
HD
MS
WD
H
Pyrobitumen

Figure 7. Photographs of the Gayna River showings and hand samples. A) The ‘A’ showing creek looking south, with a person for scale. B) An outcrop at the ‘B’ showing with bright orange sphalerite mineralization. HD – host dolomite, WD – main white dolomite, MS – main sphalerite. C) Sample 77-102 147.2, showing HD with organic wisps. D) Sample A30 231.3, showing recrystallized HD with WD veining, note vein orientation is mirroring stylolites in some places. E) Sample A30 453, showing the relationship of the carbonate phases HD, GD – main grey dolomite, WD, and LC – late calcite. F) Sample SG5, showing orange MS mineralization in WD hosted by HD. G) Sample BWGRR014, showing pale green ES – early sphalerite replacing HD. H) Sample 07R008, showing large chunks of pyrobitumen in dolomite. All hand sample scale bars are in centimeters.

3.1.2 Hand Samples and Petrography

A petrographic study was carried out on 95 samples from Gayna River. This study, along with hand sample descriptions, led to the definition of three distinct paragenetic stages of hydrothermal mineral formation which post-date the host carbonates and are described below and in Appendix 3.

Host Carbonate

The limestones and dolostones at the Gayna River deposit that host the subsequent hydrothermal alteration were not extensively studied. Where no alteration has taken place original textures of the host rocks can be seen. Figure 7C displays unaltered host dolostone with wispy organic layers. The carbonates are mudstones to wackestones with laminations and stromatolites commonly seen (Figure 8A). Ooids and chert clasts are often present.

The Host units commonly contain micrometer to millimeter thick wispy black bands that are likely to be concentrated organic matter and/or clays. Stylolites also occur and, typically, have a jagged appearance and are usually 0.5 to 4 mm in width. The stylolites contain mainly pyrite and organic material but also have rare rutile grains and chert fragments. The stylolites are most commonly perpendicular to the core axis and sometimes control dolomite cement precipitation as well as pyrite and sphalerite mineralization. Moderate veining often follows original host rock features such as laminations as well as stylolites (Figure 7D). Pyrite is found scattered throughout the host carbonate and ranges from 0.5% to 5% of the rock in most cases, with 1% being most common.

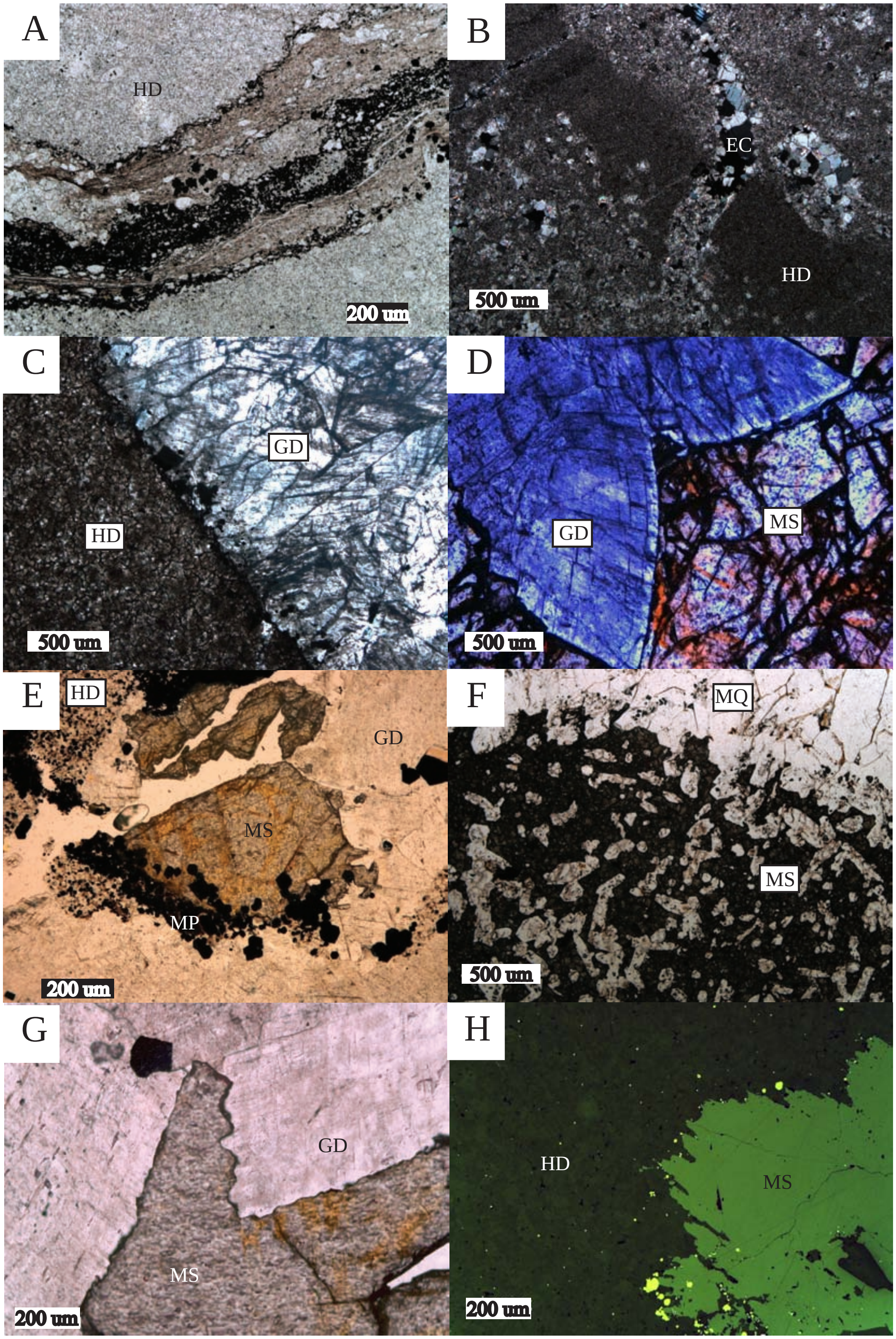
A
HD
200 um
B
EC
HD
500 um
C
GD
HD
500 um
D
GD
MS
500 um
E
HD
GD
MS
MP
200 um
F
MQ
MS
500 um
G
GD
MS
200 um
H
HD
MS
200 um

Figure 8. Selected photomicrographs of Gayna River samples. A) Sample 77-102 147.2 is under plane polarized light (PPL). The HD – host dolomite has a band of organics and insoluble material. B) Sample CAGRR001 is under cross polarized light (XPL). The HD has EQ – early quartz and EC – early calcite alteration. C) Sample SG6 is under PPL. The GD – main grey dolomite is elongate perpendicular to the boundary with the HD. There is pyrite and insoluble matter concentrated at the phase boundary. D) Sample SG5 is under PPL. The curved GD crystals are in contact with bright orange MS – main sphalerite. This is typical of the main stage mineralization. E) Sample A30 411.5 is under PPL. This shows MS with MP – main pyrite hosted in GD. The HD contains abundant detrital pyrite. F) Sample BWGRR022 is under PPL. The MQ – main quartz is intergrown with the MS. G) Sample A30 400 is under PPL. There is a scalloped contact between the MS and the GD. H) Sample BWGRR014 is under reflected light. The HD is in contact with the MS. Note the jagged contact between the host and mineralization.

Early Ore Stage

Early Calcite

The earliest hydrothermal phase observed at Gayna River is calcite. The calcite replaces host limestone and dolostone partially destroying the carbonate fragments, but also is found as the first phase in vein fills (Figure 8B). Early calcite grains are generally 10 µm to 2 mm in size but can form grains up to 5 mm and are subhedral and clear in colour.

Early Quartz

The early quartz has a similar occurrence to the early calcite phase. These quartz grains range from 10 µm to 1 mm in size, are clear or milky in colour and tend to be subhedral. The quartz grains sometimes contain remnant organic matter or inclusions of the host dolostone. In the case of organic matter it appears the host dolostone was destroyed by the early quartz phase leaving concentrated bands of organics which were not dissolved. The host dolostone may have undergone minor to complete silicification on a centimeter scale. Small, 0.1 to 0.2 mm fractures and larger millimeter size veins in the host may also be filled with the early quartz phase. The veins commonly contain interlocking grains which do not show growth zoning. In some cases the quartz grains increase in size outwards from the host/quartz boundary suggesting they were growing into open space.

Early Pyrite

The early pyrite grains tend to be very small (less than 0.01 mm to 0.2 mm) and most have cubic shapes. They commonly occur as a fringe along the edges of host rock clasts in the breccias and in clusters of ~0.5 mm size with the replacive early sphalerite.

Early Sphalerite

The early sphalerite phase occurs as small, usually 0.05 to 0.1 mm, grains which rarely reach up to 2 mm in length. This sphalerite is light green, white, pale yellow, pale orange or pale brown in colour. Most grains are subhedral but rounded grains are present in some samples.

The early sphalerite most commonly replaces the host dolostone (Figure 7E) or occurs as rims on dolostone clasts in the breccias. The sphalerite can replace less than 0.5% of the host and in some areas, and it can totally replace the hostrock on a centimeter scale. When occurring as rims on clasts in breccias the sphalerite is intensely fractured with fragments sometimes displaced. Sphalerite is most often seen in areas with moderate to intense early quartz alteration.

Main Ore Stage

Ore Stage Dolomite

The ore stage dolomite commonly has an average grain size of 0.1 to 2 mm with some grains reaching over 6 mm. The grain size tends to increase with distance from the contact with the host carbonate. Crystals which are elongated perpendicular to the contact with the host rock are common (Figure 8C). Saddle dolomites (Figure 8D) are also common and form when the dolomite is growing into open space. When the crystals have this distinctive saddle morphology they are commonly highly zoned. In both hand specimen and thin section the dolomite can have either a grayish or white colour. Crystals appear cloudy due to a high abundance of very small fluid inclusions.

The grey dolomite is usually found in contact with the host carbonate and may also replace it. The white dolomite can grow in continuity with the grey dolomite (Figure 7F) or be found directly at the contact with the host carbonate. Where both are observed, in all cases the grey dolomite clearly predates the white dolomite. The boundaries between both types of dolomite and the host carbonate can be completely gradational to very sharp. Gradational boundaries often retain original features of the carbonate host such as ooid ghosts and compositional laminations. The dolomite crystals can have internal ghosts of the original, smaller, carbonate host grains indicating recrystallization has occurred. Sharp boundaries are seen when the dolomite does not appear to have reacted with the host carbonate and is filling open space.

Ore Stage Pyrite

The main ore stage pyrite grains are most commonly 0.2 to 2 mm in size and have subhedral to euhedral forms. The ore stage pyrite is usually associated with ore stage dolomite, sphalerite, and quartz (Figure 8E). The pyrite grows between grain boundaries of these minerals and commonly appears to be coeval with them.

Ore Stage Quartz

The ore stage quartz grains can be up to 4 mm in size and are colourless. Most grains are euhedral. Commonly, the ore stage quartz is growing on the ore stage dolomite into open space. The quartz is generally surrounded by the ore stage sphalerite although may also be intergrown. Rarely, ore stage quartz occurs as subhedral inclusions in sphalerite (Figure 8F) and as small 0.1 mm veins crosscutting the host and ore stage dolomite.

Ore Stage Sphalerite

The main ore stage sphalerite phase is medium to large grained (0.5 to 3 mm) although, less commonly, small crystals (0.05 to 0.2 mm) also occur. Bright orange, red, and yellow colours are typical of this paragenetic phase although green and brown main ore stage sphalerite is also observed. Generally the sphalerite forms granular masses of anhedral crystals however euhedral crystals are seen in places. Zoning is often well defined and can occur as evenly spaced bands which mirror the tetrahedral crystal form or irregular patchy zones.

The main ore stage sphalerite most common occurs filling space around ore stage dolomite (Figure 7G, 8D, E). Scalloped and jagged edges at main ore stage sphalerite boundaries with host carbonate, main ore stage dolomite, and main ore stage quartz indicate that sphalerite-bearing fluids partially dissolved these phases (Figure 8G, H).

Ore Stage Galena

The galena at Gayna River is a volumetrically minor phase, estimated to make up less than 0.1% of the rock (Hardy, 1979), and was observed in only 4 samples. The galena grains are 0.25 to 4 mm in size and are usually subhedral. The galena is commonly found filling space around main ore stage sphalerite by nucleating on these grains.

Late Ore Stage

Late Pyrite

The last pyrite to be precipitated in the system ranges in grain size from 0.25 to 3 mm and is usually in the form of euhedral crystals. This pyrite is found filling space around main ore stage dolomite and sphalerite and in vugs with late calcite.

Late Quartz
The late stage quartz tends to form large (centimeter size) prismatic crystals in vugs and is found with late calcite.

Late Calcite
The late calcite phase crystals can be from 0.05 mm up to several centimeters in size. This calcite is colourless to milky and often has an abundance of highly birefringent twin lamellae. The late calcite is subhedral to euhedral in form. The main occurrence of late calcite is infilling the remaining porosity after the main ore stage mineralization. It also occurs as thin millimeter size veins crosscutting previous phases.

Late Sphalerite
The late sphalerite phase is volumetrically extremely minor. Millimeter size granular bright orange and red sphalerite may appear in vugs with calcite crystals.

Pyrobitumen
The last phase in the paragenesis at Gayna River is pyrobitumen. The pyrobitumen is found filling in remaining porosity adjacent to main ore stage dolomite or late calcite (Figure 7H). The pyrobitumen is found in micrometer to centimeter size amounts and has a matte to shiny black appearance. It may be found in small flecks or larger fragments with irregular shapes.

Oxidation
Some outcrop samples contain oxidized pyrite and zinc oxides (hydrozincite and smithsonite). Surface rocks may contain minor to moderately oxidized sulphides.

3.1.3 Paragenetic Summary

The paragenesis presented above is summarized in Figure 9 and is the framework used for the geochemical studies presented in subsequent sections. Differences between the paragenetic sequence presented here and in Hardy (1979) include the introduction of three defined ore stages and a more detailed observation of phase relationships. As a result of the limited sample set used in this study there may be some discrepancies: for example, barite and fluorite observed by Hardy (1979) were not found in any of the samples examined in this study.

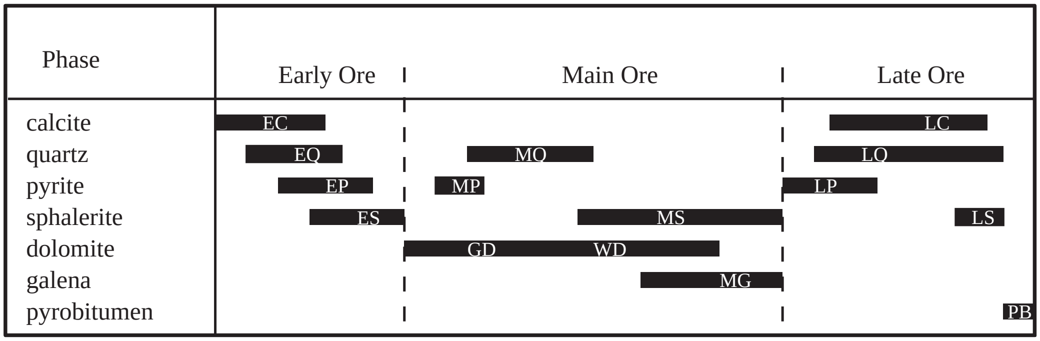

Figure 9. The paragenetic sequence for the Gayna River deposit, which is divided into early, main, and late ore stages. Abbreviations are as follows; EC - early calcite, EQ - early quartz, EP - early pyrite, ES - early sphalerite, GD - main grey dolomite, WD - main white dolomite, MP - main pyrite, MQ - main quartz, MS - main sphalerite, MG - main galena, LP - late pyrite, LQ - late quartz, LC - late calcite, LS - late sphalerite, PB - pyrobitumen.

3.2 Main Ore Stage Sphalerite Trace Element Composition

A total of 1096 individual points in 35 transects, of varying lengths, from 15 main ore stage sphalerite samples (Appendix 4), in addition to 4 qualitative element concentration maps of individual sphalerite crystals (Figure 10), were analyzed by electron microprobe. Twenty-one trace elements have been identified in the sphalerite grains (Table 1). Arsenic, Cu, Ga, Bi, and Pb are consistently above detection limits in the sphalerites, Fe, Ni, Sb, Mn, Ba, V, Ca, Au, Cr and Se are inconsistently above detection limits, and Ag, Co, Cd, Ge, In, and Ti are rarely above detection limits.

The concentrations of Ag, Cu, and Ga plus S and Zn (samples SG4, SG5, SG3) or Pb and As (SG4B) were mapped in 4 individual sphalerite crystals. The Ga distribution is heterogeneous: some crystals show clear growth zoning with respect to Ga whereas others have uniformly low Ga concentrations. Copper values have a strong positive correlation with Ga in all high Ga crystals analyzed thus far (Figure 11). Ag, Pb, and As were uniformly low in the 4 crystals analyzed.

Bright orange and red zones in sphalerite grains had higher Cu values than less intensely coloured zones. No systematic variation with colour for other elements was observed.

Table 1. Summary of trace element data for sphalerite from the Gayna River deposit.

Consistent		Inconsistent		Rare	
element	ppm (dl)[1]	element	ppm (dl)	element	ppm (dl)
Bi	1694 (350)	Se	bdl (200)	Ag	bdl (300)
Cu	547 (150)	Ni	bdl (100)	Co	bdl (100)
Pb	1049 (400)	Sb	bdl (200)	Ge[2]	
As	284 (120)	Mn	103 (100)	Cd[2]	
Ga	494 (150)	Ba	bdl (300)	In[2]	
		V	bdl (85)	Ti[2]	
		Ca	bdl (100)		
		Au	bdl (550)		
		Cr	bdl (160)		
		Fe	252 (250)		

[1] mean for all microprobe points in ppm (detection limit* in ppm)

*detection limits vary for each analysis, reported are means to 2 significant figures

[2] data from Carrière and Sangster (1999)

bdl = mean is below detection limit

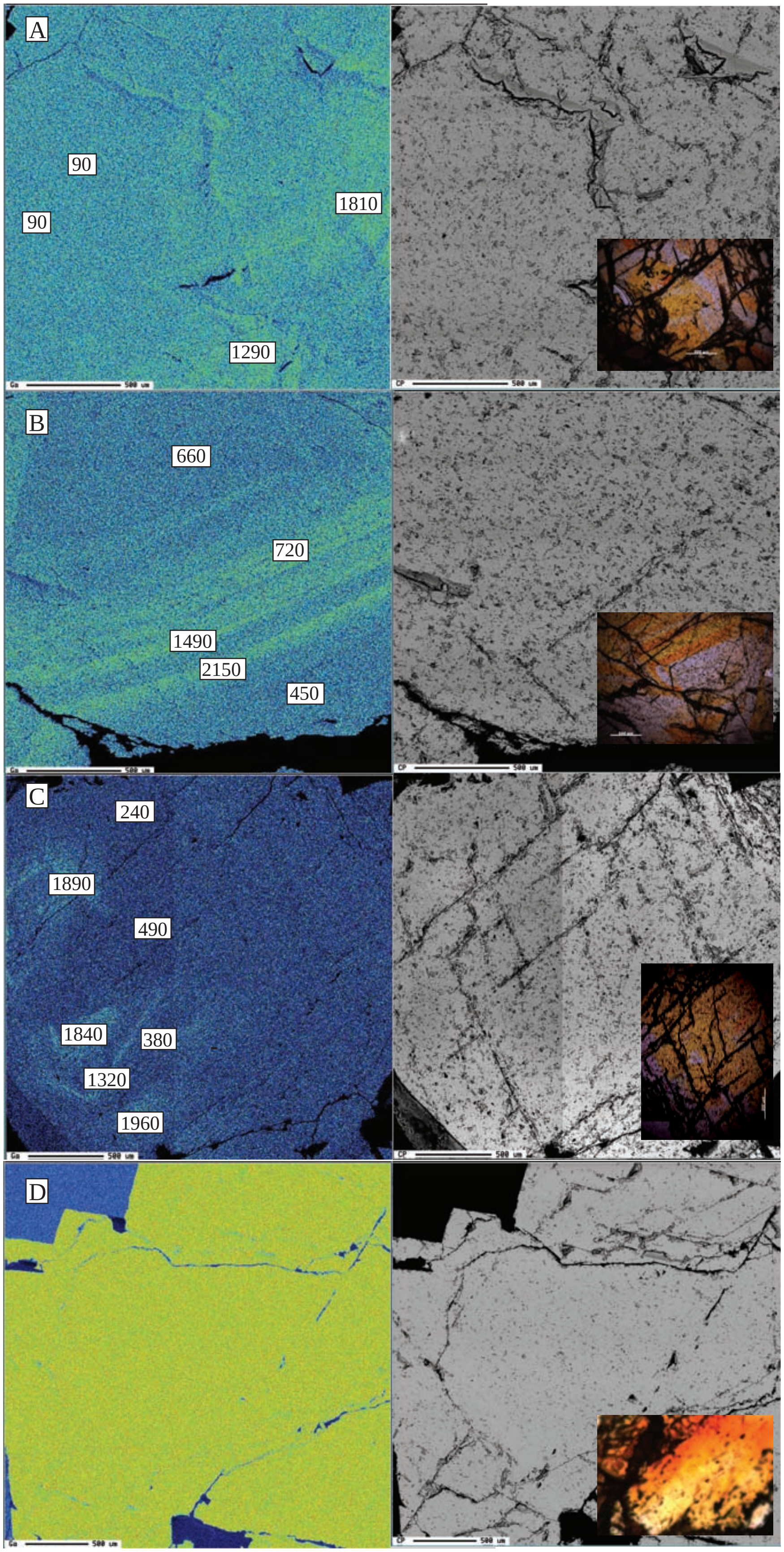
A
90
90
1810
1290
B
660
720
1490
2150
450
C
240
1890
490
1840
380
1320
1960
D

Figure 10. Qualitative Ga microprobe maps with spot analyses of Ga concentrations noted in ppm. Backscattered electron images of the same field of view are beside each map. The insets are plane polarized light photomicrographs of each sphalerite crystal. (A) Sample A27 149 m shows a heterogeneous distribution of Ga. (B) Sample A27 144 m shows distribution of Ga in bands, where the high Ga concentrations correspond to bright orange coloured areas. (C) Sample A27 144.5 m shows both some banded distribution and random distribution of Ga. Note that the right side of image is unreliable due to a beam current jump during analysis. (D) Sample A27 152 m shows a homogeneous distribution of Ga. No spot analyses were obtained for this sample.

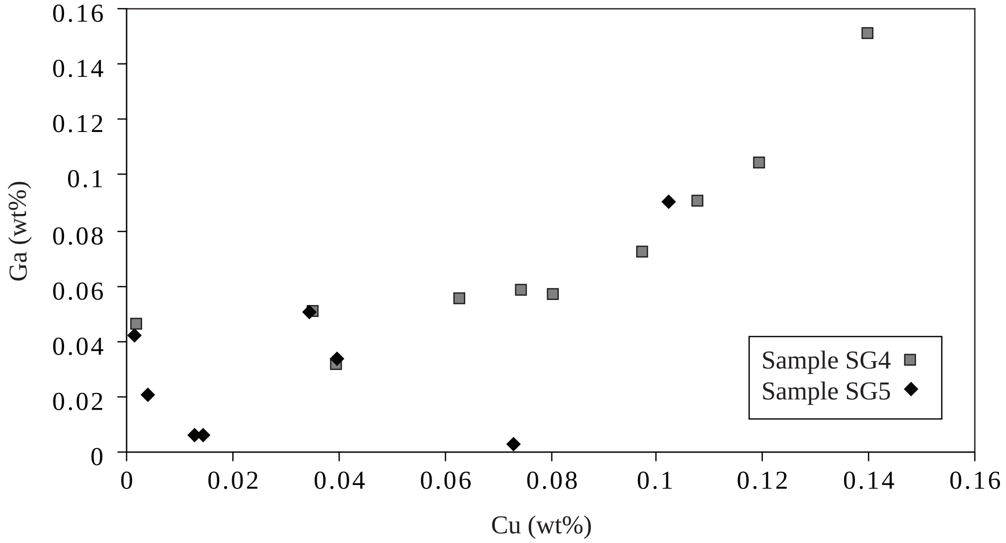

Figure 11. A cross-plot of Cu and Ga concentrations for selected Gayna River samples.

3.3 Lead, Rhenium, and Osmium Isotopes

Lead/Lead

Lead isotope data were acquired on 4 main-ore stage galena samples from various locations on the Gayna River property. These were obtained to supplement 9 previous Pb isotope results, analyzed by thermal ionization mass spectrometry, for main-ore stage galena at Gayna River from Sharp (2004). In addition, 10 main-ore stage sphalerite samples were analyzed.

The Pb isotope ratios for both galena and sphalerite, presented in Table 2, are indistinguishable and are comparable with the earlier study of Sharp (2004). The $^{206}Pb/^{204}Pb$ values range from 18.683 to 18.888 for galena and from 18.455

to 19.424 for sphalerite. The ^{207}Pb/^{204}Pb values for galena and sphalerite range from 15.638 to 15.660 and 15.612 to 15.673 respectively. Finally, the ^{208}Pb/^{204}Pb values for galena range from 38.288 to 38.529 and for the sphalerite they range from 37.950 to 38.549. There is no variation in Pb isotope data with paragenesis or sphalerite colour. All the data are all relatively radiogenic in nature and are tightly clustered in ^{207}Pb/^{204}Pb space (Figure 12).

Table 2. Pb/Pb isotopic data for sulphides from the Gayna River deposit.

Sample	**Phase**	**^{206}Pb/^{204}Pb**	**± 2σ** [1]	**^{207}Pb/^{204}Pb**	**± 2σ**	**^{208}Pb/^{204}Pb**	**± 2σ**
BSB001	sphalerite	18.818	0.019	15.657	0.021	38.440	0.062
75C001	sphalerite	18.834	0.026	15.656	0.028	38.448	0.083
A30 347	sphalerite	18.517	0.028	15.629	0.030	38.116	0.086
MBGRR013	sphalerite	18.963	0.023	15.659	0.024	38.485	0.069
BWGRR014	sphalerite	18.455	0.015	15.612	0.017	37.950	0.054
77-102 410.5	sphalerite	18.578	0.024	15.630	0.026	38.174	0.075
A30 400	sphalerite	18.981	0.025	15.657	0.023	38.549	0.063
B28 212.2	sphalerite	18.894	0.022	15.673	0.025	38.441	0.075
77-102 318.9	sphalerite	18.820	0.031	15.657	0.031	38.440	0.091
A32 59.1	sphalerite	19.424	0.032	15.662	0.030	38.475	0.087
06F001	galena	18.747	0.031	15.646	0.030	38.363	0.081
BWGRR022	galena	18.888	0.020	15.660	0.019	38.529	0.056
77-102 318.9	galena	18.683	0.017	15.638	0.018	38.288	0.055
BSB001	galena	18.754	0.026	15.647	0.023	38.367	0.059
GR 04-01 [2]	galena	18.743	0.090	15.669	0.113	38.417	0.338
GR 04-02 [2]	galena	18.706	0.090	15.675	0.113	38.389	0.338
GR 04-03 [2]	galena	18.763	0.090	15.667	0.113	38.388	0.338
GR 04-04 [2]	galena	18.851	0.090	15.684	0.113	38.570	0.339
GR 04-05 [2]	galena	18.745	0.090	15.672	0.113	38.430	0.338
GR 04-06 [2]	galena	18.659	0.090	15.657	0.113	38.307	0.337
GR 04-07 [2]	galena	18.433	0.088	15.641	0.113	38.035	0.335
GR 04-08 [2]	galena	18.612	0.089	15.650	0.113	38.238	0.336
GR 04-09 [2]	galena	18.878	0.091	15.686	0.113	38.562	0.339

[1] ± 2σ error (absolute) for this study [2] Data from Sharp (2004), ± 2σ (percent)

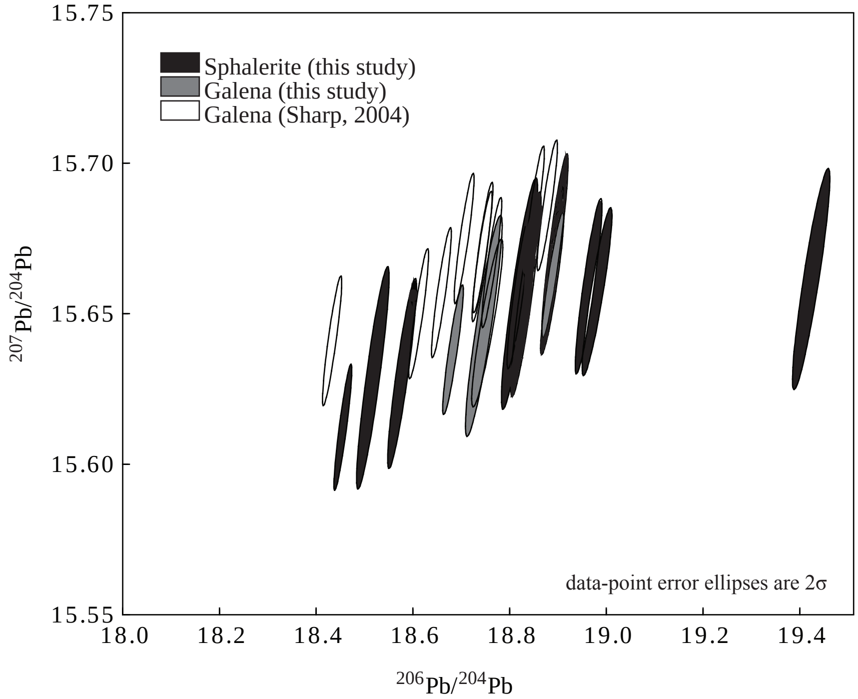

Figure 12. A detailed view of the lead isotope data for sphalerite and galena samples (this study) with additional lead isotope data from galena (Sharp, 2004).

Rhenium/Osmium

Rhenium concentrations in 7 samples range from 0.224 to 48.00 ppb and Os concentrations range from 3.36 to 413.53 ppt. The ^{187}Re/^{188}Os ratios are fairly high, ranging from 44.4 to 2638, and the ^{187}Os/^{188}Os ratios are low ranging from 0.716 to 1.784 (Table 3).

Table 3. Re/Os isotopic data for pyrobitumen from the Gayna River deposit.

Sample	Re ppb	± 2σ[1]	Os ppt	± 2σ	^{187}Re/^{188}Os	± 2σ	^{187}Os/^{188}Os	± 2σ	Rho
07R001	0.224	0.015	21.89	0.92	53.1	6.4	0.716	0.078	0.752
07R006	9.766	0.041	109.29	1.18	491.2	12.6	1.206	0.033	0.923
07R007	2.731	0.018	175.7	3.09	81.6	3.3	0.814	0.056	0.575
07R008	3.349	0.021	413.53	1.45	44.4	0.4	1.185	0.013	0.576
A30 350	1.807	0.024	178.51	1.51	55.6	1.3	1.197	0.025	0.776
BWGRR001	0.493	0.017	3.36	0.66	783	368	0.961	0.474	0.948
BWGRR006	48.00	0.18	106.6	1.6	2638	81	1.784	0.071	0.769

[1] ± 2σ error (absolute)

3.4 Fluid Inclusions

A total of 65 samples were petrographically examined for fluid inclusions. The petrographic study confirms the presence of two phase, liquid plus vapour, inclusions in all the Gayna River samples. No daughter minerals are observed in any inclusions. The fluid inclusions in most samples have small vapour bubbles (0.95 degree of fill) but, rarely, other degrees of fill are observed (0.80 to 0.98).

Samples generally contain a mixture of primary and secondary fluid inclusions. Primary inclusions are classified on the basis of fluid inclusion assemblages having a three-dimensional random distribution, or being isolated from adjacent inclusions, and/or a large size relative to the host crystal (Shepherd at al., 1985). Rarely, fluid inclusions clearly form in distinct growth zones. Secondary inclusions are classified on the basis of occurrence as planar groups trapped in healed fractures, cross-cutting grain boundaries, and/or inclusions which have thin, flat, or irregular morphologies. In all mineral phases, but most commonly in the carbonates and quartz, some of the inclusions are of irregular shape, have tails, are surrounded by very small inclusions, and/or are in groups with variable degrees of fill. These inclusions are interpreted to have been modified after trapping and were not selected for microthermometry.

Most of the fluid inclusions in the samples are very small (<5 μm) and not suitable for the microthermometric study. In total only 18 fluid inclusion wafers had some measurable fluid inclusions, and data were acquired from early ore stage sphalerite, main ore stage dolomite, quartz, and sphalerite and late ore stage quartz and calcite. Hydrohalite is not observed in any inclusions, although it may be present but not visible due to the small inclusion size.

The microthermometry results for all inclusions are reported in Table 4 and Appendix 5 and displayed in Figures 14, 15, and 16. Results are reported below by paragenetic phase.

Early Ore Stage

Sphalerite

The primary inclusions in this phase range in size from 1 to over 30 μm with a mean of ~5 μm. Inclusions are commonly elongate but sometimes have a tetrahedral shape and they occur in random clusters or as single isolated inclusions in crystals. Only a small number, ~ 5%, of crystals contain primary inclusions and these, in addition, always have secondary inclusions. Many crystals only contain secondary inclusions, other crystals contain few inclusions. Secondary inclusions are generally small, 1 μm or less, and occur in planes with equidimensional to slightly elongate habits.

Table 4. Microthermometric data for carbonates, quartz and sphalerite from the Gayna River deposit.

Sample	Host Mineral	Ore Stage	Inclusion Origin	Tm ice (°C)			Th (°C)		
				range	mean	number	range	mean	number
B28 212.2	sphalerite	early	primary	-	-	-	178 to 195	189	3
B28 212.2	sphalerite	early	secondary	-23.8	-	1	192	192	2
BWGRR012	sphalerite	early	primary	-12.5 to -10.3	-11.9	4	179 to 214	190	6
BWGRR023B	sphalerite	early	primary	-26.7 to -10.7	-14.5	9	107 to 183	138	9
BWGRR023B	sphalerite	early	secondary	-10.7 to -10.6	-10.7	2	135	-	1
A30 120	dolomite	main	primary	-	-	-	152 to 202	177	7
A30 322.5	dolomite	main	primary	-33.2 to -18.5	-26.7	11	151 to 198	177	11
A30 322.5	dolomite	main	secondary	-	-	-	185	-	1
A30 347	dolomite	main	primary	-	-	-	155	-	1
A30 400	dolomite	main	primary	-	-	-	153 to 159	156	2
B28 194.5	dolomite	main	primary	-28.5 to -17.3	-23.1	7	154 to 225	191	9
B28 212.2	dolomite	main	primary	-22	-	1	215 to 231	223	2
BWGRR008	dolomite	main	primary	-17.8 to -0.8	-9.5	3	65 to 110	83	3
BWGRR012	dolomite	main	primary	-34.3 to -2.1	-14.7	3	132 to 172	146	6
BWGRR014B	dolomite	main	primary	-15.3 to -2.1	-6.5	3	146 to 182	161	6
MBGRR013	dolomite	main	primary	-13.9 to -11.0	-12.0	4	162 to 178	170	5
SG7	dolomite	main	primary	-	-	-	126 to 213	157	4
BWGRR022A	quartz	main	primary	-23.8 to -15.8	-20.4	7	132 to 222	163	8
CAGRR001	quartz	main	primary	-36.1 to -9.8	-22.6	22	120 to 233	177	17
CAGRR001	quartz	main	secondary	-20.7 to -20.6	-20.7	4	83 to 201	180	7
A30 347	sphalerite	main	primary	-14.7 to -10.1	-11.3	4	161 to 171	167	4
A30 400	sphalerite	main	primary	-38.0 to -31.0	-35.7	14	192 to 227	206	16
MBGRR013	sphalerite	main	primary	-16.1 to -13.8	-15.4	4	177 to 182	179	9
RTS2B	sphalerite	main	primary	-32.5 to -16.1	-28.0	6	178 to 268	206	8
SG7	sphalerite	main	primary	-21	-	1	-	-	-
75C001	quartz	late	primary	-15.5 to -11.8	-13.4	5	148 to 223	173	5
BWGRR023B	quartz	late	primary	-20.2 to -10.7	-13.7	20	84 to 175	140	21
BWGRR023B	quartz	late	secondary	-11.5	-	1	148 to 156	151	5
SG7	quartz	late	secondary	-	-	-	108	-	1
A30 120	calcite	late	primary	-	-	-	105 to 181	146	5
A30 400	calcite	late	primary	-21.2	-	1	-	-	-
A33 250	calcite	late	primary	-22.0 to -9.7	-15.1	27	56 to 123	85	20
A35 346.2	calcite	late	primary	-18.3	-	1	74 to 118	101	4
BWGRR008	calcite	late	primary	-16.4 to -13.7	-15.7	9	83 to 176	161	12
BWGRR008	calcite	late	secondary	-15.9	-15.9	2	164 to 168	166	5
MBGRR013	calcite	late	primary	-31.8 to -18.0	-22.5	10	102 to 150	124	11

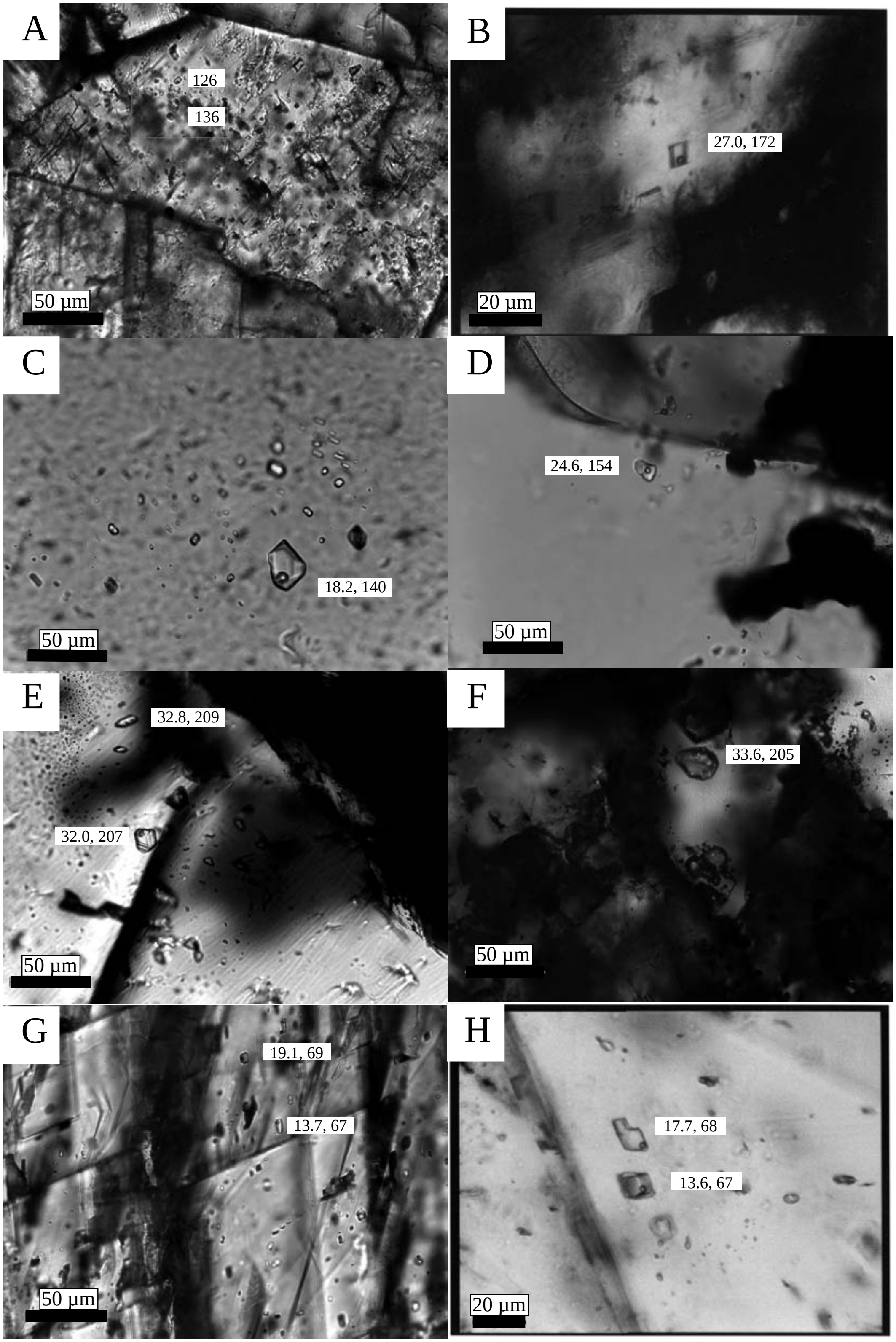
A
126
136
50 µm
B
27.0, 172
20 µm
C
18.2, 140
50 µm
D
24.6, 154
50 µm
E
32.8, 209
32.0, 207
50 µm
F
33.6, 205
50 µm
G
19.1, 69
13.7, 67
50 µm
H
17.7, 68
13.6, 67
20 µm

Figure 13. Photomicrographs of Gayna River fluid inclusions which are labeled with microthermometry results (salinity in wt% NaCl equivalent, homogenization temperature in °C; single numbers are homogenization temperatures in °C when final melting temperatures were unobtainable). A) A photomicrograph of main dolomite with abundant fluid inclusions, mostly less than 1 μm in size, from sample SG7. B) A photomicrograph of main dolomite, with a rare large negative crystal shape inclusion, from sample BWGRR012. C) A photomicrograph of late quartz, with a cluster of negative crystal shape inclusions, from sample BWGRR021. D) A photomicrograph of an irregularly shaped inclusion in main quartz, from sample BWGRR022. E) A photomicrograph of a large negative crystal shape inclusion in main sphalerite with smaller irregularly shaped inclusions and a plane of secondary inclusions, from sample A30 400. F) A photomicrograph of an isolated large inclusion in main sphalerite, from sample BWGRR014. G) A photomicrograph of randomly distributed inclusions in late calcite, from sample A33 250. H) A photomicrograph of large, negative crystal shape inclusions in late calcite, from sample A33 250.

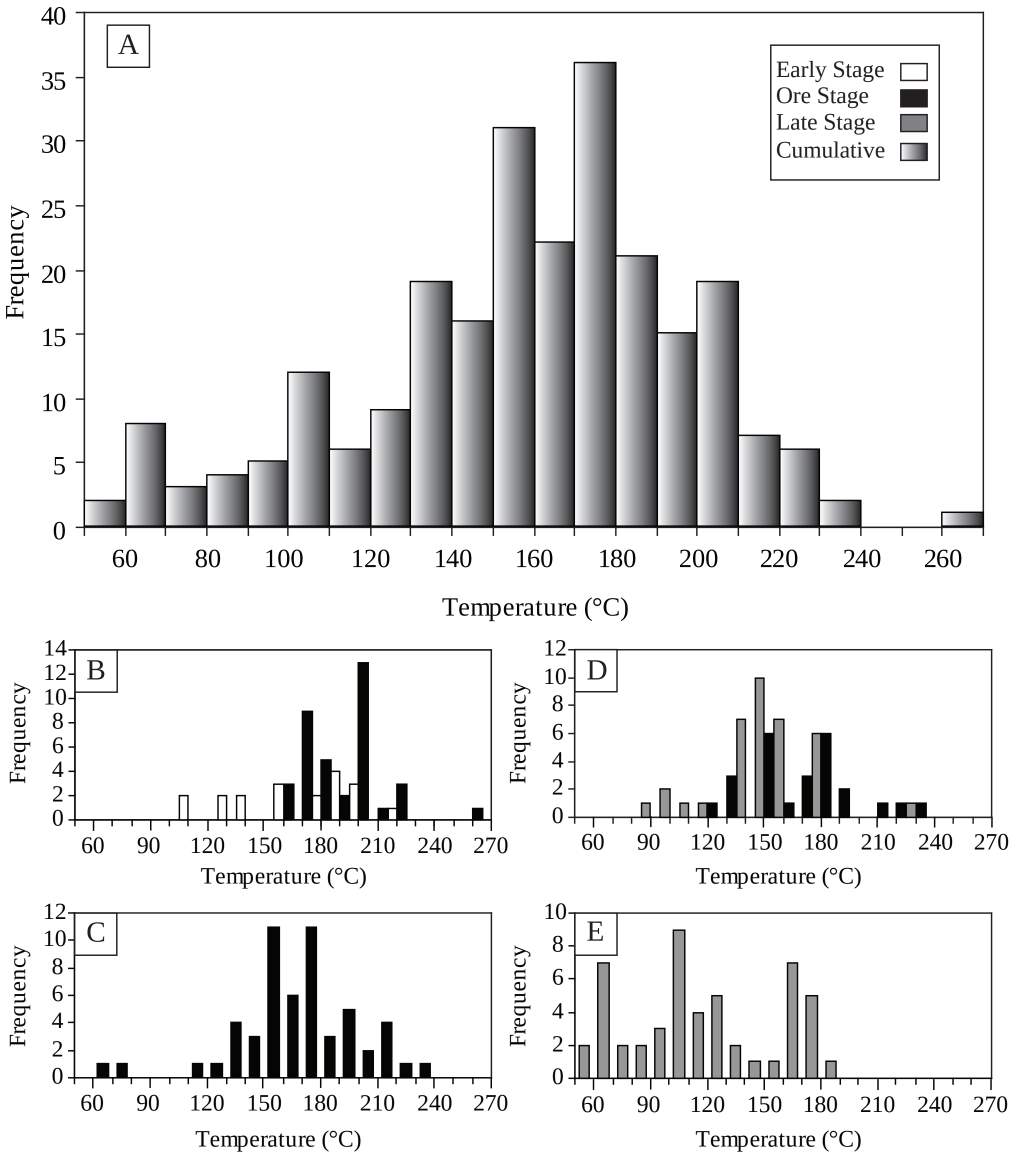

Figure 14. The fluid inclusion homogenization temperatures for samples from Gayna River. A) Cumulative data for all of the phases. B) Data from sphalerite. C) Data from dolomite. D) Data from quartz. E) Data from calcite samples.

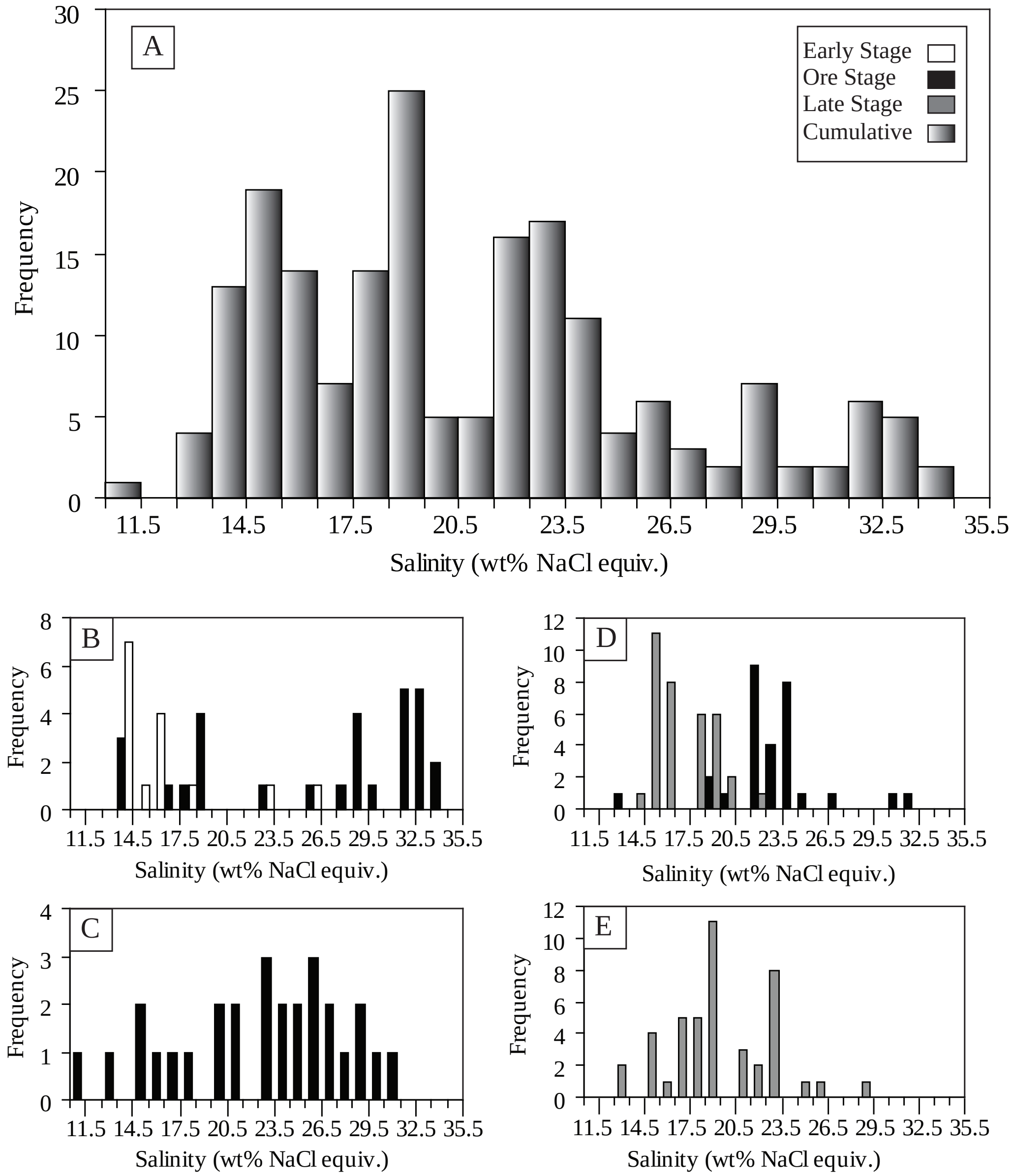

Figure 15. The fluid inclusion salinities for samples from Gayna River. A) Cumulative data for all of the phases. B) Data from sphalerite. C) Data from dolomite. D) Data from quartz. E) Data from calcite.

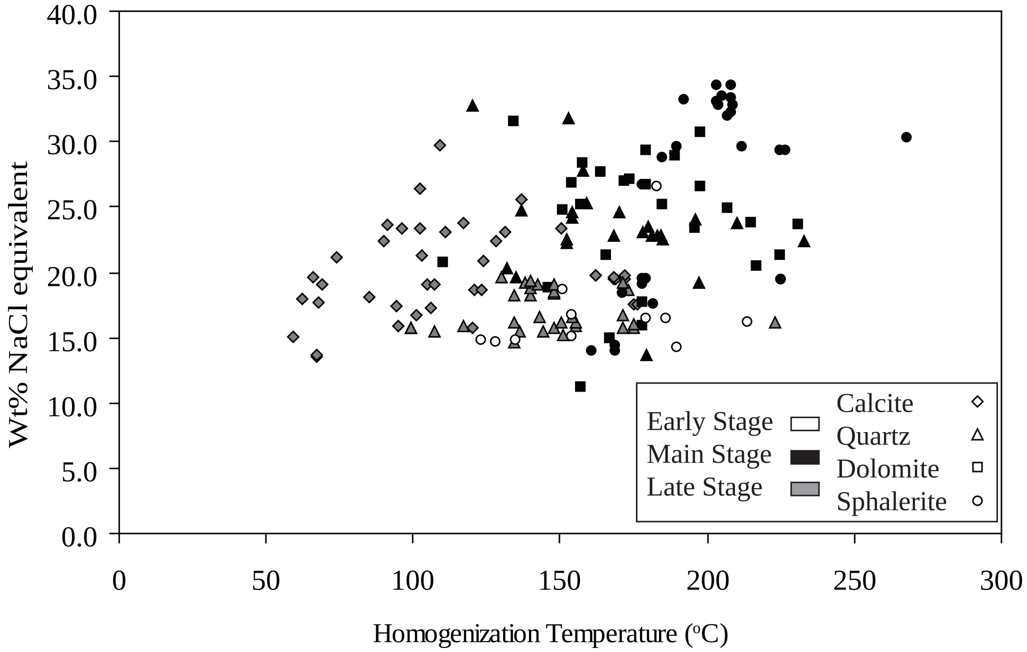

Figure 16. A cross-plot of fluid inclusion homogenization temperatures and fluid inclusion salinities for the early, main, and late ore stage samples from Gayna River.

Microthermometric results were obtained from 20 early ore phase primary inclusions in sphalerite. In approximately half of these inclusions first melting occurs near -70°C, whereas in the other half first ice melting occurs near -55°C. Hydrate melting was not observed in the inclusions. Final ice melting temperatures range from -26.7 to -10.3°C, and have corresponding salinities of 26.6 to 14.2 wt% NaCl equivalent. The mean salinity of early ore phase sphalerite inclusions is 17.2 wt% NaCl equivalent. The homogenization temperatures in these inclusions range from 107 to 214°C, with a mean of 164°C.

<u>Main Ore Stage</u>

Dolomite

In the dolomite crystals the primary inclusions tend to be extremely small with the vast majority being less than 1 µm in size (Figure 13A). Rarely, inclusions are up to 15 µm in size (Figure 13B). Most primary inclusions are equidimensional to slightly elongate in shape with some rhombohedral inclusions present. In some cases inclusions occur in groups orientated parallel to grain boundaries. These are interpreted as primary inclusions. Most primary inclusions, however, occur in randomly distributed, densely populated clusters with adjacent secondary inclusions in planar groups. Secondary inclusions in dolomite are extremely small, almost all less than 1 μm in size. These inclusions are equidimensional to slightly elongate or irregular in shape.

The extremely small size of most inclusions in the dolomite makes microthermometry difficult and restricts the accuracy of measurements. However, 62 ore phase dolomite primary inclusions were microthermometrically analysed. Temperatures of first melting are generally near -70°C. Final ice melting occurs between -34.3 and -7.6°C corresponding to salinities of 31.5 to 11.2 wt% NaCl equivalent with a mean of 23.2 wt% NaCl equivalent. These results exclude 3 inclusions with high final melting temperatures of -2.2, -2.1, and -0.8°C. These inclusion had apparent final ice melting temperatures of approximately -27°C, but then the bubble continued moving until final melting occurred at -2.2 to -0.8°C. These final melting temperatures possibly represent clathrate melting and indicate the presence of small amounts of volatile phases in these inclusions. Their size precludes more detailed investigation and they are not included in Figure 16. Homogenization temperatures range from 65 to 231°C with a mean of 168°C.

Quartz

The primary main stage quartz inclusions are most commonly 1 to 4 μm in size but large, 10 to 30 μm, inclusions can occur. Inclusions with negative crystal shapes are common (Figure 13C), as well as rectangular to equidimensional habits. Primary inclusions occur in random clusters or bands mirroring crystal boundaries which are interpreted as being growth zones. Secondary trails commonly comprise 90% of all inclusions. These secondary inclusions are mostly less than 1 μm in size with some ranging up to 4 μm. The dominant fluid inclusion habits are irregular (Figure 13D), elongate, or equidimensional.

Upon freezing, in approximately half of these quartz-hosted inclusions, the solid is brown in appearance. The first liquid is observed at -70°C in the primary main ore phase quartz inclusions (n=30). Final melting occurs between -36.1 and -9.8°C. The calculated salinities range from 32.9 to 13.7 wt% NaCl equivalent with a mean of 23.6 wt% NaCl equivalent. The temperature of homogenization ranges from 120 to 233°C with a mean of 172°C.

Sphalerite

Inclusions in the main stage sphalerite are petrographically similar to the early ore stage sphalerite. Primary inclusions range in size from 1 to over 50 μm with a mean of ~5 μm. Primary inclusions are commonly elongate or tetrahedral in shape, are seen in only ~5% of crystals, and occur in random clusters or as single isolated inclusions (Figure 13E, F). Many crystals contain only planes of secondary inclusions or are inclusion free. Secondary inclusions are generally small, 1 μm or less and have equidimensional to elongate habits.

Microthermometry was carried out on 40 primary main ore phase sphalerite inclusions. First melting was observed at low temperatures, approximately -70° C. Final ice melting temperatures range from -38 to -10.1°C corresponding to 34.3 to

14.0 wt% NaCl equivalent. The mean wt% NaCl equivalent is 26.9, however the inclusions appear to have a weak bimodal distribution of salinity, with modes at 19 and 32-33 wt% NaCl equivalent (Figure 15). The homogenization temperatures of the fluid inclusions range from 161 to 268°C, have a mean of 195°C, and do not have a bimodal distribution.

Late Ore Stage

Quartz

The largest inclusions at Gayna River are found in the late stage quartz where some primary inclusion can be larger than 1 mm in size. Most commonly inclusions are 1 to 4 µm in size with some 10 to 20 µm inclusions. Crystals are usually ~1% inclusions by volume. Primary inclusions have negative crystal, rectangular, and equidimensional shapes and occur in random clusters or are isolated. Secondary inclusions are small, less than 1 to 4 µm, and are mostly slightly elongate or irregular in shape. Secondary inclusions occur in trails, commonly healing fractures.

The primary late ore phase quartz inclusions (n=37) commonly have first melting temperatures near -70°C, but can remain completely frozen up to -30°C. Final ice melting temperatures range from -20.2 to -10.7°C corresponding to salinities of 22.5 to 14.7 wt% NaCl equivalent with a mean of 17.4 wt% NaCl equivalent. Homogenization temperatures range from 99 to 223°C with a mean of 145°C.

Calcite

Primary inclusions in calcite are mostly less than 1 µm in size but rarely range up to 20 µm. Inclusions commonly have rhombohedral negative crystal shapes but can be equidimensional, elongate, or irregular (Figure 13G, H). Primary inclusions occur in randomly distributed clusters within crystals whereas secondary inclusions occur in trails in healed fractures across and within crystals. Secondary inclusions are almost always less than 1 µm in size, have equidimensional to elongate habits, and comprise 10 to 90% of inclusions in any crystals.

The primary late ore phase calcite fluid inclusions (n=60) develop brown coloured solids upon freezing and mostly have temperatures of first melting near -70°C. Final ice melting temperatures range from -31.8 to -9.7°C giving salinities of 29.8 to 13.6 wt% NaCl equivalent. The mean salinity is 17.4 wt% NaCl equivalent. These inclusions have homogenization temperatures in the range of 59 to 181°C with a mean of 117°C.

Secondary Inclusions

Few secondary inclusions were studied due to their generally very small size. Secondary inclusions in all minerals have final melting and homogenization temperatures within the range of the primary inclusions (Table 4). As proposed by Carrière and Sangster (1992), these secondary inclusions likely represent a continuum in the hydrothermal activity.

Fluid inclusion summary

The temperatures of first ice melting for all inclusions at Gayna River are lower than the eutectic temperature of the H_2O-NaCl system, -21.1°C (Linke, 1965), indicating the presence of other salts in the fluids. Misinterpretation of first ice melting temperatures is possible, especially in very small inclusions, due to melting or crystallization of metastable assemblages (Davies et al., 1990, Samson and Walker, 2000). In this study, the very low observed first melting temperatures may well represent metastable eutectics or crystallization, but without further study this cannot be delineated. However, in light of the observed brown coloured ice in some inclusions and the final melting temperatures which are often lower than the eutectic for a pure H_2O-NaCl system, other salts are likely present in the system (Roedder, 1984; Samson and Walker, 2000). The probable candidates are NaCl-$CaCl_2$-H_2O and/or NaCl-$MgCl_2$-H_2O, with eutectic temperatures of -52°C and -33°C respectively (Spencer et al., 1990; Samson and Walker, 2000; Bakker, 2004). The NaCl-$MgCl_2$-H_2O system has metastable eutectics at -37°C, ~ -55°C, and ~ -80°C and the NaCl-$CaCl_2$-H_2O system has a metastable eutectic at ~ -70°C (Davis et al., 1990), which would account for first melting temperatures in this study.

The fluid inclusions at Gayna River have a wide range of homogenization temperatures and salinities but these vary with the paragenesis (Figure 16). The early ore phase inclusions have salinities in the lower range of the entire dataset (Table 4) but have variable homogenization temperatures. The main ore phase mineralizing fluids generally have higher salinities and homogenization temperatures than the early or late phases. Finally, the late ore phase inclusions have salinities and homogenization temperatures at the lower end of the range of data.

3.5 Sulphur isotopes

Sixty-six mineral separates including pyrite, sphalerite and galena from Gayna River were analyzed (Table 5). In total the $\delta^{34}S$ composition of sulphides at Gayna River range from -4 to 25.7‰ (CDT) (Figures 17 and 18).

Early Ore Stage

The lowest S isotope values are for the early ore stage pyrite samples (n = 5) which range from -4 to 2‰ with a mean of -2‰. The early ore stage sphalerites (n = 7) have $\delta^{34}S$ values at the low and high end of the results (0.5 to 5.2‰, 25.1‰ and 25.7‰). The lowest $\delta^{34}S$ values are seen in pale yellow, pale brown, and pale green sphalerite. The two highest $\delta^{34}S$ values are from brown coloured sphalerites.

Main Ore Stage

The main ore stage sphalerites (n = 31) have values of 12.2 to 25.4‰ with a mean of 21.0‰. Dark red and dark orange sphalerites have mid-range values while bright orange sphalerites are dominant in the 21 to 24‰ range. The brown coloured sphalerites have high $\delta^{34}S$ values. The 7 galena samples range from $\delta^{34}S$ = 14.9 to 23.2‰ with a mean of 19.3‰.

Late Ore Stage

Pyrites from the late ore phase (n = 15) have δ^{34}S values of 11 to 21‰ with a mean of 18‰. One sample with oxidized pyrite (MBGRR005), has a δ^{34}S value of 25‰.

Summary

The early ore stage pyrite and sphalerite δ^{34}S values are distinctly different from the main and late ore stages. The early ore stage is characterized by low δ^{34}S values between -4 to 5‰. The main and late ore stages have overlapping S isotope ranges from 12 to 25‰.

Table 5. S isotopic data for sulphides from the Gayna River deposit.

Sample	**Phase**	**Colour**	**δ^{34}S (‰)**
75002	Early Sph	pale	0.5
A17 204.2	Early Sph	pale	0.5
A32 214.1	Early Sph	brown	25.7
B28 212.2	Early Sph	pale	1.5
B28 212.2	Early Sph	pale	4.5
B28 212.2	Early Sph	pale	5.2
BWGRR018	Early Sph	brown	25.1
75002	Main Sph	red/dark	13.6
06BSW	Main Sph	orange	22.6
06BSW	Main Sph	orange	23.0
75C001	Main Sph	orange	21.4
75C002	Main Sph	orange	23.6
77-102 318.9	Main Sph	orange	18.9
77-102 404	Main Sph	orange	17.1
77-102 410.5	Main Sph	red/dark	14.2
77-102 452	Main Sph	red/dark	13.4
A30 400	Main Sph	orange	23.3
A30 347	Main Sph	orange	19.7
A30 347	Main Sph	orange	22.7
A30 347	Main Sph	red/dark	19.6
A30 353.5	Main Sph	brown	22.1
A30 353.5	Main Sph	orange	21.0
A30 364	Main Sph	pale	23.4
A30 400	Main Sph	orange	23.4
A30 400	Main Sph	orange	24.2
A30 457.8	Main Sph	orange	22.9
A32 200.1	Main Sph	brown	25.4
A32 58.3	Main Sph	red/dark	19.3
A32 59.1	Main Sph	orange	21.1
A32 59.1	Main Sph	orange	22.5
A32 59.2	Main Sph	orange	20.7
A32 59.2	Main Sph	orange	23.0
B14 73.2	Main Sph	orange	22.4
BSB001	Main Sph	orange	24.5
BSB001	Main Sph	red/dark	23.8
BWGRR009	Main Sph	red/dark	12.2
BWGRR022	Main Sph	red/dark	23.5
A30 174.4	Early Pyr		2
A30 380	Early Pyr		-4
A30 380	Early Pyr		-3
B28 212.2	Early Pyr		-3
B28 642	Early Pyr		-2
77-102 452	Late Pyr		17
A17 250	Late Pyr		12
A30 322.5	Late Pyr		13
A30 347	Late Pyr		16
A30 347	Late Pyr		17
A30 364	Late Pyr		21
A32 58.3	Late Pyr		19
A32 59.1	Late Pyr		19
A32 59.2	Late Pyr		13
A32 59.2	Late Pyr		16
B28 312.2	Late Pyr		19
B28 506.5	Late Pyr		11
B28 551.8	Late Pyr		15
B28 583.5	Late Pyr		19
B28 597	Late Pyr		19
MBGRR005	Late Pyr		25
06BSW	Main Gal		20.4
75C002	Main Gal		14.9
77-102	Main Gal		15.0
BWGRR022	Main Gal		22.2
BWGRR022	Main Gal		23.0
BWGRR022	Main Gal		23.2
F showing	Main Gal		16.5

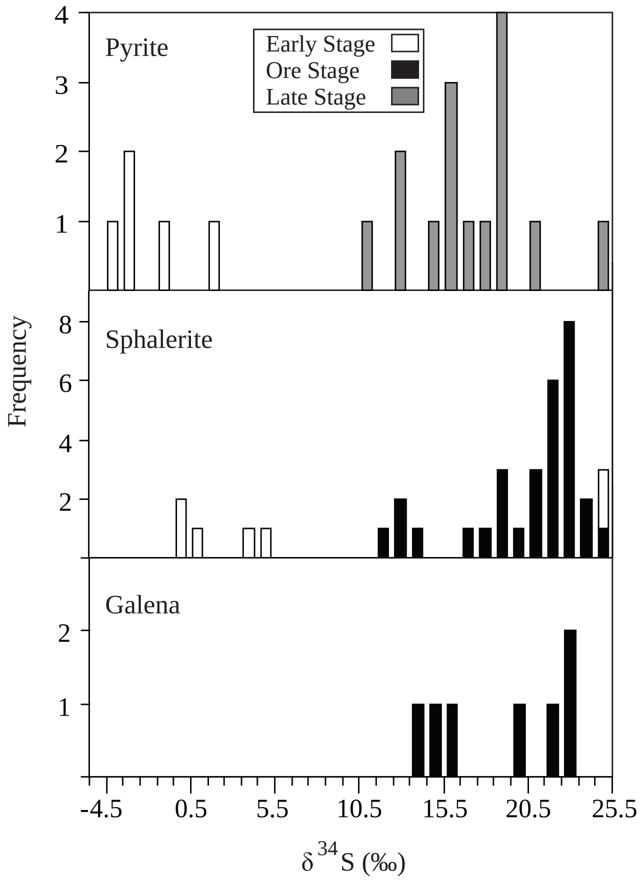

Figure 17. The sulphur isotope results for the pyrite, sphalerite, and galena samples from Gayna River.

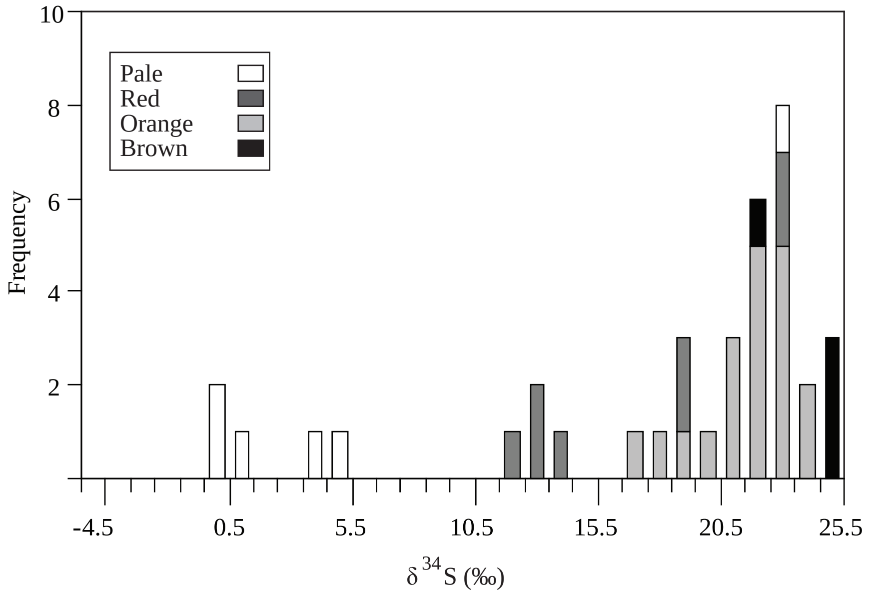

Figure 18. The sulphur isotope results for the various colours of sphalerite from Gayna River.

3.6 Carbon and Oxygen isotopes

The total data obtained from this stable isotope study of 56 carbonate and 9 quartz samples are presented in Table 6 and Figure 19. The samples were analyzed according to the paragenetic scheme presented in Figure 9 and the paragenetic stages are discussed in turn.

Host Carbonate

The host dolomite has a range of $\delta^{13}C$ values from 1.5 to 4.6‰ (VPDB) with a mean of 3.2‰ and $\delta^{18}O$ values range from 22.1 to 27.2‰ (VSMOW) with a mean of 24.5‰.

Main Ore Stage

The grey dolomite cement samples have $\delta^{13}C$ values of 1.7 to 4.1‰ (VPDB) with a mean of 2.8‰ and $\delta^{18}O$ values of 23.6 to 27.4‰ (VSMOW) with a mean of 25.6‰. The white dolomite cement samples have $\delta^{13}C$ values of 0.2 to 2.6‰ (VPDB) with a mean of 1.4‰ and $\delta^{18}O$ values of 19.9 to 23.0‰ (VSMOW) with a mean of 20.9‰. The main ore stage quartz samples have $\delta^{18}O$ values of 21.5 to 24.2‰ (VSMOW) with a mean of 22.6‰.

Late Ore Stage

The late ore stage quartz samples all have tightly clustered $\delta^{18}O$ isotopic values with a range from 21.5 to 23.1‰ (VSMOW) and a mean value of 22.0‰. The late calcite has $\delta^{13}C$ values of -4.3 to 3.0‰ (VPDB) with a mean of -1.6‰ and $\delta^{18}O$ values of 15.9 to 20.5‰ (VSMOW) with a mean of 18.7‰.

Summary

The grey and host dolomite groups have a very similar mean and range of isotopic compositions. Some grey dolomites are almost identical in isotopic composition to the host dolomite from the same sample whereas others are significantly different and there is no consistent relationship. The white dolomites have lower C and O isotope values than the grey dolomites. The late calcite samples have the lowest C and O isotope values. All of the quartz $\delta^{18}O$ values fall within those seen in the carbonate samples.

3.7 Strontium Isotope Results

Strontium isotope results are reported in Table 7 and Figure 20. The host dolostone has $^{87}Sr/^{86}Sr$ values of 0.7102 to 0.7303. The main ore stage grey dolomite has $^{87}Sr/^{86}Sr$ ratios ranging from 0.7087 to 0.7129 and the white dolomite has $^{87}Sr/^{86}Sr$ ratios ranging from 0.7084 to 0.7219. The late ore stage calcite has $^{87}Sr/^{86}Sr$ ratios between 0.7095 and 0.7148. Carbon and O isotope compositions and Sr concentrations show no correlation with the $^{87}Sr/^{86}Sr$ ratios.

Table 6. C and O isotopic data from the Gayna River deposit.

Sample	**Phase**	**δ^{13}C ‰ (VPDB)**	**δ^{18}O ‰ (VSMOW)**
06F001	host	4.3	25.6
75C001	host	1.9	24.0
A30 120	host	4.0	24.3
A30 185	host	4.0	23.6
A30 347	host	4.0	25.2
A30 378	host	2.7	25.9
A30 45.4	host	3.4	24.5
A30 78	host	3.0	25.0
A33 250	host	4.6	22.1
A33 68	host	4.0	23.5
A34 244	host	3.1	25.7
A34 457	host	4.1	27.2
B Showing	host	1.8	23.0
B14 73.2	host	3.8	26.1
B28 212.2	host	4.0	22.5
B28 312.2	host	1.6	25.7
BWGRR022	host	1.5	23.0
MBGRR013	host	1.7	23.9
A30 185	grey dolomite	1.7	24.0
A30 322.5	grey dolomite	3.4	25.1
A30 378	grey dolomite	3.0	26.3
A30 403.8	grey dolomite	2.5	26.6
A30 453	grey dolomite	2.8	24.8
A32 58.3	grey dolomite	2.2	26.7
A32 59.2	grey dolomite	2.0	27.4
A33 68	grey dolomite	4.1	23.6
A34 244	grey dolomite	4.1	27.1
A34 457	grey dolomite	2.9	27.0
B28 212.2	grey dolomite	2.4	24.2
B28 312.2	grey dolomite	1.8	25.8
BWGRR018	grey dolomite	4.0	23.9
75C001	white dolomite	1.5	21.2
A30 120	white dolomite	0.7	23.0
A30 347	white dolomite	1.7	20.4
A30 378	white dolomite	2.2	20.2
A30 400	white dolomite	0.8	20.7
A30 45.4	white dolomite	1.1	19.9
A33 68	white dolomite	1.1	22.7
A34 457	white dolomite	0.2	20.2
B28 212.2	white dolomite	1.8	20.9
B28 312.2	white dolomite	1.9	20.2
BWGRR022	white dolomite	2.6	20.7
B14 216	quartz	-	22.2
BSB001	quartz	-	21.6
BSW06	quartz	-	21.7
BWG021	quartz	-	24.2

Table 6 (con't). C and O isotopic data from the Gayna River deposit.

Sample	Phase	$\delta^{13}C$ ‰ (VPDB)	$\delta^{18}O$ ‰ (VSMOW)
BWG022	quartz	-	21.5
BWR020	quartz	-	23.1
CAR001	quartz	-	22.0
CAR005	quartz	-	22.9
MBR005	quartz	-	21.5
77-102 386	calcite	3.0	19.6
A17 255	calcite	-1.3	20.2
A30 120	calcite	-2.7	20.5
A30 120	calcite	-3.0	19.7
A30 453	calcite	-3.3	19.4
A30 78	calcite	-2.6	20.0
A33 102.8	calcite	-2.4	16.5
A33 250	calcite	-0.9	19.0
A35 346.2	calcite	-1.2	15.9
A35 346.2	calcite	-1.3	16.6
BWGRR008	calcite	-0.3	18.8
BWGRR014	calcite	-4.3	19.4
F showing	calcite	-2.3	18.8
MBGRR013	calcite	-0.4	18.0

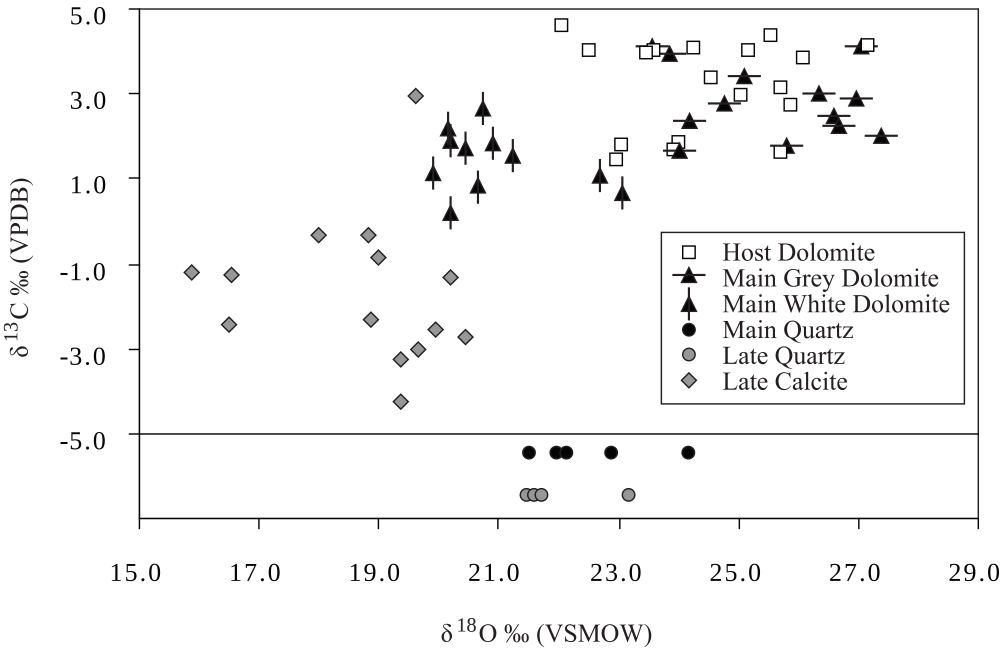

Figure 19. The carbon and oxygen isotope results for the carbonate and quartz phases from Gayna River.

Table 7. Sr isotopic data from the Gayna River deposit.

Sample	Phase	^{87}Sr/^{86}Sr	± 2σ	Total Sr (Volts)
06F001	calcite	0.7105	0.0002	1.04
06F001	calcite	0.7115	0.0002	1.05
06F001	calcite	0.7095	0.0002	0.79
06F001	calcite	0.7103	0.0002	0.94
A30 378	grey dolomite	0.7110	0.0002	0.60
A30 378	grey dolomite	0.7105	0.0003	0.51
A30 378	host	0.7303	0.0017	0.47
A30 378	host	0.7113	0.0004	0.66
A30 378	white dolomite	0.7219	0.0001	2.90
A30 378	white dolomite	0.7131	0.0002	0.84
A30 378	white dolomite	0.7122	0.0002	0.84
A30 453	calcite	0.7099	0.0002	0.93
A30 453	calcite	0.7118	0.0002	1.97
A30 453	calcite	0.7114	0.0001	2.03
A30 453	grey dolomite	0.7091	0.0002	0.79
A30 453	grey dolomite	0.7100	0.0002	0.71
A30 453	host	0.7174	0.0004	1.44
A30 453	host	0.7157	0.0004	1.25
A33 68	grey dolomite	0.7095	0.0004	0.29
A33 68	grey dolomite	0.7087	0.0005	0.26
A33 68	host	0.7102	0.0002	0.88
A33 68	host	0.7164	0.0005	0.58
A33 68	host	0.7172	0.0006	0.47
A33 68	host	0.7107	0.0003	0.56
A33 68	white dolomite	0.7093	0.0004	0.31
A33 68	white dolomite	0.7084	0.0004	0.32
A34 457	grey dolomite	0.7129	0.0002	0.80
A34 457	host	0.7120	0.0002	0.93
A34 457	host	0.7122	0.0002	0.90
A34 457	host	0.7118	0.0001	0.98
A34 457	white dolomite	0.7131	0.0002	0.95
A34 457	white dolomite	0.7131	0.0002	0.77
A35 346	calcite	0.7126	0.0001	3.67
A35 346	calcite	0.7145	0.0002	2.98
A35 346	calcite	0.7148	0.0001	3.27
B28 212	grey dolomite	0.7104	0.0003	0.38
B28 212	grey dolomite	0.7117	0.0003	0.40
B28 212	host	0.7196	0.0006	1.01
B28 212	host	0.7143	0.0003	0.88
B28 212	white dolomite	0.7107	0.0003	0.40
B28 212	white dolomite	0.7106	0.0003	0.40

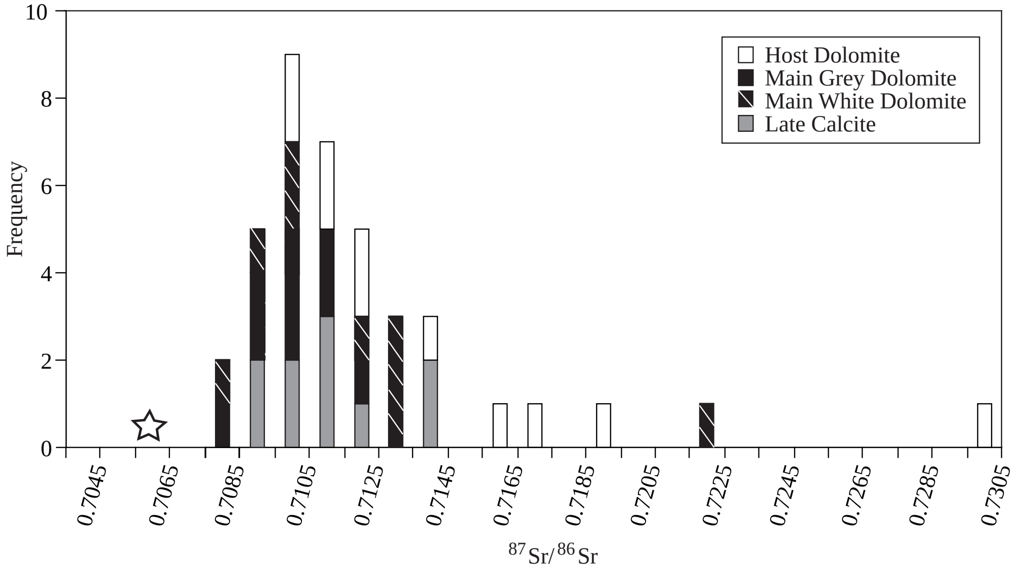

Figure 20. The laser-ablation Sr isotope data for the Gayna River carbonate samples. The star indicates the seawater Sr ratio when the Little Dal Group was deposited (Halverson et al., 2007).

Chapter 4
Discussion

4.1 Composition of the Host Carbonate

The host carbonate was not a major focus of the geochemistry study, and only C, O, and Sr isotopic ratios were obtained for this phase. The C and O values for the host dolomite, ranging from 1.5 to 4.6‰ (VPDB) and 22.1 to 27.2‰ (VSMOW) respectively, are similar to values for other early Neoproterozoic carbonates which are not associated with glaciations (e.g. Jacobsen and Kaufman, 1999; Walter et al., 2000; Lindsay et al., 2005).

The host dolostone samples have high $^{87}Sr/^{86}Sr$ ratios, ranging form 0.7102 to 0.7303. The seawater $^{87}Sr/^{86}Sr$ ratio when the Little Dal Group was deposited was ~0.7055 to 0.7063 (Halverson et al., 2007) and reached a maximum $^{87}Sr/^{86}Sr$ ratio of ~0.7091 during the Late Cambrian-Early Ordovician (Burke et al., 1982). Therefore, the high $^{87}Sr/^{86}Sr$ ratios seen for the Gayna River host rocks must originate from some other source. The radiogenic Sr could have been introduced during dolomitization of the host rocks. However, the C and O isotope values correspond well with other Neoproterozoic carbonate rocks and the original depositional features are well preserved in the host rocks suggesting that extensive fluid alteration did not take place. Additionally, the host rock $^{87}Sr/^{86}Sr$ ratios are higher than in the main and late ore stage carbonates (see section 4.3.2) indicating that they are not a result of the same fluid event.

There may be impurities in the host carbonate with high Rb concentrations, such as clay minerals, which can significantly affect $^{87}Sr/^{86}Sr$ ratios (Banner, 1995). This is supported by the petrographic study which identified clays and other insoluble material within the host carbonate often as wisps, stylolites, or very small inclusions. In addition, the measured net ion signals for ^{87}Rb and ^{85}Rb are 100 to 1000 times greater for the host carbonate than the other carbonate phases (see Appendix 6). Therefore, the high $^{87}Sr/^{86}Sr$ ratios seen in the host carbonate rocks are likely not initial ratios and are a result of Rb containing phases included in the rocks during deposition and will not be discussed further.

4.2 Genesis of the Early Ore Stage Minerals

Fluid inclusion data from the early ore stage minerals suggest that they formed from a warm, moderately saline fluid. Both the salinity and temperature have a wide range, with salinities from 14.2 to 26.6 wt% NaCl equivalent and temperatures from 107 to 214°C. The origins of the brines in the system are unknown. The brines could have been formed by the dissolution of halite bearing evaporite sequences, possibly by meteoric water. The Little Dal Gypsum unit does not contain a significant halite component and there are no other local evaporite sequences which could be invoked as a halite source, although salt casts have been very rarely observed in the Little Dal

Group (Hardy, 1979). Yet, the mineralizing fluids may have encountered a halite source at any point in the fluid migration history. Equally, the high salinities could be the result of brine generation by sub-aerial evaporation of seawater. Such brines have been implicated in the formation of many other carbonate-hosted systems, such as the Irish midlands, the United States Mississippi Valley, and the Pine Point districts (Viets et al., 1996; Banks et al., 2002; Gleeson and Turner, 2007).

There are no available data to place any time constraints on the early ore stage mineralization. The wide range of homogenization temperatures with no corresponding changes in fluid salinity, may suggest that the mineralization could have formed from a single fluid which cooled over some unknown period of time.

The early ore stage pyrite and sphalerite S isotope values range from -5 to 5‰. If the mean homogenization temperature for the early ore stage sphalerites (164°C) is used, along with the fractionation equations from Sakai (1968) and Li and Liu (2006), then the isotopic compostion of sulphate in equilibrium with the early ore stage sulphides can be calculated. The resulting calculated range, ~24 to 32‰, corresponds to the isotopic composition of Neoproterozoic-Ordovician time seawater sulphate (Sheilds et al., 2004), suggesting that the isotopic data generated in this study could be explained by the reduction of seawater sulphate. Alternatively, the early sulphide $\delta^{34}S$ values may reflect remobilization of the diagenetic pyrite in the host carbonate (Ohmoto et al., 1990). There is textural evidence that dissolution of the host rock occurred during mineralization and the dissolution of diagenetic pyrite would provide a limited sulphide source which is consistent with the small amount of mineralization seen during the early ore phase. In summary, in the early ore stage, the data suggest a warm saline brine carrying metals precipitated sphalerite when it encountered sulphide from either reduced Neoproterozoic-Ordovician age seawater or the dissolution of diagenetic pyrite.

4.3 Genesis of the Main Ore Stage Minerals

The fluid inclusion results indicate that the main ore stage mineralization was formed by a relatively high temperature, high salinity brine. The salinity of the mineralizing fluid(s) is variable but most fluid inclusion salinities are between 23 and 27 wt% NaCl equivalent. The fluid inclusion homogenization temperatures vary widely for all main ore stage phases.

The main ore stage sphalerite fluid inclusions suggest that mixing occurred in the main ore stage (Figure 16). The main ore stage sphalerite fluid inclusions have one end member, ~170°C and ~15 wt% NaCl equiv., which is comparable to the early ore stage sphalerite fluid inclusions which have a modal salinity around 15 wt% NaCl equivalent with a wide range of homogenization temperatures. The main ore stage sphalerite fluid inclusions range to a higher temperature and salinity cluster, ~210°C and ~34 wt% NaCl equivalent. This distribution can be explained by mixing between a lower temperature and salinity fluid and a higher temperature and salinity fluid in the main stage. The higher temperature and salinity fluid may have displaced the early ore fluid resulting in some mixing of these two fluids.

However, this is not convincing over the whole dataset: the main stage dolomite and quartz fluid inclusions have a wide distribution of temperatures and salinities which do not define a mixing trend.

The mean $\delta^{18}O$ values decrease throughout the main stage from 25 to 21‰ (VSMOW). The main stage quartz samples have $\delta^{18}O$ values similar to the white dolomite (Figure 19). To determine if these observations are a result of equilibrium fractionation the fluid inclusion homogenization data were used to calculate the isotopic composition of the mineralizing fluids. Most of the calculations used fluid inclusion homogenization temperatures from the same paragenetic phase. For the samples that had no available microthermometric data, estimates from other minerals in the same paragenetic stage were used.

The O isotopic compositions of the mineralizing fluids in carbonate samples were calculated using the fractionation equation for dolomite → H_2O proposed by Zheng (1999) and the mineralizing fluid compositions of the quartz samples were calculated using the fractionation equation proposed by Zheng (1993). These equations were chosen because the experimental data span the temperature range of Gayna River samples. The mineralizing fluid composition results are displayed in Figure 21 and reported below.

The grey dolomite samples have calculated fluid $\delta^{18}O$ values of 10.9 to 15.0‰ (VSMOW) with a mean of 13.0‰. The white dolomite samples have fluid $\delta^{18}O$ values of 6.8 to 11.8‰ (VSMOW) with a mean of 8.9‰. The main stage quartz samples have fluid $\delta^{18}O$ values of 8.6 to 10.6‰ (VSMOW) with a mean of 9.3‰. As for the early ore stage, the origins of the brines in the system are unknown. As previously discussed, brine formation by the dissolution of halite-bearing evaporite sequences is possible or the high salinities may be a result of brine generation by sub-aerial evaporation of seawater. The O isotopes have higher values than expected for meteoric fluids and seawater and instead have compositions that have been strongly affected by water-rock interaction. The main ore stage fluid has higher $\delta^{18}O$ values than the late ore stage fluid. This may be because the main ore stage fluid is hotter and thus may have undergone more extensive isotopic exchange with country rocks. The amount of water rock interaction is unknown and so the isotopes do not help to constrain whether the mineralizing fluids originated as evaporated seawater or by dissolution of halite by meteoric water (Taylor, 1997).

The mean $\delta^{13}C$ values decrease throughout the stage from 2.8 to 1.4‰ (VPDB). The isotopic compositions of the mineralizing fluids were calculated using the methods described above for O. For the C isotopes the mineralizing fluid compositions were calculated using the fractionation equation for dolomite → CO_2 proposed by Ohmoto and Rye (1979). CO_2 was selected as the parent species based on the evidence for thermochemical sulphate reduction (see section 4.3.1) and the proposed equations for this reaction (e.g. Orr, 1982; Machel et al., 1995; Thom and Anderson, 2008). The mineralizing fluid composition results are displayed in Figure 21. The grey dolomite samples have mineralizing fluid $\delta^{13}C$ values of 3.2 to 6.2‰ (VPDB) with a mean of 4.8‰. The white dolomite samples have mineralizing fluid $\delta^{13}C$ values of 2.0 to 4.8‰ (VPDB) with a mean of 3.1‰.

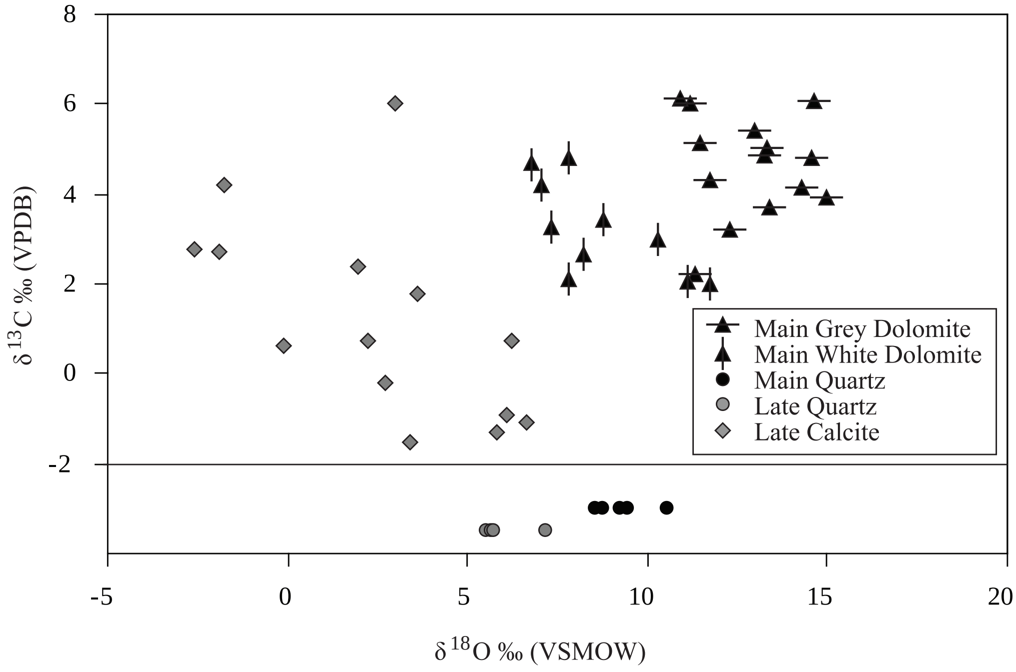

Figure 21. The mineralizing fluid compositions for the carbonate and quartz phases from Gayna River. See section 4.3 for calculation methods.

In general, the $\delta^{18}O$ and $\delta^{13}C$ compositions of the mineralizing fluids get progressively enriched in the lighter isotopes throughout the paragenesis (Figure 21). There are two possibilities for the difference in isotopic composition between the grey and white dolomite phases. One is that they were formed by two different fluids that had different initial isotopic compositions. This is unlikely due to the overlapping temporal and spatial relationships between these phases and the fluid inclusion data which indicate these phases both formed at the same temperature and from a fluid with the same salinity. There is petrographic evidence that the fluid precipitating the grey dolomite caused dissolution of the host dolostone. This supports an interpretation whereby both dolomite phases were formed by one fluid with an isotopic composition similar to the white dolomite mineralizing fluid, and the grey dolomite was formed by the same fluid but also has a contribution of material though recystallization or local dissolution and reprecipitation of the host dolostone. The main ore stage quartz mineralizing fluid $\delta^{18}O$ values are comparable to the white dolomite mineralizing fluid, indicating that both these phases were likely precipitated from the same fluid.

4.3.1 Evidence for thermochemical sulphate reduction

The mean main ore stage S isotopic values are 19‰ and 20‰ for galena and sphalerite, respectively. These values are significantly higher than those seen in the early ore stage sulphides and suggest that the sulphide must have originated from a different source. Isotopic data for Neoproterozoic sulphates have δ^{34}S values that range from 11.6 to 25.2‰ (CDT) (Walter et al., 2000). The Little Dal Group includes the Gypsum formation, a sequence of evaporites which is locally greater than 250 m thick in the Gayna River area (Hewton, 1982). The Gypsum formation occurs within the Silty Dolostone unit which overlies the mineralized host rock. δ^{34}S values of 13.9 to 17.7‰ (CDT) have been reported for this formation (Turner, pers. comm.), however, these are based on limited sampling. The presence of a local source of sulphate, in this case gypsum, means that sulphate reduction could have occurred near the site of ore deposition.

The reduction of sulphate to sulphide can occur via bacterial sulphate reduction (BSR) or thermochemical sulphate reduction (TSR). BSR is common in shallow, low-temperature settings and sulphate is reduced by bacteria such as *Desulfovibrio* and *Desulfotomaculum* (Postgate and Campbell, 1966). TSR is common in deeper, high temperature settings and sulphate is reduced by abiotic processes (Machel, 2001). Framboidal pyrite is typically a by-product of BSR whereas cubic or prismatic pyrite is commonly associated with TSR (Machel, 1989). Cubic pyrite is common in the samples from Gayna River and no framboidal pyrite has been observed. Fluid inclusion data from Gayna River suggest the temperatures of the system were above the BSR window of 0 to 60-80°C (Machel et al., 1995) and are higher than the 127°C lower limit of TSR (Machel, 2001). The δ^{13}C values of carbonates decrease throughout the main and late stages and the δ^{34}S values increase from the early to the main and late stages at Gayna River. δ^{13}C depletion, caused by isotopically light C being released from hydrocarbons during the reduction of sulphate, and δ^{34}S enrichment, caused by S not undergoing significant fractionation from the sulphate source when bacteria are not involved, are both further evidence of TSR (Machel et al., 1995; Machel, 2001). Finally, the presence of hydrocarbons is required for TSR because they act as the reducing agent. At the Gayna River deposit pyrobitumen is commonly the last paragenetic phase observed, indicating that at some time hydrocarbons migrated through the deposit.

Although the exact fractionation mechanism which occurs between the S isotopes in SO_4^{2-} and H_2S during TSR is unknown, Kiyosu and Krouse (1990) proposed an equation for TSR S isotope fractionation. Using this equation, with the mean fluid inclusion homogenization temperature for the main ore phase sphalerite, a fractionation of ~11‰ between SO_4^{2-} and H_2S is predicted at Gayna River. Seawater is not considered as a sulphate source because for TSR the sulphate is almost invariably derived from the dissolution of gypsum and/or anhydrite (Machel, 2001). If the sulphate source was the local gypsum with δ^{34}S values from 13.9 to 17.7‰, the corresponding sulphide δ^{34}S values would be ~ 3 to 7‰. If the isotopic compositions of other Neoproterozoic sulphates are considered (δ^{34}S values between 11.6 and 25.2‰ (CDT); Walter et al., 2000) the corresponding sulphide δ^{34}S values formed from a TSR reaction would be ~ 1 to 14‰. These values are all lower than those seen in the main ore stage sulphides from Gayna River. In some cases of TSR there is no fractionation between SO_4^{2-} and H_2S due to, for example, closed system behavior (Machel et al., 1995). Closed system TSR could account for the $\delta^{34}S$ values of 12.2 to 25.4‰ seen in the main ore stage sulphides. However, even with closed system reduction the isotopic compositions of the ore phase minerals cannot be accounted for by the current small dataset from the Little Dal Gypsum formation. This suggests that either another source of sulphate is necessary or the small amount of data from the Little Dal Gypsum is not representative of the whole formation. Either way closed system thermochemical sulphate reduction is the likely S source for the main ore stage sulphides.

4.3.2 Source of metals

The trace elements in the Gayna River sphalerites are unusual, both in the range of detected elements and the concentrations of those elements. The trace elements are similar to those found in sphalerites from other Northern Cordillera carbonate rocks in that they are enriched in Cu and Pb but depleted in Fe concentrations (McLaren and Godwin, 1979). The Ga values at Gayna River are high whereas most other carbonate-hosted zinc-lead deposits in the Mackenzie platform do not contain detectable Ga (Carrière and Sangster, 1999). However, microprobe data from sphalerites at the Prairie Creek Zn-Pb-Ag deposit to the south of Gayna River (Figure 22) have Ga values (up to 1500 ppm), that are approximately double to triple those in Gayna River sphalerites (Fraser, 1996). The source for the Ga in the hydrothermal fluids in both deposits is unknown. It is possible that both deposits share some fluid history involving a Ga rich metal source. However, the lack of Ga in the other Zn-Pb showings in the Mackenkie Platform does not support this hypothesis. The Prairie Creek deposit has three styles of mineralization: stratiform, MVT, and quartz veins which are hosted by Middle Ordovician through upper Devonian rocks. The deposit is bounded by the Prairie Creek Fault and the Gate Fault, both major reverse faults (Fraser, 1996). In comparison, the Gayna River deposit has only MVT style mineralization and is hosted by Neoproterozoic rocks. The structures present at Gayna River are the adjacent Plateau Fault and numerous minor normal and reverse faults (Figure 6). The age of the mineralization at both deposits is poorly constrained; however, at Prairie Creek the quartz vein style mineralization may be Cretaceous in age (Fraser, 1996). The lack of Ga in most deposits in the vicinity of Gayna River and the differences in the structural setting and mineralization styles between Prairie Creek and Gayna River suggest it is more likely that the Ga (and possibly other elements) are sourced locally for the deposits.

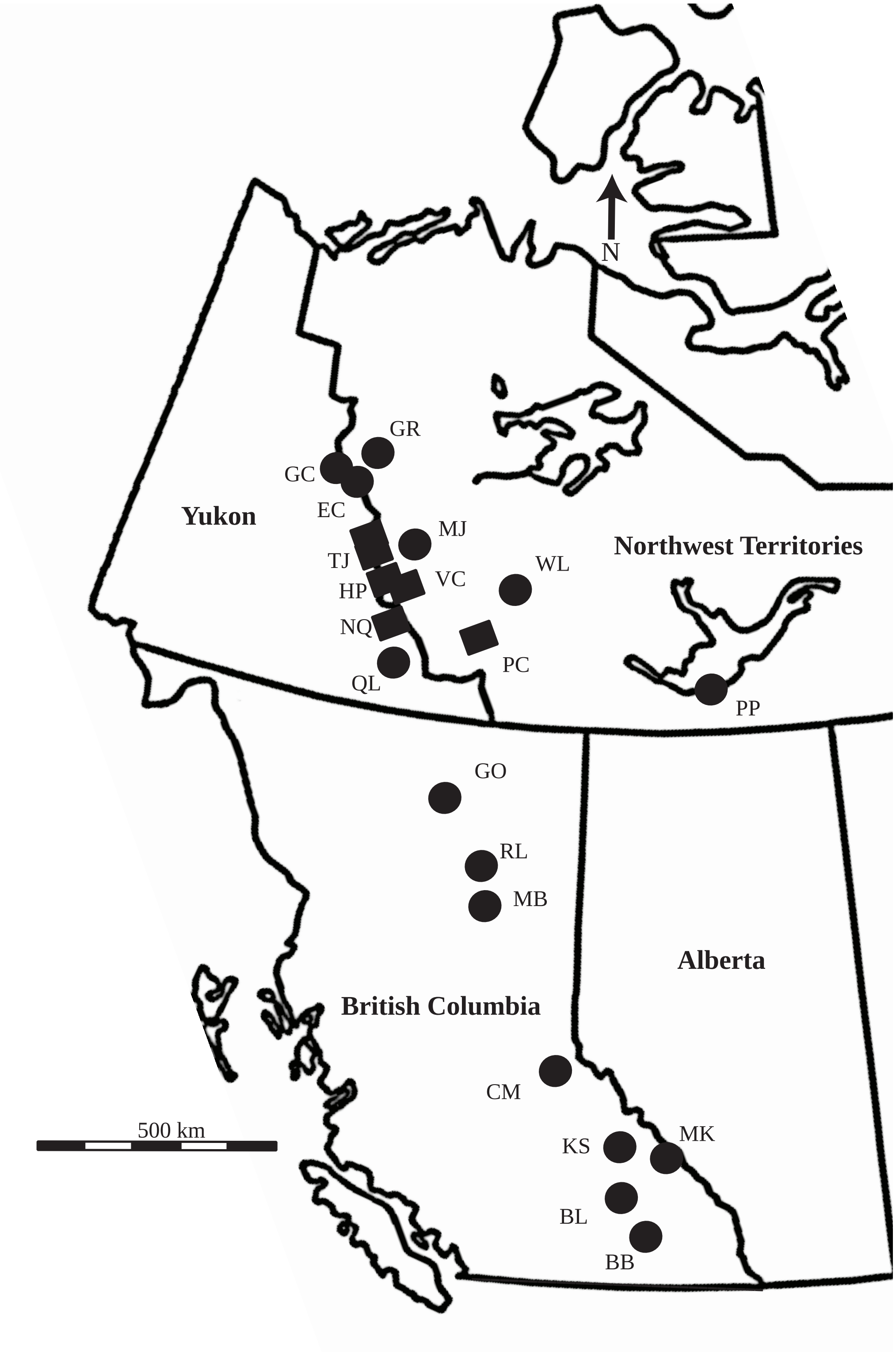

Figure 22. A location map of selected western Canadian base metal deposits. The circles are MVT style deposits and the squares are other deposit types. Abbreviation are; GR - Gayna River, GC - Goz Creek, EC - Economic, TJ - Tom/Jason, MJ - Majesty, HP - Howards Pass, VC - Vulcan, NQ - Norquest, WL - Wrigley Lou, QL - Quartz Lake, PC - Prairie Creek, PP - Pine Point, GO - Goat, RL - Robb Lake, MB - Mt. Burden, CM - Comin, KS - Keystone, BL - Big Ledge, MK - Monarch/Kicking Horse, BB - Bluebell.

The major trace elements in the sphalerite at Gayna River, Bi, Cu, Pb, As, and Ga, can be derived from shales (Viets et al., 1992). However, as far as we are aware there are no trace element data for shales in the Gayna area so identifying the exact metal source for Gayna River is not possible. Studies of the Selwyn basin shales in the vicinity of the Tom stratiform Pb-Zn-Ba deposit, to the south of Gayna River, found no significant enrichment of Fe, Mn, or Cu near the mineralized area, and Zn and Pb concentrations were lower than expected for carbonaceous shales (Large, 1981). Carrière and Sangster (1999), however, suggested that the unusual trace element compositions of sphalerites in the Gayna River region are most likely a result of fluid interaction with shales in the Selwyn Basin to the west of the deposit. Alternatively, Young et al. (1979) identified an estimated several kilometers thick package of sedimentary rocks underlying the Mackenzie Mountain Supergroup containing shales, which is also a plausible source of metals at Gayna River. It is also possible, considering evidence that the metals may have had a local source, that trace elements were sourced from the Little Dal Group Dead End Shale unit. The 180 m thick Dead End Shale unit sits ~ 150 m below the base of the Host units (Figure 6).

The source of metals for the deposit may be further elucidated by the Sr isotopic data from the ore stage carbonates. The main ore stage dolomites have $^{87}Sr/^{86}Sr$ ratios ranging from 0.7084 to 0.7219. At the time of the Little Dal Group deposition the seawater $^{87}Sr/^{86}Sr$ ratio was ~0.7055 to 0.7063 (Halverson et al., 2007) and seawater reached a maximum $^{87}Sr/^{86}Sr$ ratio of ~0.7091 during the Late Cambrian-Early Ordovician (Burke et al., 1982). This suggests there must be another source of radiogenic Sr present to produce the higher ratios seen in the main ore stage carbonates at Gayna River. Possible sources of high $^{87}Sr/^{86}Sr$ ratios include; crystalline basement rocks, igneous rocks, and clastic sediments (e.g. Morrow et al., 1990; Mountjoy et al., 1992). There is no evidence to support interaction with crystalline basement or igneous rocks. Fluids would have to be derived from depths of > 10 km (Young et al., 1979) to have interacted with basement rocks and fluid inclusion temperatures do not indicate mineralizing fluids reached such depths. Intrusive rocks have not been identified in the Gayna River region (Figure 2). Shales have been shown to contribute high $^{87}Sr/^{86}Sr$ ratios in other systems. In the Western Canada Sedimentary Basin, Machel and Cavell (1999) defined a maximum Sr isotope ratio of basinal shale of 0.7120, which is thought to be valid for rocks from the base of the Cambrian to the Pleistocene in age. Many of the $^{87}Sr/^{86}Sr$ ratios from Gayna are higher than this value which suggests that the source of the high $^{87}Sr/^{86}Sr$ ratios at Gayna River could be older shale packages, such as those that underlie the Gayna River deposit. As mentioned above, the Little Dal Group includes the Dead End Shales which may be the source of metals and trace elements at Gayna River, equally, the metal source may be located in the thick package of rocks (including shales) underlying the Mackenzie Mountain Supergroup which is unnamed as it is not exposed in the Mackenzie Mountains. Therefore, the data suggest that the metals at Gayna are likely to be derived from either the Dead End Shales or the thick shale packages underlying the Gayna River deposit.

4.4 Genesis of the Late Ore Stage Minerals

The lower salinities and homogenization temperatures seen in the late ore stage fluid inclusions provide evidence for a third fluid in the system. These inclusions have a mean salinity of 17.4 wt% NaCl equivalent and the temperatures decrease throughout the stage from a mean of 145°C for late quartz to a mean of 117°C for late calcite. A broad mixing line from a higher temperature fluid (~170°C and ~17 wt% NaCl equivalent) to a lower temperature fluid (~60°C and ~17 wt% NaCl equivalent) is defined in Figure 16.

The $\delta^{18}O$ values for the late stage samples are similar to the main stage, with means of 22 and 19‰ (VSMOW) for quartz and calcite respectively. The fluid inclusion homogenization data were used to calculate the isotopic composition of the mineralizing fluids to determine if these observations are a result of temperature dependent fractionation. As above, the mineralizing fluid compositions for the O isotopes in carbonate samples were calculated using the fractionation equation for calcite → H_2O proposed by Zheng (1999) and the mineralizing fluid compositions of the quartz samples were calculated using the fractionation equation proposed by Zheng (1993). The late stage quartz samples have mineralizing fluid $\delta^{18}O$ values of 5.6 to 7.2‰ (VSMOW) with a mean of 6.0‰ (Figure 21). The late calcite samples have mineralizing fluid $\delta^{18}O$ values of -2.6 to 6.6‰ (VSMOW) with a mean of 2.5‰. The late ore stage quartz mineralizing fluid $\delta^{18}O$ values overlap the calcite mineralizing fluid, indicating these phases were likely precipitated from similar fluids. The origin of the salinities of the late ore stage fluid, as discussed for the early and main stages, are unknown but are most likely a result of either brine formation by the dissolution of halite-bearing evaporite sequences or brine generation by sub-aerial evaporation of seawater (Viets et al., 1996; Banks et al., 2002; Gleeson and Turner, 2007). The late calcite $\delta^{18}O$ values are somewhat depleted which may indicate a meteoric water component in the late ore stage fluid (Taylor, 1997).

The $\delta^{13}C$ values for the late ore stage range from -4.3 to 3.0‰ (VPDB). The isotopic compositions of the mineralizing fluids were determined using the methods described above. The mineralizing fluid compositions were again calculated using the fractionation equation for calcite → CO_2 proposed by Ohmoto and Rye (1979). The late calcite samples have mineralizing fluid $\delta^{13}C$ values of -1.5 to 6.0‰ (VPDB) with a mean of 1.2‰ (Figure 21).

The late calcite phase mineralizing fluid has the isotopically lightest C for most samples, supporting the previous argument for TSR involving hydrocarbons. TSR can release light C isotopes into carbonate reservoirs (Krouse et al. 1988) resulting in lower $\delta^{13}C$ values in carbonate hosted deposits (Huizenga et al. 2006). Pyrobitumen occurs in the late stage of the Gayna River deposit confirming hydrocarbons were present and oxidation of these could be the cause of the lower $\delta^{13}C$ values of the late calcite mineralizing fluid. The late ore stage quartz mineralizing fluid $\delta^{18}O$ values match the calcite mineralizing fluid, indicating these phases were likely precipitated from the same fluid.

4.4.1 Origin of Sulphide

The $\delta^{34}S$ values for the late pyrite (mean of 17‰) are slightly lower than those of the main stage sulphides. The highest local gypsum $\delta^{34}S$ value (Gypsum Formation), 17.7‰ (Turner, pers.comm.), is comparable with the mean late ore stage sulphide value (17‰). Based on the discussion of S fractionation for the main ore stage, closed system thermochemical sulphate reduction of local gypsum is a plausible S source for the late ore stage sulphides.

4.4.2 Source of metals

The late ore stage calcite has $^{87}Sr/^{86}Sr$ ratios, 0.7095 to 0.7148, within the range of the main ore stage values. This suggests that the late ore stage has a similar metal source to the main ore stage. Thus, the Dead End Shales or the thick shale packages underlying the Gayna River deposit, enriched in radiogenic Sr in addition to metals, are a likely metal source for the late ore stage as well.

4.5 Link between Sphalerite Colour, trace elements, and $\delta^{34}S$ values

Several studies have linked dark colours in sphalerite to high Fe content (Roedder and Dwornik, 1968). The sphalerites at Gayna River have very low Fe content and occur in a wide range of colours. The lack of Fe in these sphalerites would suggest they should be very light in colour; however, the range of colours suggests there must be other trace elements occupying colour centers. Sphalerites observed in Northern Arkansas, Tri-State, and Central Missouri MVT deposits all had higher Ga and Cu concentrations in orange and red/orange sphalerites than in pale, green, or brown sphalerites (Viets et al., 1992). High Ga and Cu concentrations combined with very low Fe concentrations may be responsible for the bright colours seen at Gayna River. The mineral gallite ($CuGaS_2$) has the same crystal structure as sphalerite with Cu replacing half of the Zn positions and Ga replacing the other half (Sheka et al., 1966). The correlation between Ga and Cu and the relatively high concentration of these elements in the sphalerite at Gayna River is likely from substitution of Ga and Cu into Zn sites in the sphalerite crystal lattice.

At Gayna River there appears to be a broad correlation between $\delta^{34}S$ values and sphalerite colour; low $\delta^{34}S$ values are seen in pale coloured sphalerite, moderate $\delta^{34}S$ values are seen in dark red and orange coloured sphalerite, moderate to high $\delta^{34}S$ values are seen in bright orange coloured sphalerite, and high $\delta^{34}S$ values are seen in brown coloured sphalerite (Figure 18). Tiegeng and Lin (1995) found a similar correlation between $\delta^{34}S$ values in sphalerite and colour in a similar study of sphalerites from the Huxu Zn-Pb Deposit, China. They report of low $\delta^{34}S$ values in light coloured sphalerites (including pale reds and yellows), medium coloured sphalerites (including red and yellow tints) had moderate $\delta^{34}S$ values, and high $\delta^{34}S$

values were measured in dark coloured sphalerites (including black, purple, and dark brown). They also showed that $\delta^{34}S$ values were negatively correlated with Zn and Ni content and positively correlated with Pb, Cu, Ag, and Au content and therefore, suggested there was a link between colour, sulphur isotope composition and trace element content (Tiegeng and Lin,1995). At Gayna River, high Ga concentrations are correlated with high Cu concentrations and these are predominately seen in intense red and orange coloured sphalerite (Figures 10 and 11). The concentration of the 17 measured trace elements is variable within single crystals and due to the difference in scale of the isotopic study (100 μg separates) and the electron microprobe data, confirmation of a correlation between trace element composition and sulphur isotope composition was impossible.

In general, at Gayna River the $\delta^{34}S$ values increase over time and the colour of the sphalerites becomes progressively darker with this increase. For the early ore stage sphalerite the lower $\delta^{34}S$ values have been explained by the recycling of S from diagenetic pyrite or reduction of contemporaneous seawater. The lighter colours in the early ore stage may indicate lower Pb, Cu, Ga and Ag contents in the metal bearing fluid. The main ore stage sphalerite fluid inclusions show evidence of fluid mixing. The multiple main ore stage fluids may have had different trace element contents, leading to different colours of sphalerite over time as the relative proportions of these fluids changed. Concurrently, if Rayleigh fractionation is taken into account as sulphate was reduced to sulphide, the $\delta^{34}S$ values in the sphalerite would increase over time. Combined these factors may provide an explanation for why $\delta^{34}S$ values appear to be higher in darker coloured sphalerite. Alternately, a main control on the sulphur isotopes and sphalerite colour in the main ore stage may have been oxygen fugacity. When oxidizing fluids are dominant, the $\delta^{34}S$ values of sulphides are lower and Fe is in the oxidized form of Fe^{3+} which does not substitute easily for Zn^{2+} in the sphalerite crystal lattice (Rye and Ohmoto, 1974). These conditions would result in the observed lower $\delta^{34}S$ values for moderately coloured sphalerites. Later, if more reducing conditions (indicated by the presence of hydrocarbons) occurred, the $\delta^{34}S$ values would be higher and more Fe would be in the reduced form of Fe^{2+} which can substitute more easily for Zn^{2+} producing darker sphalerites.

4.6 Age constraints for the Gayna River Deposit

The mineralization at Gayna River is hosted by Neoproterozoic rocks and this has been interpreted as suggesting that the deposit may be Neoproterozoic in age (e.g. Hardy, 1979; Hewton, 1982). The homogenous $^{207}Pb/^{204}Pb$ isotopic composition of the galena and sphalerite data means that it difficult to extract any meaningful age information. Isochron regressions using the program Isoplot (Ludwig, 2003) yielded Pb-Pb ages of 1555 ± 660 Ma with the Stacey and Kramer (1975) growth curve intercepts at 171 and 1455 Ma (2σ, MSWD=0.34, Model 1) for the galena samples and 2158 ± 1000 Ma with growth curve intercepts at 136 and 2095 Ma (2σ, MSWD=3.4, Model 2) for the galena and sphalerite samples (Figure 23). The large errors associated with these ages, due to the clustered nature of these data, mean that these ages are essentially meaningless.

The "shale curve" of Godwin and Sinclair (1982) is often used to model the evolution of Pb in the SEDEX deposits of the Selwyn basin. Previous workers have used this curve to suggest the age of the mineralization at Gayna River is Devono-Mississippian (Dewing et al., 2006), since the Gayna River deposit may share the same Pb source as the SEDEX systems. Lead isotope data from various Canadian deposits in the vicinity of Gayna River (Figure 22) are shown in Figure 24. The Gayna River Pb ratios are most similar to the SEDEX type deposits (Tom, Jason, Vulcan, and Howards Pass); however, there is a greater range in ^{206}Pb/^{204}Pb values for the Gayna River samples than for the SEDEX deposits. The Kicking Horse and Monarch, Economic, and Goat Zn-Pb deposits have lead in the same ^{206}Pb/^{204}Pb range as Gayna River but, similarly to the SEDEX deposits, these deposits have ^{207}Pb/^{204}Pb values which range to higher values and data which lie in distinct linear arrays, whereas at Gayna River the data do not form a linear array. Other major Western Canada carbonate hosted Zn-Pb deposits, such as Pine Point and Robb Lake, have significantly different Pb isotope signatures and likely have no genetic relationship to Gayna River.

If the data from this study for Gayna River are plotted on the Godwin and Sinclair (1982) shale curve (Figure 23), the distribution suggests there must have been mixing of an older and a younger Pb source. The least radiogenic Pb results correspond to lower Cambrian deposits in the area such as Goz Creek and Economic (Godwin et al., 1982). The majority of samples correspond to the Devono-Mississippian age proposed for the Selwyn Basin SEDEX deposits, and as these deposits have similar ^{206}Pb/^{204}Pb values to Gayna River (Figure 24), it is possible that one of the fluids carrying Pb to Gayna River shared a Pb source with these Devono-Mississippian deposits. The most radiogenic Pb results correspond to a Tertiary age which may be related to the Laramide orogeny. These Pb isotope data do not support a Neoproterozoic or Lower Paleozoic age as suggested previously (Hardy, 1979; Kesler and Reich, 2006; Dewing, et al., 2006) and there is a strong case for mixing of several Pb sources.

Rhenium-Os dating was carried out on the pyrobitumen found as the latest paragenetic phase at Gayna River. When plotted on an isochron diagram, the Re and Os isotopic data did not fall on a single isochron. The data fit reasonably onto two possible isochrons (Figure 25) with 4 samples in one grouping and 4 samples in the other (with one datum included in both groups). Regression of these two data groups using the program Isoplot (Ludwig, 2003) with λ^{187}Re of 0.666e^{-11}yr^{-1} (Smoliar et al., 1996), yield Re-Os ages of 14 ± 7 Ma with an initial ^{187}Os/^{188}Os ratio of 1.2 ± 0.1 (2σ, MSWD=13, Model 3) and 24 ± 2 Ma with an initial ^{187}Os/^{188}Os ratio of 0.75 ± 0.05 (2σ, MSWD = 1.9, Model 1) respectively.

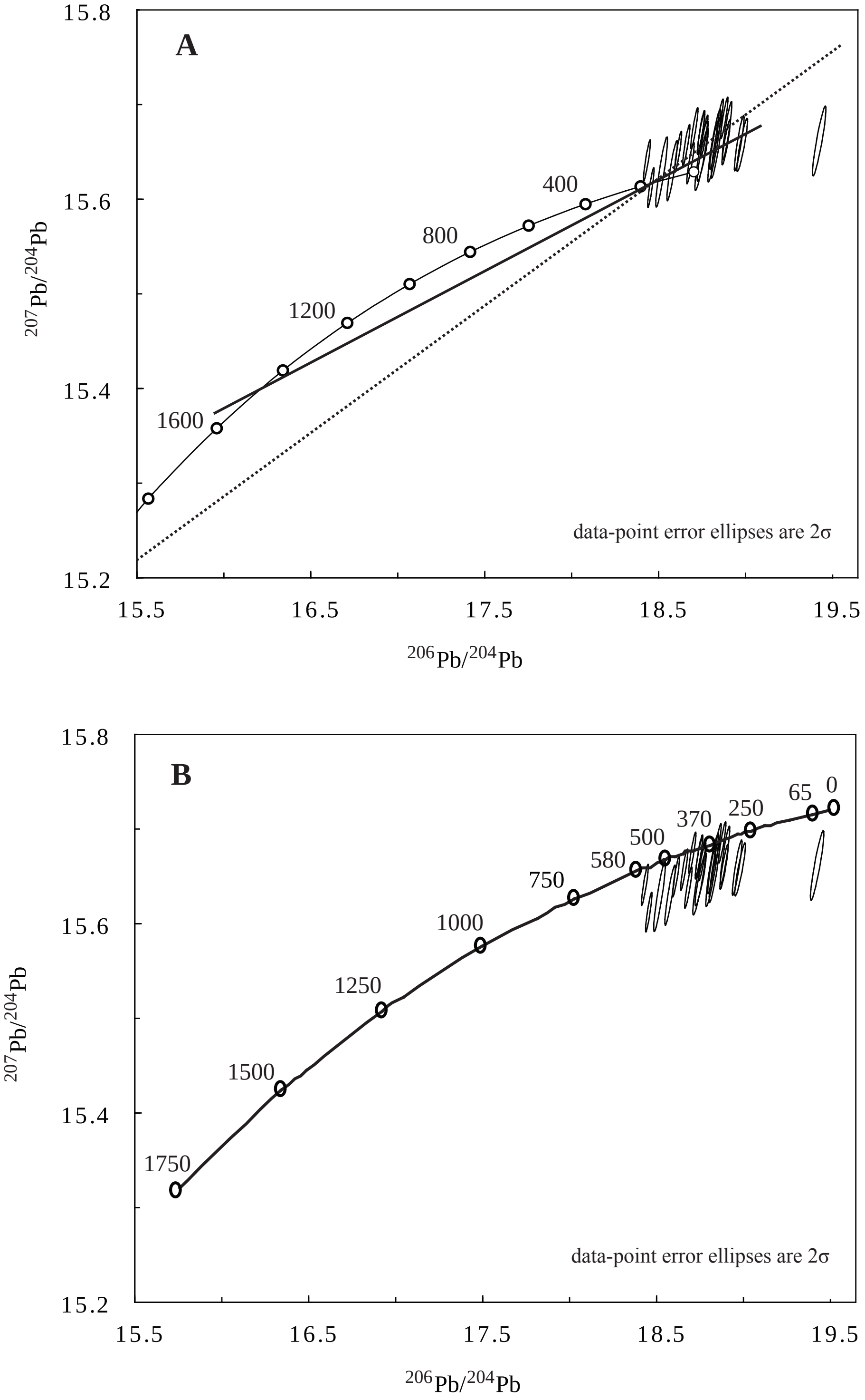

Figure 23. The lead isotope data for Gayna River sphalerite and galena samples (this study) with additional lead isotope data from galena (Sharp, 2004) plotted on (A) the lead growth curve of Stacey and Kramer (1975) with ages in Ma and isochrons for galena samples only (solid line) and all samples (dashed line), and (B) the 'shale curve' of Godwin and Sinclair (1982) with ages in Ma. See section 4.6 of text for disscussion of isochrons.

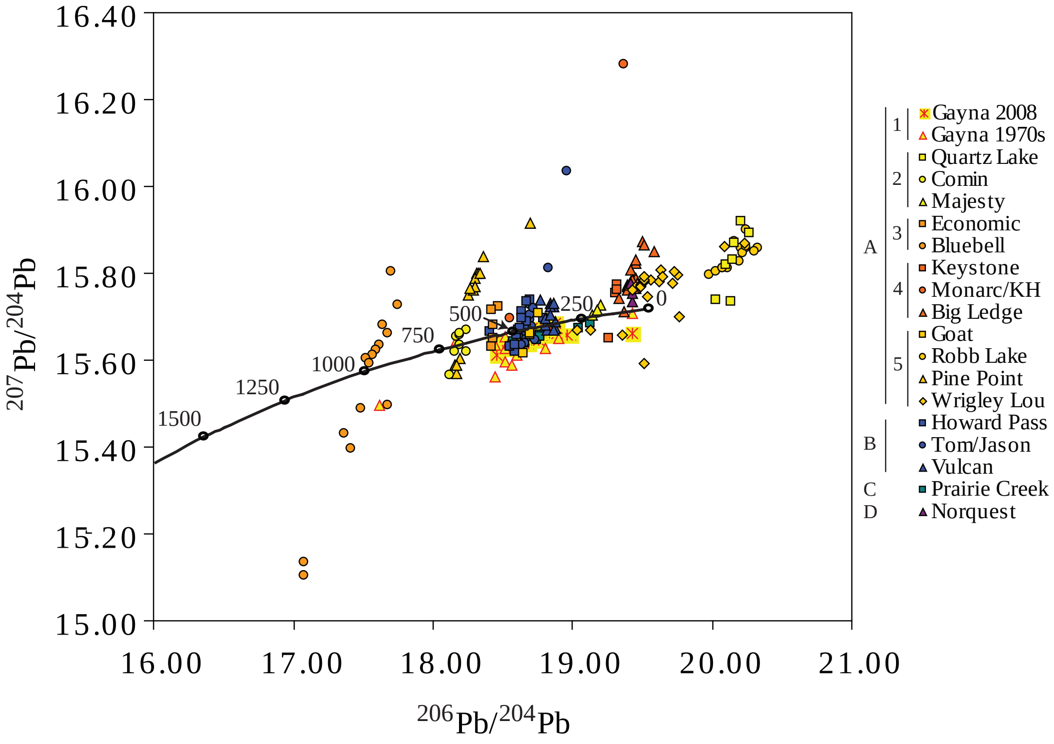

Figure 24. The lead isotope data from selected deposits in the Foreland Belt and Selwyn Basin areas. A - Stratabound deposits of host rock age 1. Helikian 2. Hadrynian 3. Cambrian 4. general Paleozoic 5. Devonian. B - Sedex deposits. C - Stratform, stratabound, and vein type deposit. D - Skarn deposit. The data are from Godwin et al. (1988) for all deposits except Gayna 2008 (this study) and Prairie Creek (Fraser, 1996). The "shale curve" of Godwin and Sinclair (1982) is shown with ages in Ma.

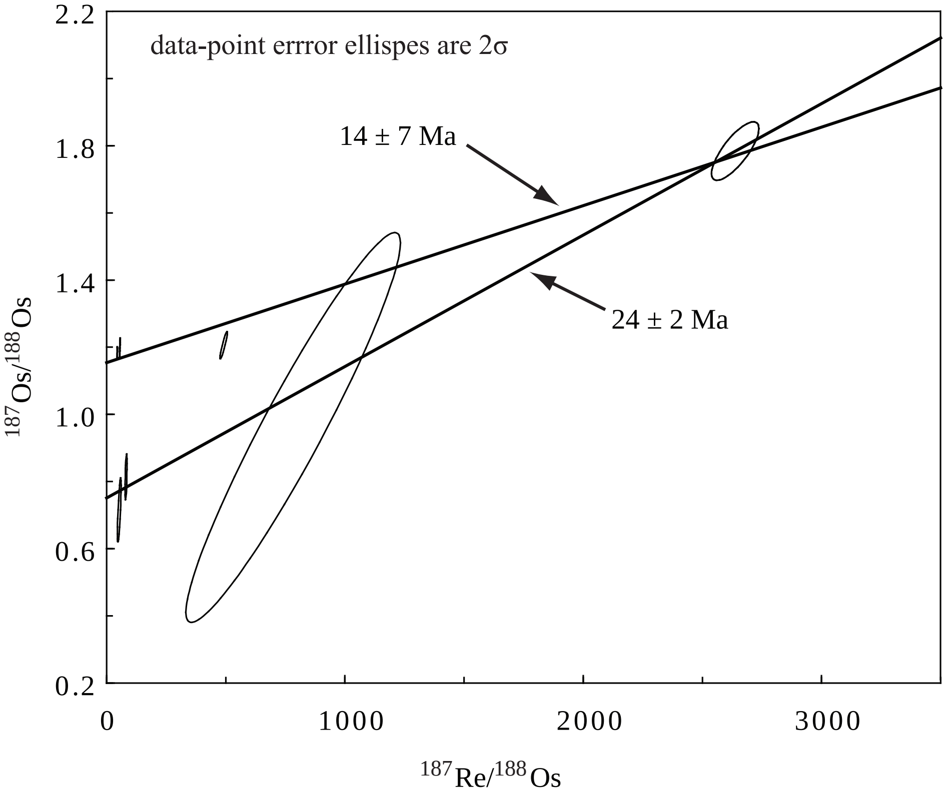

Figure 25. The Re/Os isotope data for Gayna River pyrobitumen samples. The two possible ages were determined using Isoplot (Ludwig, 2003).

The lack of fit on a single Re/Os isochron for the Gayna River pyrobitumen samples may suggest either that the samples did not form at the same time, that the samples had different initial ^{187}Os/^{188}Os ratio, and/or that the samples have lost or gained Re and/or Os since formation (Dickin, 1995). Although all the samples analyzed in this study occur late in the paragenesis it cannot be demonstrated that all the pyrobitumen was emplaced in a single flow event. Equally, the initial Os composition of the hydrocarbons could vary as a result of inhomogeneities in a large source region, different source rocks and/or fluid pulses. The likelihood of the extremely young age proposed for the pyrobitumen being the result of isotopic resetting must also be addressed. Selby et al. (2007) found that the process of biodegradation does not have a great effect on Re-Os isotopic systematics because the Re and Os are primarily associated with the heavy fractions of oils which are not destroyed during biodegradation. Additionally, Re and Os mobility have been shown to be positively correlated with C_{org} (Peucker-Ehrenbrink and Hannigan, 2000; Jaffe et al., 2002). If this is the case, then surficial weathering of pyrobitumen, composed of C_{org}, should not affect the Re-Os systematics. As well, a study of shale weathering by Jaffe et al. (2002) indicated that weathered samples had low ^{187}Re/^{188}Os ratios. At Gayna River the ^{187}Re/^{188}Os ratios are moderate to high, and if the lowest ^{187}Re/^{188}Os ratios are excluded from the isochron, the calculated age is not significantly different. As a result it does not appear that Re and Os were reset and we consider a Tertiary age for the hydrocarbon emplacement at Gayna River to be plausible.

The initial ^{187}Os/^{188}Os ratio of a system can be used to delineate the nature of the source petroleum reservoir (e.g., Selby and Creaser, 2005). Using the typical ingrowth trajectory for average organic-rich sediments (Ravizza et al. 1998) and the marine Os isotope record presented by Peuker-Ehrenbrink and Ravizza (2000) the oldest possible source rocks which could result in the initial ^{187}Os/^{188}Os ratios seen in this study (0.75 and 1.2) are late Cretaceous and mid-late Cretaceous in age respectively. This suggests that in either case the pyrobitumen at Gayna River is sourced from petroleum that is late Cretaceous or younger in age.

The Keel Tectonic Zone (KTZ), located within several hundred kilometers of the Gayna River deposit, has been investigated as a potential hydrocarbon source area (Issler et al., 2005). The maximum burial for the KTZ was during the Cenozoic and the maximum temperatures were reached during the Devonian and Early Cretaceous. The maximum burial in this area may have initiated hydrocarbon migration to Gayna River during the Cenozoic. In total therefore, the Pb-Pb and Re-Os isotopic data suggest that the Gayna River deposit may have formed at some time between the Cretaceous to Tertiary and is likely not of Neoproterozoic age.

4.7 Deposit Classification, Comparison, and Genesis

The Gayna River deposit has been classified as a Mississippi Valley Type deposit in several studies (e.g. Hardy, 1979; Hewton, 1982; Kesler and Reich, 2006) on the basis of mineralogy, ore textures, and the epigenetic nature of the mineralization. However, the high temperatures of the mineralizing fluids and quartz and barite have led some workers to challenge this classification (Dewing et al., 2006) and argue that Gayna River and other Zn-Pb showings in the Mackenzie Mountains may in fact be better classified with Irish-style, polymetallic vein or SEDEX deposits. The Tom and Jason SEDEX deposits, located to the south of the Gayna River deposit (Figure 22) and hosted by Devonian clastic rocks, have similar Pb isotopes to Gayna River. However, a fluid inclusion study shows that the ore-forming fluids at these deposits had ~ 9 wt% NaCl equivalent salinity and a temperature of ~250°C (Gardner and Hutcheon, 1985; Ansdell et al., 1989), which is completely different from those seen at Gayna River. Thus, the Tom/Jason deposits may possibly share a Pb source with Gayna River but the mineralizing fluids are not related.

The fluid inclusion temperatures at Gayna River are higher than typical for many MVT deposits, but are comparable with carbonate hosted deposits such as those of the Irish Midlands and Gays River (Banks and Russell, 1992; Chi and Savard, 1995; Samson and Russell, 1987). In all other respects, this study finds that the Gayna River deposit clearly fits within the Mississippi Valley Type (MVT) definition. This deposit is epigenetic, stratabound, and hosted by carbonate rocks. Mineralization occurs mainly as open-space filling, collapse breccias and replacement of the carbonate host rock (this study; Paradis et al., 2007). Very few minerals are present at Gayna River; carbonates, sphalerite, and galena are common, quartz and pyrite are occasionally seen, and barite and fluorite have been observed as rare accessory minerals (Hardy, 1979). The simple mineralogy seen at Gayna River is considered a main characteristic of MVT deposits (Sangster, 1996). The wide range of salinity at Gayna River is typical for MVT deposits (Leach et al., 2005; Basuki and Spooner, 2002) as are the S isotope values at Gayna River, excluding those deposits with bacterially-derived reduced S. Perhaps the main issue is the definition of MVT, discussed by Leach et al. (2005), and if this term should be used for a broad group of carbonate hosted Zn-Pb deposits with diversity as a feature of the deposit type, or if it these deposits should be split into distinct types based on their diverse attributes. At this time, there does not appear to be a definite solution and the term 'carbonate-hosted Zn-Pb deposit' effectively avoids the controversy but does not insinuate any genetic origin and is purely descriptive.

The fluid inclusion salinity and homogenization temperatures at Gayna River are similar to the MVT style fluid inclusions measured at Prairie Creek Zn-Pb-Ag deposit (Fraser, 1996), in addition to the previously mentioned similarly high Ga concentrations in sphalerite from both deposits. At Prairie Creek, for the stratiform style mineralization, sphalerite fluid inclusions have an average salinity of 20 wt% NaCl equivalent, and homogenization temperatures ranging from 110 to 220°C. The MVT style mineralization has sphalerite fluid inclusions with an average salinity of 22 wt% NaCl equivalent, and homogenization temperatures ranging from 155 to 220°C, almost identical to the main ore stage sphalerite fluid inclusions measured at Gayna River. The late vein style mineralization at Prairie Creek, however, is different to Gayna River and is characterized by low salinities and homogenization temperatures around 140°C (Fraser, 1996). The MVT style mineralization at Prairie Creek possibly has some genetic relationship to Gayna River based on similar fluid inclusion and trace element results.

There are several carbonate hosted Zn-Pb deposits found further south in the Cordillera. The Robb Lake carbonate hosted Zn-Pb deposit, located in Northern British Columbia (Figure 22), is dissimilar to Gayna River. The age of the Robb Lake deposit, hosted by Silurian to Middle Devonian dolostones, is contentious and has been described as Eocene based on paleomagnetism (Smethurst et al., 1999) and alternatively as Paleozoic based on Rb-Sr radiometric dating combined with fluid inclusion data (Nelson et al., 2002; Paradis and Nelson 2007). A fluid inclusion study by Sangster and Carrière (1991) at Robb Lake found salinities of 16 to >23 wt% NaCl equivalent, which are somewhat lower than those for the main ore stage at Gayna River. Fluid inclusion homogenization temperatures were also significantly lower at Robb Lake, ranging from 87 to 154°C. Based on the interpreted age and fluid inclusion differences, the Robb Lake deposit is unlikely to be genetically related to the Gayna River deposit. The Kicking Horse and Monarch carbonate hosted Zn-Pb deposits, located in southern British Columbia in the Foreland Belt, have significantly lower fluid inclusion homogenization temperatures, 66 to 99°C, for sphalerite than at Gayna River but they have comparable salinity with a mean of 23 wt% NaCl equivalent (Vandeginste et al., 2007). The Kicking Horse and Monarch deposits are interpreted by Vandeginste et al. (2007) to be of either Ordovician-Devonian or Early Tertiary based on a reconstructed burial temperature curve and fluid inclusion temperatures. If the age is Early Tertiary, these deposits may be genetically related to Gayna River and as the salinities for both the Gayna River and Kicking Horse/Monarch deposits are also similar to those reported from Paleozoic dolomite throughout the Western Canada Sedmimentary Basin, (e.g. Aulstead et al., 1988; Mountjoy et al., 1999; Qing and Mountjoy, 1994; Vandeginste et al., 2005; Wendte et al., 1998) it is possible a basin wide fluid system was present which was then differentiated by locate fluid-rock interaction producing the variation seen between Cordilleran deposits.

4.7.1 Fluid Flow

Various models for the origin of the Cordilleran MVT deposits have been suggested by many authors. Garven (1985) and subsequently others (e.g., Qing and Mountjoy,1992, 1994; Qing et al., 1995; Adams et al., 2000) proposed a Cretaceous-Tertiary Laramide model invoking topographically driven regional fluid flow. In this model, subsurface brines are flushed out of the basin by groundwater flow from topographic highs to topographically low areas. These brines are rich in Zn and Pb and can form deposits where they become concentrated in permeable units. A Devonian-Mississippian Antler orogenic model, similar to Garven's (1985) model, has been advocated for by various authors (Nesbitt and Muehlenbachs, 1994; Amthor et al, 1993; Mountjoy et al, 1999). This model involves similar topographically driven regional fluid flow due to uplift. Evidence is largely based on fluid inclusion homogenization temperatures and isotopes which indicate east to west fluid flow, and dating which indicates mineralization events occurred during the Devonian-Mississippian. A third model from Nelson et al. (2002) argues for mineralization being associated with mid-Paleozoic tectonism, where far-field effects of subduction caused the fluid migration that formed these deposits through development of deep hydrothermal convection systems. Thermal convection systems involve deep circulation of hydrothermal brines by convection due to temperature and salinity variations (Morrow, 1998). These authors suggest that such systems can account for the high temperatures and salinities seen in many Cordilleran MVT deposits.

At Gayna River there is no evidence for meteoric water in the main ore stage. Thus, the topographically driven flow models invoking groundwater flushing may not be appropriate. The Pb and Re/Os isotopic evidence, suggesting that the Gayna River mineralization is likely Cretaceous-Tertiary in age, rules out thermal convection related to mid-Paleozoic tectonism. The Plateau Fault (Figure 1) developed during the Late Cretaceous to Early Tertiary (Eisbacher, 1981; Cook, 1991) during a period of major compression related to the Laramide Orogeny. It has been traced over a length of 270 km and the fault appears to have detached above the Little Dal Gypsum unit (Cecile et al., 1982; Cook, 1991). Previous workers (Hardy, 1979; Hewton, 1982) disregarded the Plateau Fault as a possible fluid conduit because they believed that the Gayna River mineralization was emplaced before the Plateau Fault was activated. However, in light of the proposed Cretaceous-Tertiary date, and the proximity of the Plateau Fault to the Gayna River mineralization (Figure 3), Laramide related tectonically driven flow is the most likely source of fluids for the Gayna River mineralization (Figure 26). As the Little Dal Gypsum is assumed to be the fault glide plane any fluids moving up the fault would encounter this gypsum, and TSR could take place, as proposed in the Gayna River deposit model. The fluid temperatures seen at Gayna River for the main stage mineralization (mean 195°C) could have been achieved by fluids originating at the base of the Plateau Fault, estimated to be under greater than 6 km of stratigraphy (Cook, 1991; MacNaughton et al., 2008), if average geothermal gradient ranges (25°C to 35° per kilometer) are considered. This model is similar to the “squeegee” model proposed by Oliver (1986) which entails an advancing thrust sheet driving fluids from the continental margin sediments into the adjacent foreland basin. The “squeegee” model has previously been applied to the Cordillera: for example, Machel and Cavell (1999) concluded that there was at least some tectonically-induced, “squeegee” fluid, related to the Laramide, responsible for the geochemical composition of Devonian carbonates in the Western Canada Sedimentary Basin. The Tertiary age determined from Re/Os isotope data corresponds with a proposed period of extension and faulting in the deposit area (Aitken, 1982) and could be related to a relaxation phase after a late pulse of the Laramide orogeny.

4.7.2 Deposition Model

The formation of carbonate hosted sulphide deposits requires both a metal and a sulphide source. In order for a single fluid to transport both metals and reduced sulphide a low pH and high temperature environment is needed (Sangster, 1990). It is difficult to envisage a role for a low pH fluid in these systems as the abundant carbonate rocks would react with any acidic fluid, dissolving the rock and releasing H_2O and CO_2^{-2}, and buffering the system at a higher pH (Leach et al., 2005). For this reason, other processes include either a metal- and sulphate-rich fluid encountering a reducing agent, a metal- and reducing agent-rich fluid encountering a sulphate source, or a metal-rich and low sulphur fluid encountering a sulphide source have been suggested (Anderson, 1975; Beales, 1975; Sverjensky 1986).

The precipitation of mineral phases is affected by many factors: pressure, temperature, pH, P_{CO2}, oxidation state, and salinity (Rimstidt, 1997). It is unlikely that pressures greatly changed during the time of the main ore stage mineralization. All of the other factors may be changed by fluid mixing, which likely occurred between a lower temperature, lower salinity fluid and a higher temperature, higher salinity fluid in the main ore stage (see section 4.3). As mentioned above, the large quantity of carbonate host rocks would have buffered the system making pH changes an unlikely cause of mineral precipitation. There is no evidence for changes in P_{CO2} throughout the main ore stage. Thus, changes in temperature, salinity, and oxidation state, as well as fluid metal composition, must have controlled the main

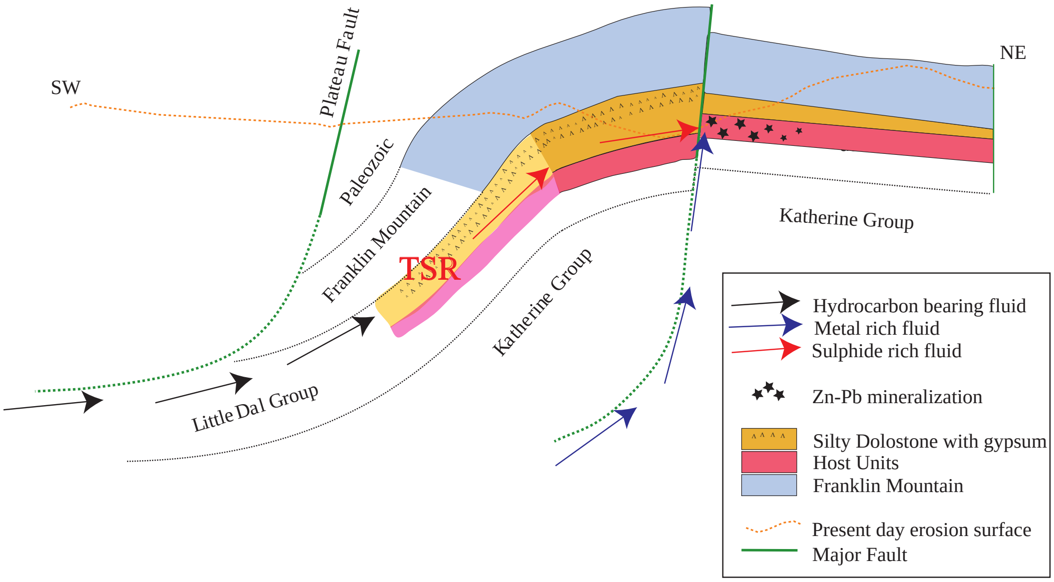

Figure 26. A cartoon representation of the main stage mineralization process. The thermochemical sulphate reduction (TSR) of the Little Dal Gypsum creates sulphide which, combined with metal rich fluids derived from underlying shales, produces mineralization in the Little Dal Upper and Lower Host Units.

ore stage mineral precipitation. Dolomite has increased solubility with increased salinity (Rimstidt, 1997) so it would be expected that dolomite would precipitate when the salinity was lower. However, solubility for dolomite also decreases with increasing temperature which has a greater affect on solubility than salinity. The main stage dolomite is present through the stage but also shows evidence of dissolution which may be due to fluctuating temperatures. For quartz, increasing salinity and temperature both increase solubility (Rimstidt, 1997) so it would be expected that the quartz would precipitate when the lower temperature and salinity fluid was dominant. The hot, saline fluid is likely the main source of metals, so it would be expected that sphalerite would be precipitated when larger amounts of this fluid were present in the system. Sphalerite mineralization may have occurred when this hot, metal-rich fluid, mixed with the cooler, lower salinity fluid, reducing the solubility of metal complexes due to a decrease in temperature (Seward and Barnes, 1997). Equally, as discussed in section 4.5, the main ore stage sphalerite precipitation may be related to changes in oxidation state. For the main stage, it appears that temperature, salinity and possibly oxidation state changes, potentially caused by fluid mixing, in addition to the metal composition of the fluid, resulted in precipitation of the various phases.

The evidence for TSR at Gayna River and fluid inclusion mixing evidence is most compatible with a main ore stage mineralization depositional process in which a metal-rich fluid encounters another fluid carrying sulphide derived from a hydrocarbon-rich fluid interacting with a sulphate source (Figure 26). TSR occurs due to the high temperature and hydrocarbon presence resulting in the production of sulphide. Closed system reduction of the gypsum leads to isotopically heavy S in the main and late ore stages. The TSR reaction releases isotopically light C which is incorporated into main and late carbonate phases. In the late ore stage a warm, saline brine becomes dominant as the high temperature and salinity fluid event ends. Mineralization is minor due to limited remaining sulphide supply or possibly limited metals carried in the late ore stage fluid.

Chapter 5
Conclusions

- The mineral deposition at Gayna River likely did not occur in the Neoproterozoic and may be Late Cretaceous – Early Tertiary age, possibly related to the Laramide Orogeny and the Plateau Fault.
- The Gayna River deposit was formed by at least three circulating $CaCl_2$ + NaCl fluids corresponding to the early, main, and late ore stages.
- The main mineralizing event was a result of fluid mixing between a hot, saline fluid (main phase sphalerite mean temperature 195°C, 26.9 wt% NaCl equivalent) which was likely a deep circulating formation water and a cooler, less saline fluid similar to the early ore stage fluid.
- The sulphide source was local Little Dal Group Gypsum which underwent closed system thermochemical sulphate reduction.
- The metal source was likely local shales which contained abundant base metals and trace elements.
- The unusually high Ga concentrations may enhance the economic potential of the deposit.

BIBLIOGRAPHY

Adams, J.J., Rostron, B.J., and Mendoza, C.A. 2000. Evidence for two-fluid mixing at Pine Point, NWT; proceedings of geofluids III; third international conference on fluid evolution, migration and interaction in sedimentary basins and orogenic belts. Journal of Geochemical Exploration, **69-70**: 103-108.

Aitken, J.D. 1982. Precambrian of the Mackenzie fold belt; a stratigraphic and tectonic overview; Precambrian sulphide deposits. Special Paper - Geological Association of Canada, **25**: 149-161.

Aitken, J.D. 1981. Stratigraphy and sedimentology of the upper Proterozoic Little Dal Group, Mackenzie Mountains, Northwest Territories; Proterozoic basins of Canada. Paper - Geological Survey of Canada, **81-10**: 47-71.

Aitken, J.D. 1974. Geological maps showing bedrock geology of the northern parts of Mount Eduni and Bonnet Plume Lake map areas, District of Mackenzie, NWT. Geological Survey of Canada, Open File 221.

Aitken, J.D. and Cook, D.G. 1975. Geology of upper Ramparts River (106G) and Sans Sault Rapids (106H) map-area, District of Mackenzie. Geological Survey of Canada, Open File 272.

Amthor, J.E., Mountjoy, E.W., and Machel, H.G. 1993. Subsurface dolomites in upper Devonian Leduc formation buildups, central part of Rimbey-Meadowbrook reef trend, Alberta, Canada. Bulletin of Canadian Petroleum Geology, **41**: 164-185.

Anderson, G.M. 1975. Precipitation of Mississippi Valley-Type ores. Economic Geology and the Bulletin of the Society of Economic Geologists, **70**: 937-942.

Ansdell, K.M., Nesbitt, B.E., and Longstaffe, F.J. 1989. A fluid inclusion and stable-isotope study of the Tom Ba-Pb-Zn deposit, Yukon Territory, Canada. Economic Geology and the Bulletin of the Society of Economic Geologists, **84**: 841-856.

Aulstead, K.L., Spencer, R.J., and Krouse, H.R. 1988. Fluid inclusion and isotopic evidence on dolomitization, Devonian of Western Canada. Geochimica et Cosmochimica Acta, **52**: 1027-1035.

Bakker, R.J. 2004. Raman spectra of fluid and crystal mixtures in the systems H_2O, H_2O-NaCl and H_2O-$MgCl_2$ at low temperatures: Applications to fluid-inclusion research. Canadian Mineralogist, **42**: 1283-1314.

Banks, D.A., Boyce, A.J., and Samson, I.M. 2002. Constraints on the origins of fluids forming Irish Zn-Pb-Ba deposits; evidence from the composition of fluid inclusions. Economic Geology and the Bulletin of the Society of Economic Geologists, **97**: 471-480.

Banks, D.A. and Russell, M.J. 1992. Fluid mixing during ore deposition at the Tynagh base-metal deposit, Ireland; proceedings of the eleventh European symposium on fluid inclusions research (ECROFI XI). European Journal of Mineralogy, **4**: 921-931.

Banner, J.L. 1995. Application of the trace element and isotope geochemistry of strontium to studies of carbonate diagenesis. Sedimentology, **42**: 805-824.

Basuki, N.I. and Spooner, E.T.C. 2002. A review of fluid inclusion temperatures and salinities in Mississippi Valley-Type Zn-Pb deposits; identifying thresholds for metal transport. Exploration and Mining Geology, **11**: 1-17.

Batten, K.L., Narbonne, G.M., and James, N.P. 2004. Paleoenvironments and growth of early Neoproterozoic calcimicrobial reefs; platformal Little Dal Group, northwestern Canada. Precambrian Research, **133**: 249-269.

Beales, F.W. 1975. Precipitation mechanisms for Mississippi Valley-Type ore deposits. Economic Geology and the Bulletin of the Society of Economic Geologists, **70**: 943-948.

Bizzarro, M., Simonetti, A., Stevenson, R.K. and Kurszlaukis, S., 2003. In situ $^{87}Sr/^{86}Sr$ investigation of igneous apatites and carbonates using laser-ablation MC-ICP-MS. Geochimica et Cosmochimica Acta, v. 67, p. 289-302.

Bodnar, R.J. 1993. Revised equation and table for determining the freezing point depression of H_2O-NaCl solutions. Geochimica et Cosmochimica Acta, **57**: 683-684.

Borthwick, J. and Harmon, R.S. 1982. A note regarding CIF_3 as an alternative to BrF_5 for oxygen isotope analysis. Geochimica et Cosmochimica Acta, **46**: 1665-1668.

Burke, W.H., Denison, R.E., Hetherington, E.A., Koepnick, R.B., Nelson, H.F., and Otto, J.B. 1982. Variations of seawater $^{87}Sr/^{86}Sr$ throughout Phanerozoic time. Geology, **10**: 516-519.

Carrière, J.J. and Sangster, D.F. 1999. A multidisciplinary study of carbonate-hosted zinc-lead mineralization in the Mackenzie platform (a.k.a. Blackwater and Lac de Bois platforms), Yukon and Northwest Territories, Canada. Geological Survey of Canada Open File 3700, 145 p.

Carrière, J.J. and Sangster, D.F. 1992. Preliminary studies of fluid inclusions in sphalerite quartz, and dolomite from Gayna River MVT deposit, Northwest Territories; current research; part A, Cordillera and Pacific margin. Geological Survey of Canada, 92-01A.

Cecile, M.P., Cook, D.G., and Snowdon, L.R. 1982. Plateau overthrust and its hydrocarbon potential, Mackenzie Mountains, Northwest Territories; current research; part A. Paper - Geological Survey of Canada, 89-94.

Chi, G.X. and Savard, M.M. 1995. Fluid evolution and mixing in the Gays River carbonate-hosted Zn-Pb deposit and its surrounding barren areas, Nova Scotia. Atlantic Geology, **31**: 141-152.

Clayton, R.N. and Mayeda, T.K. 1963. The use of bromine pentafluoride in the extraction of oxygen from oxides and silicates for isotopic analysis. Geochimica et Cosmochimica Acta, **27**: 43-52.

Cook, D.G. 1991. Mackenzie Mountains, Franklin Mountains and Colvitte Hills: Structural Styles. *In* Geology of the Cordilleran Orogen in Canada *Edited by* H. Gabrielse and C.J. Yorath. Geologic Survey of Canada, Ottawa, ON, Canada, pp. 642-647.

Creaser, R.A., Sannigrahi, P., Chacko, T., and Selby, D. 2002. Further evaluation of the Re-Os geochronometer in organic-rich sedimentary rocks: A test of hydrocarbon maturation effects in the Exshaw Formation, Western Canada Sedimentary Basin. Geochimica et Cosmochimica Acta, **66**: 3441-3452.

Davies, D.W., Lowenstein, T.K., and Spencer, R.J. 1990. Melting behavior of fluid inclusions in laboratory-grown halite crystals in the systems NaCl–H_2O, NaCl–KCl–H_2O, NaCl–$MgCl_2$–H2O, NaCl–$CaCl_2$–H_2O. Geochimica et Cosmochimica Acta, **54**, 591-601.

Dewing, K., Sharp, R.J., Ootes, L., Turner, E.C., and Gleeson, S. 2006. Geological assessment of known Zn-Pb showings, Mackenzie Mountians, Northwest Territories. Geological Survey of Canada Current Research, 2006-A4.

Dickin, A.P. 1995. Radiogenic isotope geology. Cambridge University Press, Cambridge, United Kingdom.

Downie, C. 2001. Geological Report on the Gayna River Property, Northwest Territories Geoscience Office Assessment Report (Mineral Exploration Report) 084410.

Eisbacher, G.H. 1981. Sedimentary tectonics and glacial record in the Windermere Supergroup, Mackenzie Mountains, northwestern Canada. Geological Survey of Canada, Paper 80-27, 40p.

Fraser, S.C. 1996. Geology and geochemistry of the Prairie Creek Zn, Pb, Ag deposits, southern Mackenzie Mountains, N.W.T. Unpublished M.Sc. Thesis, University of Alberta, Edmonton, Alberta, 146p.

Gabrielse, H. and Campbell, R.B. 1991. Upper Proterozoic assemblages. *In* Geology of the Cordilleran Orogen in Canada. *Edited by* H. Gabrielse and C.J. Yorath. Geologic Survey of Canada, Ottawa, ON, Canada, pp. 125-150.

Gardner, H.D. and Hutcheon, I. 1985. Geochemistry, mineralogy, and geology of the Jason Pb-Zn deposits, Macmillan Pass, Yukon, Canada. Economic Geology and the Bulletin of the Society of Economic Geologists, **80**: 1257-1276.

Garven, G. 1985. The role of regional fluid flow in the genesis of the Pine Point deposit, Western Canada Sedimentary Basin. Economic Geology and the Bulletin of the Society of Economic Geologists, **80**: 307-324.

Gleeson, S.A. 2006. A microthermometric study of fluid inclusions in sulfides and carbonates from Gayna River and the Bear base metal prospects, Mackenzie Mountains, NWT. Northwest Territories Geoscience Office Open Report 2006-005, pp. 1-10.

Gleeson, S.A. and Turner, W.A. 2007. Fluid inclusion constraints on the origin of the brines responsible for Pb–Zn mineralization at Pine Point and coarse non-saddle and saddle dolomite formation in southern Northwest Territories. Geofluids, **7**: 51-68.

Glesemann, A., Jäger, H.-J., Norman, A.L., Krouse, H.R. and Brand, W.A., 1994. Online sulfur-isotope determination using an elemental analyzer coupled to a mass spectrometer. Analytical Chemistry, **66**: 2816-2819.

Godwin, C.I., Gabites, J.E., and Andrew, A. 1988. Leadtable; a galena lead isotope data base for the Canadian Cordillera; with a guide to its use by explorationists. Paper - Ministry of Energy, Mines and Petroleum Resources, **1988-4**: 188.

Godwin, C.I. and Sinclair, A.J. 1982. Average lead isotope growth curves for shale-hosted zinc-lead deposits, Canadian Cordillera. Economic Geology and the Bulletin of the Society of Economic Geologists, **77**: 675-690.

Godwin, C.I., Sinclair, A.J., and Ryan, B.D. 1982. Lead isotope models for the genesis of carbonate-hosted Zn-Pb, shale-hosted Ba-Zn-Pb, and silver-rich deposits in the northern Canadian Cordillera. Economic Geology and the Bulletin of the Society of Economic Geologists, **77**: 82-94.

Halverson, G.P., Dudas, F.O., Maloof, A.C., and Bowring, S.A. 2007. Evolution of the ^{87}Sr/^{86}Sr composition of Neoproterozoic seawater; Neoproterozoic to Paleozoic ocean chemistry. Palaeogeography, Palaeoclimatology, Palaeoecology, **256**: 103-129.

Hardy, J.L. 1979. Stratigraphy, brecciation and mineralization, Gayna River, Northwest Territories. Unpublished M.Sc. Thesis, University of Toronto, Toronto, Ontario, 467p.

Hewton, R.S. 1982. Gayna river; a Proterozoic Mississippi Valley-Type zinc-lead deposit; Precambrian Sulphide deposits. Special Paper - Geological Association of Canada, **25**: 667-700.

Hewton, R.S. 1976. Gayna River Project - Geology, Geochemistry and Diamond Drilling - 1976, RT Claims, Northwest Territories Geoscience Office Assessment Report (Mineral Exploration Report) 080567.

Hewton, R.S. and Wilson, N. 1977. Gayna River Assessment Report, Northwest Territories Geoscience Office Assessment Report (Mineral Exploration Report) 080724.

Huizenga, J., Gutzmer, J., Banks, D., and Greyling, L. 2006. The Paleoproterozoic carbonate-hosted Pering Zn-Pb deposit, South Africa; II, fluid inclusion, fluid chemistry and stable isotope constraints. Mineralium Deposita, **40**: 686-706.

Issler, D.R., Grist, A.M., and Stasiuk, L.D. 2005. Post-early Devonian thermal constraints on hydrocarbon source rock maturation in the Keele Tectonic Zone, Tulita area, NWT, Canada, from multi-kinetic apatite fission track thermochronology, vitrinite reflectance and shale compaction. Bulletin of Canadian Petroleum Geology, **53**: 405-431.

Jacobsen, S.B. and Kaufman, A.J. 1999. The Sr, C and O isotopic evolution of Neoproterozoic seawater; earth system evolution; geochemical perspective. Chemical Geology, **161**: 37-57.

Jaffe, L.A., Peucker-Ehrenbrink, B., and Petsch, S.T. 2002. Mobility of rhenium, platinum group elements and organic carbon during black shale weathering. Earth and Planetary Science Letters, **198**: 339-353.

Kesler, S.E. and Reich, M.H. 2006. Precambrian Mississippi Valley-Type deposits; relation to changes in composition of the hydrosphere and atmosphere; evolution of early earth's atmosphere, hydrosphere, and biosphere; constraints from ore deposits. Memoir - Geological Society of America, **198**: 185-204.

Kesler, S.E., Cumming, G.L., Krstic, D., and Appold, M.S. 1994. Lead isotope geochemistry of Mississippi Valley-Type deposits of the southern Appalachians. Economic Geology and the Bulletin of the Society of Economic Geologists, **89**: 307-321.

Kiyosu, Y. and Krouse, H.R. 1990. The role of organic acid in the abiogenic reduction of sulfate and the sulfur isotope effect. Geochemical Journal, **24**: 21-27.

Krouse, H.R., Viau, C.A., Eliuk, L.S., Ueda, A., and Halas, S. 1988. Chemical and isotopic evidence of thermochemical sulphate reduction by light hydrocarbon gases in deep carbonate reservoirs. Nature (London), **333**: 415-419.

Large, D. 1981. The geochemistry of the sedimentary rocks in the vicinity of the Tom Pb-Zn-Ba deposit, Yukon Territory, Canada; geochemical exploration 1980. Journal of Geochemical Exploration, **15**: 203-217.

Leach, D.L., Sangster, D.F., Kelley, K.D., Large, R.R., Garven, G., Allen, C.R., Gutzmer, J., and Walters, S. 2005. Sediment-hosted lead-zinc deposits; a global perspective. *In* Economic Geology; one hundredth anniversary volume, 1905-2005, *Edited by* J.W. Hedenquist, J.F.H. Thompson, R.J. Goldfarb and J.P. Richards. Society of Economic Geologists, Littleton, CO, United States (USA).

Li, Y. and Liu, J. 2006. Calculation of sulfur isotope fractionation in sulfides. Geochimica et Cosmochimica Acta, **70**: 1789-1795.

Lindsay, J.F., Kruse, P.D., Green, O.R., Hawkins, E., Brasier, M.D., Cartlidge, J., and Corfield, R.M. 2005. The Neoproterozoic-Cambrian record in Australia; a stable isotope study. Precambrian Research, **143**: 113-133.

Linke, W. F. 1965. Solubilities of Inorganic and Metal Organic Compounds, Vols. 1 and 2, 4th edn. American Chemical Society.

Ludwig, K. 2003. Isoplot/Ex, version 3: A Geochronological Toolkit for Microsoft Excel., Geochronology Center Berkeley.

Machel, H.G. 2001. Bacterial and thermochemical sulfate reduction in diagenetic settings; old and new insights; sedimentary and diagenetic transitions between carbonates and evaporites. Sedimentary Geology, **140**: 143-175.

Machel, H.G. 1989. Relationships between sulphate reduction and oxidation of organic compounds to carbonate diagenesis, hydrocarbon accumulations, salt domes, and metal sulphide deposits; Mississippi Valley-Type sulfide diagenesis and its relation to carbonate paragenesis and basin hydrologic systems; special session of annual midyear meeting of SEPM. Carbonates and Evaporites, **4**: 137-152.

Machel, H.G. and Cavell, P.A. 1999. Low-flux, tectonically-induced squeegee fluid flow ("hot flash") into the rocky mountain foreland basin; lithoprobe; Alberta basement transects; synthesis issue. Bulletin of Canadian Petroleum Geology, **47**: 510-533.

Machel, H.G., Krouse, H.R., and Sassen, R. 1995. Products and distinguishing criteria of bacterial and thermochemical sulfate reduction. Applied Geochemistry, **10**: 373-389.

MacNaughton, R.B., Fallas, K.M., and Zontvoort, W. 2008. Qualitative Assessment of the Plateau Fault (Mackenzie Mountains, NWT) as a Conceptual Hydrocarbon Play. Geological Survey of Canada, Open File 5831, 29p.

McCrea, J. M., 1950. On the isotopic chemistry of carbonates and a paleotemperature scale. The Journal of Chemical Physics, **18**: 849-857.

McLaren, G.P. and Godwin, C. I. 1979. Minor Elements in sphalerite from carbonate-hosted zinc-lead deposits, Yukon Territory and adjacent district of Mackenzie, Northwest Territories; Mineral Industry Report, 1977. Yukon Economic Geology Survey, 1978-1979 p. 5-21.

Morrow, D. 1998. Regional subsurface dolomitization; models and constraints. Geoscience Canada, **25**: 57-70.

Morrow, D.W., Cumming, G.L., and Aulstead, K.L. 1990. The gas-bearing Devonian Manetoe facies, Yukon and Northwest Territories. Geological Survey of Canada, Bulletin 400, 54 p.

Mountjoy, E.W., Green, D., Machel, H.G., Duggan, J., and Williams-Jones, A.E. 1999. Devonian matrix dolomites and deep burial carbonate cements; a comparison between the Rimbey-Meadowbrook reef trend and the deep basin of west-central Alberta; lithoprobe; Alberta basement transects; synthesis issue. Bulletin of Canadian Petroleum Geology, **47**: 487-509.

Mountjoy, E.W., Qing, H., and McNutt, R.H. 1992. Strontium isotopic composition of Devonian dolomites, Western Canada Sedimentary Basin; significance of sources of dolomitizing fluids. Applied Geochemistry, **7**: 59-75.

Narbonne, G.M. and Aitken, J.D. 1995. Neoproterozoic of the Mackenzie Mountains, northwestern Canada; Neoproterozoic stratigraphy and earth history. Precambrian Research, **73**: 101-121.

Nelson, J., Paradis, S., Christensen, J., and Gabites, J. 2002. Canadian cordilleran Mississippi Valley-type deposits; a case for Devonian-Mississippi back-arc hydrothermal origin. Economic Geology and the Bulletin of the Society of Economic Geologists, **97**: 1013-1036.

Nesbitt, B.E. and Muehlenbachs, K. 1994. Paleohydrogeology of the Canadian Rockies and origins of brines, Pb-Zn deposits and dolomitization in the western Canada sedimentary basin. Geology (Boulder), **22**: 243-246.

Ohmoto, H., Kaiser, C.J., and Geer, K.A. 1990. Systematics of sulphur isotopes in recent marine sediments and ancient sediment-hosted basemetal deposits; proceedings of the conference on stable isotopes and fluid processes in mineralization. Publication - Geology Department and Extension Service, University of Western Australia, **23**: 70-120.

Ohmoto, H. and Rye, R.O. 1979. Isotopes of sulfur and carbon. *In* Geochemistry of hydrothermal ore deposits, *Edited by* H.L. Barnes. John Wiley & Sons, New York, NY, United States (USA).

Oliver, J. 1986. Fluids expelled tectonically from orogenic belts: their role in hydrocarbon migration and other geologic phenomena. Geology, **14**: 99–102.

Orr, W.L. 1982. Rate and mechanism of non-microbial sulfate reduction. Geological Society of America Annual Convention, Abstracts with Programs, p.580.

Paradis, S., and Nelson, J.L., 2007, Metallogeny of the Robb Lake carbonate-hosted zinc-lead district, northeastern British Columbia. *In* Mineral Deposits of Canada: A Synthesis of Major Deposit-Types, District Metallogeny, the Evolution of Geological Provinces, and Exploration Methods: Geological Association of Canada, Mineral Deposits Division, *Edited by* Goodfellow, W.D., Special Publication No. 5, p. 633-654.

Paradis, S., Hannigan, P., and Dewing, K. 2007. Mississippi valley-type lead-zinc deposits (MVT). *In* Mineral Deposits of Canada: A Synthesis of Major Deposit-Types, District Metallogeny, the Evolution of Geological Provinces, and Exploration Methods: Geological Association of Canada, Mineral Deposits Division, *Edited by* Goodfellow, W.D., Special Publication No. 5, p. 185-203.

Peucker-Ehrenbrink, B. and Hannigan, R.E. 2000. Effects of black shale weathering on the mobility of rhenium and platinum group elements. Geology (Boulder), **28**: 475-478.

Peucker-Ehrenbrink, B. and Ravizza, G. 2000. The marine osmium isotope record. Terra Nova, **12**: 205-219.

Postgate, J.R. and Campbell, L.L. 1966. Classification of *Desulfovibrio* Species, the Nonsporulating Sulfate-reducing Bacteria. Bacteriological Reviews, **30**: 732-738.

Qing, H., Mountjoy, E.W., Nesbitt, B.E., and Muehlenbachs, K. 1995. Paleohydrogeology of the Canadian Rockies and origins of brines, Pb-Zn deposits and dolomitization in the Western Canada Sedimentary Basin; discussion and reply. Geology (Boulder), **23**: 189-190.

Qing, H. and Mountjoy, E.W. 1994. Rare earth element geochemistry of dolomites in the middle Devonian Presqu'ile barrier, Western Canada Sedimentary Basin; implications for fluid-rock ratios during dolomitization. Sedimentology, **41**: 787-804.

Qing, H. and Mountjoy, E.W. 1992. Large-scale fluid flow in the middle Devonian Presqu'ile barrier, Western Canada Sedimentary Basin. Geology (Boulder), **20**: 903-906.

Ravizza, G., Peucker-Ehrenbrink, B., and Tuit, C.B. 1998. Osmium isotopes as tracers of organic matter weathering; AGU 1998 fall meeting, EOS, Transactions. American Geophysical Union, **79**: 427.

Rimstidt, D. 1997. Gangue Mineral Transport and Deposition. *In* Geochemistry of Hydrothermal Ore Deposits, third edition, *Edited by* Barnes, University Park, Pennsylvania, USA, pp 487-515.

Roedder, E. 1984. Fluid inclusions. Reviews in Mineralogy, **12**: 644.

Roedder, E. and Dwornik, E.J. 1968. Sphalerite color banding; lack of correlation with iron content, Pine Point, Northwest Territories, Canada. American Mineralogist, **53**:1523-1529.

Rye, R. O. and Ohmoto, H. 1974. Sulfur and carbon isotopes and ore genesis: A review. Economic Geology and the Bulletin of the Society of Economic Geologists, **69**: 826-842.

Sakai, G. 1968. Isotopic properties of sulfur compounds in hydrothermal processes. Geochemical Journal, **2**: 29.

Samson, I. M. and Walker, R.T. 2000. Cryogenic Raman spectroscopic studies in the system NaCl-$CaCl_2$-H_2O and implications for low-temperature phase behavior in aqueous fluid inclusions. Canadian Mineralogist, **38**: 35-43.

Samson, I.M. and Russell, M.J. 1987. Genesis of the Silvermines zinc-lead-barite deposit, Ireland; fluid inclusion and stable isotope evidence. Economic Geology and the Bulletin of the Society of Economic Geologists, **82**: 371-394.

Sangster, D.F. 1996. Mississippi Valley-type lead-zinc. *In* Geology of Canadian Mineral Deposit Types, *edited by* Eckstrand, O.R., Sinclair, W.D., and Thorpe, R.I., Geological Survey of Canada, Geology of Canada, No. 8, p. 253-261.

Sangster, D.F. 1990. Mississippi Valley-type and SEDEX lead-zinc deposits: a comparative examination. Institution of Mining and Metallurgy, Transactions, Section B: Applied Earth Science, **99**: 21-42.

Sangster, D.F. and Carrière, J.J. 1991. Preliminary studies of fluid inclusions in sphalerite from the Robb Lake Mississippi Valley-Type deposit, British Columbia; current research; part E--recherches en cours; partie E. 91-01E. Geological Survey of Canada, Ottawa, ON, Canada.

Schmidberger, S.S., Simonetti, A. and Francis, S.D. Sr., 2003. Small-scale Sr isotope investigation of clinopyroxenes from peridotite xenoliths by laser ablation MC-ICP-MS–Implications for mantle metasomatism. Chemical Geology, **199**: 317-329.

Selby, D., Creaser, R.A., and Fowler, M.G. 2007. Re-Os elemental and isotopic systematics in crude oils. Geochimica et Cosmochimica Acta, **71**: 378-386.

Selby, D. and Creaser, R.A. 2005. Direct radiometric dating of hydrocarbon deposits using rhenium-osmium isotopes. Science, **308**: 1293-1295.

Selby, D., Creaser, R.A., Dewing, K., and Fowler, M. 2005. Evaluation of bitumen as a ^{187}Re-^{187}Os geochronometer for hydrocarbon maturation and migration; a test case from the Polaris MVT deposit, Canada. Earth and Planetary Science Letters, **235**: 1-15.

Selby, D. and Creaser, R.A. 2001. Re–Os geochronology and systematics in molybdenite from the Endako porphyry molybdenum deposit, British Columbia, Canada. Economic Geology and the Bulletin of the Society of Economic Geologists, **96**: 197–204.

Seward, T.M. and Barnes, H.L. 1997. Metal Transport by Hydrothermal Ore Fluids. *In* Geochemistry of Hydrothermal Ore Deposits, third edition, *Edited by* Barnes, University Park, Pennsylvania, USA, pp 435-486.

Sharp, R. 2004. Geological Report for the Gayna River Property. Eagle Plains Resources Ltd. Internal Report.

Sheka, I.A., Chaus, I.S., and Mityureva, T.T. 1966. The Chemistry of Gallium. Elsevier, Amsterdam, The Netherlands, 302p.

Shepherd, T.J., Miller, M.F., Scrivener, R.C., Darbyshire, D.P.F., and Halls, C. 1985. Hydrothermal fluid evolution in relation to mineralization in southwest England with special reference to Dartmoor-Bodmin area; high heat production (HHP) granites, hydrothermal circulation and ore genesis. *In* High heat production (HHP) granites, hydrothermal circulation and ore genesis, St. Austell, Cornwall, United Kingdom.

Shields, G.A., Kimura, H., Yang, J., and Gammon, P. 2004. Sulphur isotopic evolution of Neoproterozoic-Cambrian seawater; new francolite-bound sulphate delta ^{34}S data and a critical appraisal of the existing record. Chemical Geology, **204**: 163-182.

Simonetti, A., Gariepy, C., Banic, C.M., Tanabe, R., and Wong, H.K. 2004. Pb isotopic investigation of aircraft-sampled emissions from the Horne smelter (Rouyn, Quebec); implications for atmospheric pollution in northeastern North America. Geochimica et Cosmochimica Acta, **68**: 3285-3294.

Smethurst, M.T., Symons, D.T.A., Sangster, D.F., and Lewchuk, M.T. 1999. Paleo-magnetic age for Zn-Pb mineralization at Robb Lake, northeastern British Columbia. Bulletin of Canadian Petroleum Geology, **47**: 548-555.

Smoliar, M.I., Walker, R.J., and Morgan, J.W. 1996. Re-Os ages of group IIA, IIIA, IVA, and IVB iron meteorites. Science, **271**: 1099-1102.

Spencer, R.J., Møller, N., and Weare, J.H. 1990. The prediction of mineral solubilities in natural waters: A chemical equilibrium model for the Na-K-Ca-Mg-Cl-SO_4-H_2O system at temperatures below 25°C. Geochimica et Cosmochimica Acta, **54**: 575-590.

Stacey, J.S. and Kramers, J.D. 1975. Approximation of terrestrial lead isotope evolution by a two-stage model. Earth and Planetary Science Letters, **26**: 207-221.

Sverjensky, D.A. 1986. Genesis of Mississippi valley-type lead-zinc deposits. Annual Review of Earth and Planetary Sciences, **14**: 177-199.

Taylor, H.P. 1997. Oxygen and Hydrogen Isotope Relationships in Hydrothermal Mineral Deposits. *In* Geochemistry of Hydrothermal Ore Deposits, third edition, *Edited by* Barnes, University Park, Pennsylvania, USA, pp 229-302.

Thom, J. and Anderson, G.M. 2008. The role of thermochemical sulfate reduction in the origin of Mississippi Valley-type deposits. I. Experimental results. Geofluids, **8**: 16-26.

Tiegeng, L. and Lin, Y. 1995. The relationship between mineralogical characteristics and isotopic composition of sphalerite, as exemplified by the Huxu Deposit, China. Chinese Journal of Geochemistry, **14**: 160-167.

Turner, E.C. and Long, D.G. 2008. Basin architecture and syndepositional fault activiy during deposition of the Neoproterozoic Mackenzie Mountains Supergroup, Northwest Territories, Canada. Canadian Journal of Earth Sciences, **45**: 1159-1184.

Turner, E.C., Narbonne, G.M., and James, N.P. 2000. Framework composition of early Neoproterozoic calcimicrobial reefs and associated microbialites, Mackenzie mountains, N.W.T., Canada; carbonate sedimentation and diagenesis in the evolving Precambrian world. Special Publication - Society for Sedimentary Geology, **67**: 179-205.

Turner, E.C., James, N.P., and Narbonne, G.M. 1997. Growth dynamics of Neoproterozoic calcimicrobial reefs, Mackenzie mountains, northwest Canada. Journal of Sedimentary Research, **67**: 437-450.

Vandeginste, V., Swennen, R., Gleeson, S.A., Ellam, R.M., Osadetz, K., and Roure, F. 2007. Geochemical constraints on the origin of the Kicking Horse and Monarch Mississippi Valley-Type lead-zinc ore deposits, southeast British Columbia, Canada. Mineralium Deposita, **42**: 913-935.

Vandeginste, V., Swennen, R., Gleeson, S.A., Ellam, R.M., Osadetz, K., and Roure, F. 2005. Zebra dolomitization as a result of focused fluid flow in the Rocky Mountains fold and thrust belt, Canada. Sedimentology, **52**: 1067-1095.

Viets J.G., Hofstra, A.H., and Emsbo, P. 1996. Solute Compositions of Fluid Inclusions in Sphalerite from North America and European Mississippi Valley-Type Ore Deposits. *In* Ore Fluids Derived from Evaporation Seawater, Society of Economic Geologists Special Publication no. 4, *Edited by* Sangster, D.L., pp. 210–265.

Viets, J.G., Hopkins, R.T., and Miller, B.M. 1992. Variations in minor and trace metals in sphalerite from Mississippi valley-type deposits of the Ozark region; genetic implications. Economic Geology and the Bulletin of the Society of Economic Geologists, **87**: 1897-1905.

Walter, M.R., Veevers, J.J., Calver, C.R., Gorjan, P., and Hill, A.C. 2000. Dating the 840-544 Ma Neoproterozoic interval by isotopes of strontium, carbon, sulfur in seawater, and some interpretative models; Neoproterozoic of Australia. Precambrian Research, **100**: 371-433.

Wendte, J., Qing, H., Dravis, J.J., Moore, S.L.O., Stasiuk, L.D., and Ward, G. 1998. High-temperature saline (thermoflux) dolomitization of Devonian Swan Hills platform and bank carbonates, Wild River area, West-Central Alberta. Bulletin of Canadian Petroleum Geology, **46**: 210-265.

Young, G.M., Jefferson, C.W., Delaney, G.D., and Yeo, G.M. 1979. Middle and late Proterozoic evolution of the northern Canadian cordillera and shield. Geology (Boulder), **7**: 125-128.

Zheng Yongfei. 1999. On calculations of oxygen isotope fractionation in minerals. Episodes, **22**: 99-106.

Zheng, Y. 1993. Calculation of oxygen isotope fractionation in anhydrous silicate minerals. Geochimica et Cosmochimica Acta, **57**: 1079-1091.

Appendix 1

Sample Locations and Descriptions

Appendix 1 includes the field location of all samples used in this study and some brief descriptions.

<u>Notes about Appendix 1</u>

1. The X/Y locations are in UTM Zone 9N (NAD 83).

2. The drill core sample depths are in meters. Core samples are named with the hole number and the sample depth. Some core samples were taken from core drilled in 1975 which was no longer in labelled boxes and thus does not have depth information. These core samples are named 75C001-75C004.

3. Further information about the drill core can be found in the core logging in Appendix 2

4. 'Code' refers to alternate names for samples which were collected prior to 2006 using a different naming system.

5. Outcrop sample names were created using the system from Eagle Plains Resources. Sample names include the following; initals of the sampler, e.g. BW is Bronwen Wallace, the code for the property, e.g. GR is Gayna River, the sample type, e.g. R is a rock sample, and a number, e.g. 001. Some samples, 06BSW, BSB001, 06F001, and 07R001-008 were collected separately and are named with the year, e.g. 06, the showing name, e.g. BSW, and/or the sample type.

6. TS indicates samples for which standard thin sections were obtained.

7. FI indicates samples for which fluid inclusion wafers were obtained.

8. Some mineral names are abbreviated; pyr is pyrite, sph is sphalerite, and qtz is quartz.

Core	Depth	Code	UTM - X	UTM - Y	Sample Description	TS	FI
77-100	30		418195	7204318	pyrobitumen		
77-102	82.5		422415	7201095	tight host		
	96.7				tight host		
	135.3				tight host		
	146.5				pyr alteration and salt		
	147.2				pyr alteration and salt	x	
	295.3				mineralization and pyr alteration		
	304.9				blocky calcite vein, stylolite		
	311				sph		
	318				sph		
	320				sph and pyr alteration	x	
	342.6				lenses of coarse grained in fine grained rock with stylolites		
	373.4				red crystalline sph mineralization		
	381.5				sph in veins		
	386				calcite with euhedral pyr		
	404.2				2 pieces, calcite with sph		
	410.5				good sph mineralization	x	x
	422.3				2 pieces, sph mineralization in sort of mosaic breccia		
	437.8				calcite with qtz		
	452				sph mineralization		
	460.7				barren with veins		
	501.3				molartooth structure		
A17	204.2		419979	7203651			
	250						
	255	SG4B				x	

Core	Depth	Code	UTM - X	UTM - Y	Sample Description	TS	FI
A27	144	SG4	418226	7205534		x	
	144	SG4b				x	
	149	SG5				x	x
	152	SG3				x	
		SG6				x	
A27?	122	SG122	418226	7205534		x	
	155	SG155				x	
	165	SG165				x	
	180.3	SG180.3				x	
	185.8	SG185.8				x	
	216.5	SG216.5				x	
	220	SG220				x	x
	257	SG257				x	x
	284	SG284				x	x
		SG002D				x	
		SG2				x	x
		SG7					x
		SG8				x	
		SG10					x
A30	45.4		417632	7205571	breccia with vugs	x	x
	52				coarse dolostone with minor veining	x	
	55.5				vugs in dolostone	x	
	57.3				horizontal veins and vugs	x	
	60.3				mosaic breccia and vugs	x	x
	77.8				crackle breccia	x	
	96.5				extensive veining and vugs	x	x
	112.6				coarse dolostone		
	115.1				brecciation stopping at stylolite		
	120				breccia with stylolites	x	x
	151				veins ending at vertical stylolite	x	
	164.6				horizontal veins and pyr alteration	x	
	174.4				pyr in vein	x	x

Core	Depth	Code	UTM - X	UTM - Y	Sample Description	TS	FI
A30	178.2		417632	7205571	mosaic brecciation with pyr		
	185				horizontal veins and pyr	x	x
	215				coarse grained light grey dolostone	x	
	230.3				horizontal plus connecting veins		
	231.3				horizontal veins and vugs	x	x
	255.3				qtz in vein	x	x
	262.7				different shades of dolostone, breccia	x	x
	265.6				breccia and large qtz		x
	278				some veining with large vug	x	x
	292				grey dolostone		
	321.5				minor crescentic veining	x	
	322.5				crackle breccia with pyr in veins	x	x
	347				massive mineralization		x
	348.6				crackle breccia		
	349				mineralization in vein		
	350				pyr alteration, pyrobitumen		
	353.5				good mineralization in mosaic breccia		
	364				mineralized vein		
	375.5				vugs, vein at angle to core axis	x	x
	378				extensive veining, some mineralization, and pyr	x	x
	380				mosaic brecciation and large vein	x	
	400				sph mineralization in vein	x	x
	403.8				coarse dolospar vein	x	
	405.6				dolospar with some vugs/breccia	x	
	411.5				pink pyr alteration	x	x
	426.5				host with some layering	x	
	445.3				light grey dolostone with minor vein	x	
	446.5				large vein/vug with pyr		
	450.3				convoluted breccia	x	
	453				large calcite	x	x
	453.3				veins, vugs and stylolites	x	x
	457.8				convoluted breccia		x
	485.5				pyrite alteration and stylolites in coarse dolostone		

Core	Depth	Code	UTM - X	UTM - Y	Sample Description	TS	FI
A32	13.5		416444	7206438	pyrobitumen		
	17				pyrobitumen		
	36.5				mosaic breccia with qtz		
	49				pyrite, qtz, calcite in vug		
	58.3				qtz/calcite vug with sph	x	x
	58.6				large qtz in vug		
	58.9				qtz/calcite vug with sph		
	59.1				qtz/calcite vug with sph		
	59.2				qtz/calcite vug with sph	x	x
	75.2				dolostone with veining and pyrobitumen		
	101.4				creamy dolospar		
	119.5				qtz and vuggy porosity		
	133.2				4 pieces, spar and qtz		
	160				2 pieces, dolospar with laminations and vugs		
	192.7				3 pieces, dark dolospar with vuggy porosity		
	200.1				coarse grained sph at edge of vein		
	203.5				sph and pyr		
	213.2				sph in clump		
	214.1				sph and qtz in sample		
	222.9				vuggy porosity, pyrobitumen		
	233.2				2 pieces, dark dolostone with vugs and pyr		
	249.4				2 pieces, dolostone with vugs, layering, pyr fractrue		
	250				2 pieces, pyr fracture and dolospar vug		
	252.5				3 pieces, crackle to mosaic breccia with pyr and stylolites		
	284.3				pyr in bands with vugs		
	293.7				coarse dolospar with big vein		
	330.6				2 pieces, crackle breccia with pyrobitumen		
	339.6				sharpstone breccia	x	

Core	Depth	Code	UTM - X	UTM - Y	Sample Description	TS	FI
A33	20.5		417030	7205597	2 pieces, altered pyr in vein	x	
	21.5				about vertical vein in fine grained dolostone		
	47.3				pyr disseminated in host		
	61.2				pyr disseminated in host	x	
	68				rust stained dark grey dolostone, with stylolites and vugs	x	x
	88				sub horizontal veins and vugs		
	96.7				blob of mosaic breccia and vugs and pyr alteration	x	x
	102.8				2 pieces, dark grey, strange feeder veins	x	x
	160.2				qtz in small vug		
	187.7				pyr alteration, stylolite and dissolution		
	227.5				messed up host rock and mosaic breccia		
A34	247		417040	7206067	very fractured, pyr alteration, rice grain qtz		
	250.5				2 pieces, large calcite infill with dissolution	x	x
	46.2				strange finger veins		
	59				2 pieces, pyrobitumen in vugs		
	61.2				pyrobitumen in vugs	x	
	75				pyrobitumen	x	x
	128.5				about vertical veining		
	138				big vugs		
	159.2				good dissolution evidence		
	172.4				good alteration and brecciated clasts	x	
	181.9				pyr and alteration along edge of calcite vein		
	184				vein with altered clast		
	184.1				vein with altered clast		
	217.9				calcite		
	220.1				calcite with qtz in vug		
	233.4				large vugs with minor pyr		
	244				3 pieces, vertical vein bounded by stylolites	x	x
	246				dark grey with pyr alteration		

Core	Depth	Code	UTM - X	UTM - Y	Sample Description	TS	FI
A34	266.1		417040	7206067	very fractured and crumbly		
	282.8				convoluted laminations	x	
	311.9				intense veining/breccia with abundant pyr		
	351.1				mosaic breccia, small amounts of pyr		
	365.4				highly fractured with pyr in veins		
	386.5				minor veining in doloston		
	426.1				laminations in host, subvertical veins		
	457				3 pieces, very broken by spar and stylolites		x
	468.5				dark grey, veining, pyr alteration		
	468.9				pyr blebs in vein		
	497.7						
A35	25.7		418179	7203923	pyrobitumen in vugs		
	346.2				calcite	x	x
A9	573		422377	7201733	gypsum		
	576				gypsum		
	580.5				gypsum	x	
B14	70.1		419363	7203066	mosaic breccia		
	72.5				beige rock with minor veining and sph, and clear calcite	x	
	73.2				2 pieces, beige rock with minor veining and sph	x	x
	85.9				some qtz in vug		
	140.1				light brown crackle breccia		
	157				breccia with sph		
	173.2				light brown primary breccia	x	
	177.8				2 pieces, thin veins and cracks, sph		
	184.4				light brown, very crumbly breccia		
	186.9				light grey, very crumbly breccia		
	193.6				dark grey dolostone, some crackling		
	199.8				mostly spar with large stylolite, pyr alteration		
	205.5				dark grey, broken up by stylolites		

Core	Depth	Code	UTM - X	UTM - Y	Sample Description	TS	FI
B14	216.5		419363	7203066	large qtz in vug		
	217				pyr alteration		
	223.5				calcite chunk		
	228.5				big vein		
	238.3				pyr filled crack, strange host appearance		
	239.9				large calcite vein with rare pyr	x	x
	250.7				sedimentary breccia		
B28	8.2		415467	7206445	silty dolostone example		
	42.8				grainy with large vugs and vertical veins		
	66.1				highly fractured cream coloured	x	
	98.8				thick vein fracturing, tan colour		
	100.8				beige coloured, highly fractured and brecciated		
	168.1				grey dolostone with stylolites and vein		
	173.2				grey with two kinds of dolostone		
	194.5				grey dolostone, veining, sph in veins and matrix, qtz	x	x
	195.5				dolostone breccia with vien		
	209.9				mostly a large vein		
	212.2				vein with sph		x
	215.5				breccia with qtz		
	219.5				dolostone with strange texture (part of stylolite)		
	223.6				dolospar with veins, vugs and porosity		
	225.5				dolospar with veins, vugs and porosity, pyrite		
	237.5				breccia with vugs and large qtz	x	x
	242.2				fine breccia and strange open vugs		
	256.5				breccia with large pyrite		
	268.5				2 pieces, breccia, coarse grained dolospar, qtz		
	276.5				2 pieces, veining, sedimentary breccia	x	
	279.5				highly fractured tan colour		
	282				mostly vug/vein with qtz		
	312.2				2 pieces, breccia with big veins and thick pyrite		x

Core	Depth	Code	UTM - X	UTM - Y	Sample Description	TS	FI
B28	380.5		415467	7206445			
	478				coarse grained with vein		
	480.6				3 pieces, stylolites and veins		
	487.1				grainy, very large qtz		x
	492.3				rusty coloured, very brecciated with stylolites		
	504.2				lots of pyrite in breccia		
	506.5				spectacular pyrite in breccia		
	508				plain dolostone with blocky calcite		
	508.5				plain dolostone with blocky calcite		
	536.5				different types of dolostone		
	551.8				2 pieces, qtz, calcite, pyr vug		
	554.8				2 pieces, veining, dissolution, pyr		
	562.2				molar tooth structure		
	574				2 pieces, grainy with dissolution veins		
	583.5				breccia with much altered pyr	x	x
	597.5				breccia with vug and pyr		
	637.2				veining with big pyr and dissolution		
	638				2 pieces, dark colour, vertical vug		
	642.1				strange breccia with some pyr		

Other Samples	Notes	UTM - X	UTM - Y	Sample Description	TS	FI
BWGRR001		419502	7203598			
BWGRR006		419553	7203588			
BWGRR008		419530	7203614		x	x
BWGRR009		419530	7203614		x	x
BWGRR012		419541	7203628		x	x
BWGRR014A		419469	7203519		x	
BWGRR014B		419469	7203519		x	x
BWGRR015		419464	7203510		x	
BWGRR018		416674	7206969		x	x
BWGRR020		416557	7206614	single very large quartz crystal		x
BWGRR021		413403	7205594	double quartz crystals		x
BWGRR022		418072	7203745		x	
BWGRR022A		418072	7203745		x	x
BWGRR023		418072	7203745		x	
BWGRR023B		418072	7203745			x
CAGRR001		421940	7205722		x	x
CAGRR005		418636	7205864			x
MBGRR005		416554	7206421		x	x
MBGRR013		418548	7205135		x	x
75C001	75 Core	418099	7203723		x	x
75C002	75 Core	418099	7203723		x	
75C003	75 Core	418099	7203723			
75C004	75 Core	418099	7203723			x
06BSW	B showing	418405	7203554		x	x
BSB001	B showing	418405	7203554	breccia, orange sph	x	x
06F001	F showing	420480	7203800		x	
07R001-07R008	A showing	418099	7203723	pyrobitumen		

Appendix 2

Drill Core Relogging

Introduction

Seven diamond-drill holes (A30, A32, A33, A34, B28, 77-102, 77-B14) from the 1976 and 1977 Rio Tinto drill programs were relogged at the old Rio Tinto drill core storage site on the Gayna River Property. The drill holes were selected where the Rio Tinto drill logs indicated the following: the presence of mineralization accompanied by either quartz or pyrobitumen; drill site location to give a geographic spread to sample data; and whether the core was still intact, hence representative. Notable features of each relogged drill hole are described. All footages were converted to metres, but an Imperial Unit log is also provided for ease of cross-referencing with the old Rio Tinto drill logs, originally recorded in feet. A list of abbreviations for the logging codes is provided below.

RF	Reef Facies
SD	Silty Dolostone
CN	Chert Nodule Unit
UH	Upper Host
AM	Argillaceous Marker
LH	Lower Host
SSBR	Sharp Stone Breccia
CRBR	Crackle Breccia
EOH	End of Hole
CA	Core Axis

Summary

Drill hole B28 spans the interval from the Lower Limestone to the Silty Dolostone units. Various colours of sphalerite, including orange and green, are present. Veining and brecciation are variable and contain up to 40% spar. Drill-hole A33 has veins up to 7 cm wide and contains quartz; no mineralization is present. Drill-hole A30 contains red sphalerite and displays evidence of fluids being controlled by stylolites. In drill-hole 77-102, orange and red sphalerite is present in calcite veins and octahedral pyrite is present. Drill-hole A34 is entirely within reef facies. It contains pyrite alteration centred on vertical stylolites and has some large (10 cm) vugs. Drill-hole 77-B14 contains sedimentary breccias and an extremely fractured rubble zone which is interpreted as a possible fault. Orange sphalerite in 77-B14 is associated with dolospar and pyrobitumen.

Drill-hole A32 contains quartz throughout and has pyrobitumen-filled vugs. Red sphalerite is present. A pyrite vein, occurring on a stylolite surface, is associated with yellow sphalerite.

Hole: B28

Feet		Meters		Major Units	Sub Units and Alteration
from	to	from	to		
7.2	161	2.19	49.07	SD	
161	173	49.07	52.73	CN	
173	439.5	52.73	133.96	UH	
439.5	456	133.96	138.99	AM	
456	657.8	138.99	200.50	LH	
657.8	677	200.50	206.35	SSBR	
10.2	43.3	3.11	13.20		pink calcite in silty dolostone
168.5	321	51.36	97.84		pyrite mineralization minor in vugs and dolostone
191.6	194.8	58.40	59.38		minor sph mineralization in dolostone vugs, 1%
193.8	194.8	59.07	59.38		mineralization of sph in dolostone matrix, 3%
213.5	216	65.07	65.84		orange and green sph in dolospar vugs with pyrite
276		84.12			sph mineralization in dolospar vein
310.5	312	94.64	95.10		up to 5mm thick pyrite veins in dolospar
430.3	456	131.16	138.99		pyrite in veins and matrix -staining?
487	508	148.44	154.84		some pyr in vugs and veins, less then 1%, concentration increases down hole, around 507 5mm thick vein
551	552	167.94	168.25		2% crystalline pyr in dolospar veins
567	568	172.82	173.13		massive pyrite in dolospar veins
574	659	174.96	200.86		pyr in veins, occasionally up to 10%
7.2	66	2.19	20.12		sparse calcite veins less then 3mm, vugs with up to 2.5cm thick dolomite (coarse and euhedral), less than 0.5%
66	110.8	20.12	33.77		more crackling veins, less then 0.5cm in width, rock is fractured (chert), fractures often not oriented, less then 1% spar total
98.1	102.3	29.90	31.18		sub-unit breccia in cherty layer, crackle to mosaic - weird texture
110.8	165	33.77	50.29		very minor veining and breccia, less then 0.5%, often coarser dolomite zones

Hole: B28 con’t

Feet		Meters		Sub Units and Alteration
from	to	from	to	
165	179.8	50.29	54.80	crackle veins and breccia up to 2cm, calcite veins perpendicular to CA, vug filled with coarse euhedral dolomite, in places crackle breccia developed
179.8	180.4	54.80	54.99	mosaic breccia with much more spar 30%
180.4	210.8	54.99	64.25	less than 6cm calcite veins with pyr, zones of mosaic breccia, 2% spar over interval
210.8	217.8	64.25	66.39	mosaic breccia and mineralization, 20% spar - veining, roughly perpendicular to CA
217.8	251	66.39	76.50	light crackle veining with some significant vugs with calcite, vugs less then 10mm, 10% spar
251	258	76.50	78.64	mosaic breccia to crackle breccia cemented by white dolomite, porosity is flooded by spar, 30%
258	282.2	78.64	86.01	crackle breccia crackle veins perpendicular to CA, dolospar, some up to 5cm in thickness, 2% spar
268	269.8	81.69	82.24	crackle to mosaic breccia, vugs and veins with extensive dissolution, 20% cement
282.2	399.4	86.01	121.74	minor crackling, fairly featureless rock, veins less than 0.5cm in general, dolospar cemented
310.4	312.9	94.61	95.37	crackle to mosaic breccia, thick up to 10cm veins, sharp base, brecciated and or dissolution in top, two types grey dolomite and white dolomite, bands of euhedral pyrite - coarse up to 0.5cm, vugs 0.5cm filled with euhedral dolomite, 30% spar
399.4	422.3	121.74	128.72	crackle to mosaic, mostly crackle , dolomite veins/vugs perpendicular to core axis, vein 18degrees to core axis, 3% spar
422.3	457	128.72	139.29	very minor veining, nothing really (argillaceous marker), 10degrees from core axis, calcite

Hole: B28 con’t

Feet		Meters		Sub Units and Alteration
from	to	from	to	
457	494	139.29	150.57	moderate crackle vein, vein thickness up to 3cm, average 0.5-1cm, 2% spar, some (1 or 2) vugs developing, 5cm by 1cm with euhedral dolomite and late prismatic quartz
494	506.7	150.57	154.44	crackle and mosaic breccia up to 5cm veins dolospar ?spar flooding in core, 3%
506.7	565.8	154.44	172.46	calcite vein with top-stylolite bottom-dissolution, weak crackling, sporatic calcite cement vugs 5cm (3 of them), less than 1% crackling dolomite
551	553	167.94	168.55	more extensive dolomite vugs with calcite in areas, pyrite and qtz, more clasts mosaic breccia, some dissolution, 40% spar
565.8	640.3	172.46	195.16	medium intensity crackle breccia with some mosaic sections, crackling and veins perpendicular to core axis, veins are banded - grey dolomite with calcite in areas, 10% spar both dolomite and calcite
640.3	665.8	195.16	202.94	euhedral pyrite, dissolution at edges of veins, coarse dolostone flooded by coarse dolospar, replacement and dissolution, late calcite, pyrite-dissemination and in veins and vugs, some areas no veining at all, huge vugs-8cm, lined with dolomite (grey) and filled with calcite, grey-dol-dolospar-py-calcite, 30% cement
665.8	677	202.94	206.35	sharpstone breccia, limestone and dolomitized, undolomitizd in general below 669.0, minor calcite veining and vugs less than 2cm, stylolites mostly horizontal to core axis

Hole: A33

Feet		Meters		Major Units	Remarks
from	to	from	to		
13.8	60.4	4.21	18.41	AM	fine grained laminated mudstone - fissile and fizzes
60.4	255	18.41	77.72	LH	coarse grained, dark grey dolostone, few pieces are light brown, grain size 2mm and smaller, irregular zones of laminations - laminations less than 1mm where they occur
255	268	77.72	81.69	SSBR	molar tooth unit - medium grained fissile, well laminated - folded etc., dolostone
					Sub Units and Alteration
13.8	60.4	4.21	18.41		disseminated lenses (framboids of pyrite), 1-2mm
62.8	262	19.14	79.86		pyrite in fractures with dolospar, up to 4mm vug
60.4	62.8	18.41	19.14		disseminated pyrite in dolostone, not clear if primary or secondary
62.8		19.14	0.00		big pyrite filled vug - runs up parallel to core axis
67.5	262	20.57	79.86		normal' vugs - cubes of pyrite with calcite and qtz 4%
13.8	60.4	4.21	18.41		2 fractures filled with dolospar up to 15mm
60.4	232.3	18.41	70.81		crackling with dolomite and later calcite, veins average 3mm up to 7cm, vugs with qtz, calcite, -/+ pyrite - size 2cm, up to 10cm patches of mosaic breccia, veins occur in 5cm intervals - getting to zebra like texture, 1cm vein, 1cm host rock 5degrees to CA in general, 5% spar
211.1	224.3	64.34	68.37		molar tooth breccia with fragments replaced by dolospar less then 5%
224.3	232.3	68.37	70.81		very minor crackling and mosaic breccia, less than 3%
232.3	233.7	70.81	71.23		replaced molar tooth
233.7	240	71.23	73.15		minor crackling, possible reworked molar tooth, less than 1%
240	244.1	73.15	74.40		replaced by spar-molar tooth, less than 5%
244.1	255	74.40	77.72		minor crackling - significant vug fill with qtz - evidence of dissolution, less than 1% cement

Hole: A30

Feet		Meters		Major Units	Remarks
from	to	from	to		
12.1	291.5	3.69	88.85	UH	UH contact gradational to AM; med to dark grey
291.5	317.8	88.85	96.87	AM	95% argillaceous with shale partings, breaks into small chips, upper interval has 10cm silt beds
317.8	489	96.87	149.05	LH	
489	527	149.05	160.63	LH/SSBR	molar tooth structure, sharpstone breccia, very altered, 20%spar last marker 527, EOH marker missing, pieces of core missing

Feet		Meters			Sub Units and Alteration
from	to	from	to		
170.4	185.6	51.94	56.57	CRBR	pyritic layering 86degrees to CA, 2-5mm thickness occurs at base of cemented vugs, lower contact sharp, upper contact is irregular crystal growth, vugs are up to 1.5cm thick filled with calcite, CRBR 1cm thick late calcite filling of dolomite, mod to weak, some irregular vertical stringers associated with pyrite
346.9	355.5	105.74	108.36	sph min	346.9-347.9; 25% coarse red sph in dolospar host fractures, up to 8mm sph in intervals, most 2-4mm 347.9-355.5; 2-5% coarse red sph in dolospar host fractures, numerous barren intervals, average 3% sph
400	401	121.92	122.22	sph min	2% few mm size coarse red sph in dolospar host fractures
316.8	504.5	96.56	153.77	pyr min	patchy pyrite intervals usually associated with fractures 85degrees to CA, 0.5-1cm wide zones of organic matter, also pyrite as individual crystals associated with dolospar veins, sporatic in occurance (every couple of m's)
322.6	323.6	98.33	98.63	CRBR	fine grained pyrite in dolospar fractures 14degrees to CA
457.2	498.2	139.35	151.85		patchy pyrite with dolospar in CRBR up to 5mm crystals in places, 5% pyrite over 10cm in zones, pyr fractures also in top of reef, 1% pyr over whole interval
18.1	49.4	5.52	15.06	CRBR	weak crackle breccia almost parallel to CA, spar veins 1-4mm thick, 5% core volume

Hole: A30 con't

Feet		Meters		Sub Units and Alteration	
from	to	from	to		
49.4	78.6	15.06	23.96	CRBR	intense CRBR numerous embayed/corroded contacts in almost horizontal fractures filled by white dolospar and calcite 1cm thick average, up to 5cm, interconnected vertical fractures between, 30% spar
78.6	120.1	23.96	36.61	CRBR	weak to moderate CRBR, 10% spar, irregular veins some 45-60degrees some almost horizontal, 3-4mm thickness, open vugs with dolospar crystals
94.5	97	28.80	29.57	CRBR	intense interval, notable embayed neomorphic replacement?
120.1	174.1	36.61	53.07	CRBR	weak CRBR, dominantly vertical fractures, 2-5mm wide fractures, 3%spar
174.1	186.1	53.07	56.72	CRBR	moderate CRBR numerous vugs of dolospar with minor late calcite, 5% spar
186.1	291.5	56.72	88.85	CRBR	weak CRBR (last 12 feet very weak) occasional vugs, 1% spar
220.2	232.2	67.12	70.77	CRBR	CR to mosaic breccia, 25% spar, most spar perpendicular to CA
317.8	345.6	96.87	105.34	CRBR	weak CRBR, vertical to subvertical veinlets, minor vugs 2% spar
345.6	403	105.34	122.83		sporatic 10cm sucrosic dolospar veins, irregular contact, rest is CRBR, sub vertical
					most stylolites perpendicular to CA, occassionally parallel to CA, dolospar often stops at stylolites

Hole: 77-102

Feet		Meters		Major Units	Remarks
from	to	from	to		
11	135	3.35	41.15	UH	light grey limestone with laminations, alternating fine and coarse grained sections, small dolomitized sections up to 10cm
135	246.2	41.15	75.04	AM	argillite is fine grained grey limestone, fissile with shale partings
246.2	477	75.04	145.39	LH	medium grained light grey limestone, some convoluted bedding, some small dolomitized sections up to 10cm, possibly ooids up to several feet thick
476	521	145.08	158.80	SSBR	contact gradational with LH, molar tooth structure, grey limestone to EOH
					Sub Units and Alteration
245.8	248	74.92	75.59		pyrite alteration, white bubbly salt crust
292.8	315	89.25	96.01		altered pyr in veins, less than 1%
295.3	315	90.01	96.01		orange-red sph in calcite vein, crystals up to 5mm, less then 1%
367.1	387.9	111.89	118.23		euhedral pyr octahedra in calcite vein, less than 1%
367	453	111.86	138.07		sph in calcite vein, less than 1%, red and orange
380	459.2	115.82	139.96		altered pyr in fractures (massive)
		0.00	0.00		
11	366.5	3.35	111.71		very minor veining parallel to CA and also steep angle, less then 5mm, less than 1% spar
295.3	315	90.01	96.01		minor crackle breccia, 5%, veins mostly perpendicular to CA, average size 5mm up to 35cm
366.5	417	111.71	127.10		thick calcite veins up to 1m coarse crystals, 40% spar, other than large calcite veins there are minor, thin, vertical veins
417	453	127.10	138.07		minor crackling, veins up to 5cm, 3% spar, calcite
453	476.1	138.07	145.12		very minor veining, less then 1%, mostly perpendicular to CA, possible reworked molar tooth structure
476.1	521	145.12	158.80		molar tooth structure with occasional calcite veins, 2cm thick, less then 1%

Hole: A34

Feet		Meters		Major Units	Remarks
from	to	from	to		
26	497.4	7.92	151.61	RF	
					Sub Units and Alteration
44.6	53.8	13.59	16.40		coarse grained, fairly massive dolostone, some have laminations sub mm
53.8	133.6	16.40	40.72		laminated, convoluted unit, stromatolites
133.6	163.6	40.72	49.87		some laminations, more massive, minor convolutions (10-15%)
163.6	194.5	49.87	59.28		mottled texture, small rounded particles of dolostone on mm scale, Sed breccia
194.5	217	59.28	66.14		laminations and some convoluted laminations (10%)
217	226.2	66.14	68.95		mottled unit
226.2	245.3	68.95	74.77		laminated unit
245.3	246.8	74.77	75.22		top of unit is black pyritic - bedded or compositional banding - fine to medium to coarse laminations 1 cm in thickness, 48degrees to CA
246.8	332.8	75.22	101.44		mottled unit - bigger wispy colour changes, dark grey and light grey sections
332.8	456.5	101.44	139.14		laminated, minor convolutions (5%), gradually convolutions increase
456.5	457.5	139.14	139.45		black unit - veins of dolostone, pyrite, coarse grained but in places laminated
476.5	497.4	145.24	151.61		very weakly laminated, massive dolostone
26	497.4	7.92	151.61	pyrite	some minor pyrite, trace to nil
204	215	62.18	65.53		pyrite cube 0.5cm and less than 1% pyrite in veins and stylolites
245.5	246	74.83	74.98		short interval of intense pyrite alteration centered on vertical stylolites
310.5	312	94.64	95.10		pyrite in fractures and along stylolites, less than 1%
365.3	365.8	111.34	111.50		pyrite in fractures, less than 1%
399.5	417.9	121.77	127.38		pyrite in fractures and isolated spots, less than 3mm in diameter
456.5	457	139.14	139.29		massive pyrite infill of vugs - most weathered away
468.3	468.9	142.74	142.92		dolomite and pyrite fractures, up to 4mm in diameter

Hole: A34 con’t

Feet		Meters		
from	to	from	to	Sub Units and Alteration
44.6	137	13.59	41.76	various veining, vugs and brecciation, minor veining - max 7cm - average 2mm, dolospar, some calcite in center, various orientations - following rock fabric, vuggy porosity developed ranging in size to 1cm filled with dolospar and some calcite, stylolites abundant (perpendicular to CA), some vugs with bitumen infills, 5% spar
137	184.7	41.76	56.30	more spar filled vugs and or veins, coarse dolomite and later calcite - some very thick calcite, veins 23cm of spar, 25% spar total
184.7	217.8	56.30	66.39	some dolomite filled vugs - 1cm or less, sometimes calcite in middle, 5%
217.8	267	66.39	81.38	much thicker veins 5cm spar - one long vein 30cm, bounded by stylolites parallel to CA, some vugs are big, have pieces of host rock, euhedral calcite crystals, aside from veins not a lot in the rest, 10% spar overall
267	308	81.38	93.88	vuggy porosity or tight with some veins up to 10cm, less than 5%, no prefered orientation
308	333	93.88	101.50	bigger vugs with dolomitization almost forming striped rocks, large veins or vugs filled with coarse euhedral dolomite, 4-5mm, 10-15% spar
333	438.5	101.50	133.65	minor veining, more perpendicular to CA, veins are up to 2mm - some vugs bounded by stylolites, 5%
376	377.5	114.60	115.06	occasional large vugs, 5cm with coarse dolospar
438.5	458.8	133.65	139.84	vug dominated, less than 10cm, spar filled, 10% spar, large euhedral dolospar 4mm
458.8	497.4	139.84	151.61	vuggy porosity - small (mm scale), less than 5% spar

Hole: 77-B14

Feet		Meters		Major Units	Remarks
from	to	from	to		
39.6	184.8	12.07	56.33		brecciated (sed) silty dolostone - conglomeratic, yellow to grey weathering, various sedimentary breccias, variable clast size from mm to 7cm, matrix and clast supported, some pieces structurally brecciated and folded, grey units are laminatd, conglomerate clasts are dominant
87.2	89.4	26.58	27.25		fracture zones - all brown fractured unit
95.1	97.2	28.99	29.63		fracture zones - all brown fractured unit
127.4	128.6	38.83	39.20		rubble yellow fractured material
180.1	193.4	54.89	58.95		zone of yellow and grey deformed unconsolidated material, earthy appearance, ex-conglomerate, both sides ?fault zone
184.8	247	56.33	75.29		coarse grained grey dolostone - featureless
247	263	75.29	80.16		fine grained laminated dolostone, sed conglomerates/fragments laminated, up to 2cm clasts, sub-angular, matrix supported, not all conglomerate but some zones
					Sub Units and Alteration
39.6	184.8	12.07	56.33		orange weathering rusty orange sph in fractures in silty dolomite, crackle veining - sometimes just sph, sometimes sph and dol +/- pyrobitumen, found throughout interval, top of hole has veins on average 1-2mm, up to 4-5mm, 1% sph over whole interval
124.8	180.1	38.04	54.89		veins up to 5mm common with sph and dol, spar and sph infills matrix in conglomerate
180.1	193.4	54.89	58.95		no sph
193.4	247	58.95	75.29		crackle veining to brecciation cemented by dolomite and some thick calcite units, vugs developed up to 6cm in diameter, lined with euhedral dolomite crystals, sometimes with calcite unfills, lack of sph, altered, rust stained pyrite, pyrite may have been in one or more vugs as infill, 10% spar, less than 1% pyrite, 0% sph
247	260	75.29	79.25		very minor dol veins, less than 1%
257	257	78.33	78.33		1cm interval of rusty iron staining, no visible pyrite

Hole: A32

Feet		Meters		Major Units	Remarks
from	to	from	to		
10.3	107	3.14	32.61		interbedded coarse and medium grained dolostone - coarse "beds" (7-30cm) and some sub cm scale laminations, laminations are 40degrees to CA, beds are perpendicular to CA
107	232.5	32.61	70.87		finely spaced laminations, laminations more convoluted, dolomite following fabric
232.5	235.7	70.87	71.84		dark massive medium to coarse grained dolostone
235.7	288.7	71.84	88.00		convoluted laminations, thinly laminated
288.7	302.3	88.00	92.14		dark massive medium to coarse grained dolostone
302.3	320.4	92.14	97.66		medium convoluted laminated unit
320.4	322.8	97.66	98.39		dark grey, muddy, fine grained laminations broken on bedding planes, dolomite
322.8	333	98.39	101.50		finely laminated grey dolostone
333	333.5	101.50	101.65		molar tooth breccia folded unit
333.5	335.9	101.65	102.38		dark finely laminated dolostone
335.9	370.8	102.38	113.02		deformed molar tooth unit
					Sub Units and Alteration
14	22.1	4.27	6.74		pyrobitumen infilled vugs with dolomite - last phase to precipitate - less than 1% of unit
					quartz in vugs - rice grains - over full hole
17	59.8	5.18	18.23		pyrite in vugs - altered - not sure - specks of pyrite, 0.25mm scale in vugs
57.9	59.8	17.65	18.23		first appearance of sph, in veins with ?calcite and quartz, coarse crystals up to 2mm in vugs lined with euhedral calcite, really rotten vuggy rock, less than 1% sph
67.7	79.1	20.63	24.11		pyrobitumen infilling vugs, one vug with a large piece 1cm

Hole: A32 con't

Feet		Meters		Sub Units and Alteration
from	to	from	to	
89.2	331.6	27.19	101.07	pyrite in calcite lined vugs, overgrowing calcite as small cubes, associated with quartz (rice grain), only trace amounts less than 1%
104.6	105.7	31.88	32.22	pyrite in veins lining wall rock, veins 0.5cm to 1cm wide, no more vugs
142.2	142.5	43.34	43.43	pyrite in veins, couple of mm thick pyrite occurances in 1cm thick veins, pyrite is lining veins of both sides and veins are infilled by dolospar with calcite in middle, less than 2% pyrite
100.2	100.8	30.54	30.72	less than 5mm thick red crystalling sph in dolospar vein against host
105.8		32.25		yellow crystalline sph in dolospar vein with pyrite
213.5	218.6	65.07	66.63	red coarse 2mm crystals of sph in fractures, tiny bit of dolostone present, yellow sph in vein, only thing in vein but pyrite in a vug above it - less than 1% sph over interval
222.9		67.94		flaky pyrobitumen infilling quartz and calcite vug
233.2		71.08		pyrite infilled vugs, 1cm, very altered
249.4	249.9	76.02	76.17	pyrite vein growing on stylolite surface - very irregular, stylolite parallel to core axis up to 5mm, associated with pale yellow sphalerite up to 5mm, vein with yellow to beige sph+pyr+dol+ small vugs with calcite in center
252.8	370.8	77.05	113.02	massive pyrite in vugs and veins, vugs 1cm in thickness, vein is 6mm - only pyrite, fine grained and altered, less than 1% over interval, veins are infrequent maybe occurring every 3 feet or so, no preferred orientation - seem to be using pre-existing structures: stylolites + earlier dolospar veins, become more frequent down hole and smaller- 2mm or less
320	322.8	97.54	98.39	mud rich interval - no pyrite seen
330.8		100.83	0.00	pyrobitumen - late vug infilling
10.3	58	3.14	17.68	minor crackling less than 3% veins with mostly dolostone and some late calcite, no preferred orientation of veins, range from mm to 3cm - average 2mm, vugs are perpendicular to CA filled with calcite, quartz, pyrite

Hole: A32 con't

Feet		Meters		Sub Units and Alteration
from	to	from	to	
58	59.6	17.68	18.17	80% calcite dolomite quartz, coarse grained less the 4mm, very altered and bleached, few floating fragments of host rock, sharp bottom contact with a little dissolution - possibly one huge vug with small rock fragments floating
59.6	152	18.17	46.33	grey dolostone with more vugs - average couple cm to 5cm, 50degrees to CA, filled with euhedral dolomite, calcite and quartz, still has minor crackle veins which become more common to top of interval, max size 1cm, vugs decrease, total 5% spar
59.6	152	18.17	46.33	rare vuggy porosity - infilled vugs mm to 3mm in size, increases to top of interval, sparkly grey dolomite lining empty vugs
152	171.1	46.33	52.15	crackling rare dolospar, dominated by ruggy porosity with grey spar and quartz - veins less then 2% spar, porosity 5%
171.1	320.4	52.15	97.66	more intense crackling - veins and vugs - some mosaic breccias - some evidence of dissolution occasional vuggy porosity, veins and vugs - dolomite -/+ quartz -/+ calcite, 10% spar, no dominant orientation for veins/vugs
320.4	332.2	97.66	101.25	minor crackling and some vugs, as above less than 3%
332.2	370.8	101.25	113.02	very rare dolomite veins, less than 1%

Appendix 3

Petrography Summary

Ore Stage: Host rock

Paragenetic Phase: Host Carbonate

Mineralogy: limestone and dolostone

Textures: laminated, banded, stromatolitic, oolitic

Distribution: significant throughout deposit

Features: many organic and insoluble (eg. clay) layers, stylolites, diagenetic pyrite

Photo A shows the plain grey host rock with a small amount of hydrothermal altheration. Photomicrograph B shows the original carbonate texture of the rock. Photomicrograph C shows host carbonate with organic/insoluble banding. Photomicrograph D shows a common organic/insoluble 'wisp' containing significant pyrite

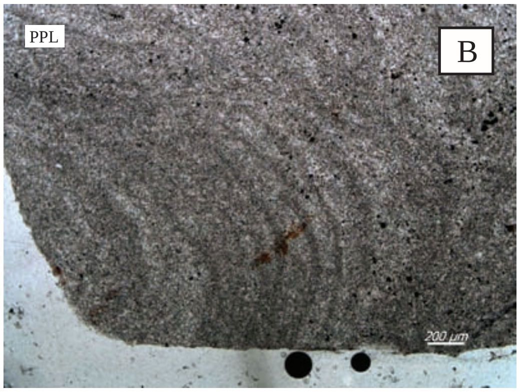

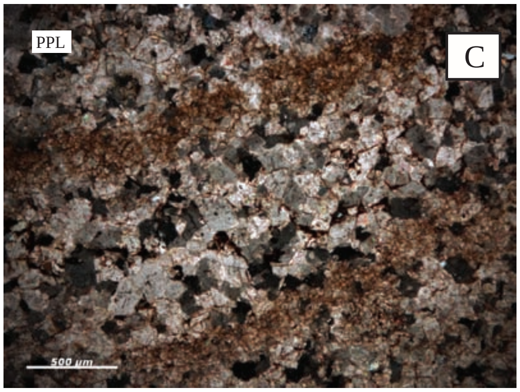

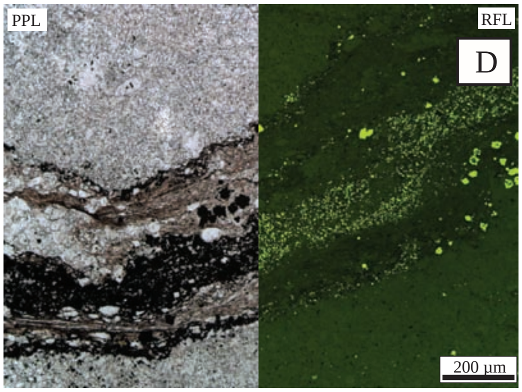

Ore Stage: Early

Paragenetic Phases: early calcite, early quartz, early pyrite, early sphalerite

Distribution: minor for all phases

Features: host carbonate is partially destroyed, minerals commonly occur in veins, sphalerite tends to be pale in colour

Photomicrographs A and B show early calcite altering the host carbonate. Photomicrograph C shows early sphalerite within host carbonate. Photomicrograph D shows early quartz with remnant organic bands from the host carbonate. The later ore stage phases cross-cut these phases.

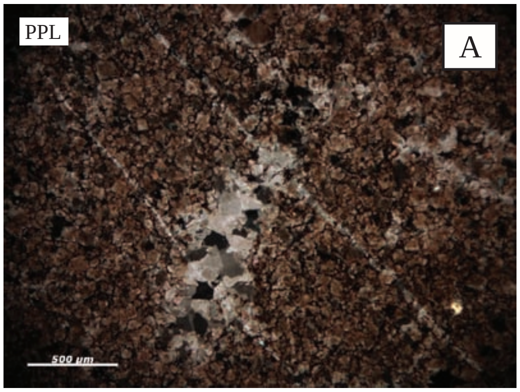

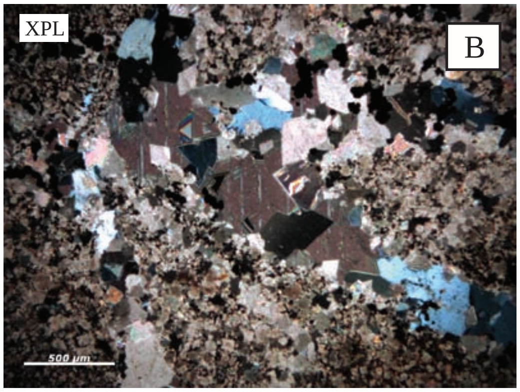

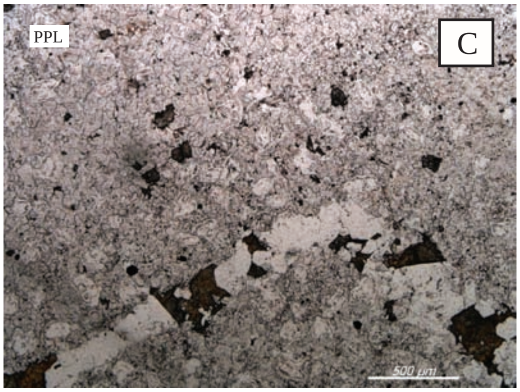

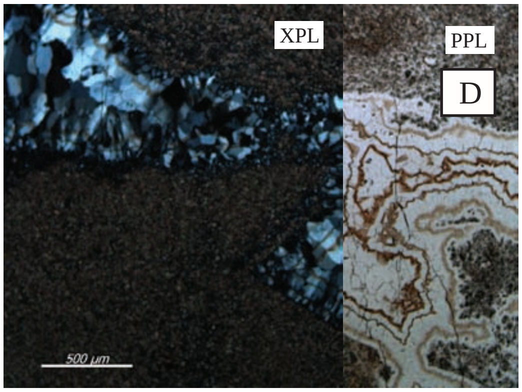

Ore Stage: Main

Paragenetic Phase: main dolomite

Distribution: significant throughout deposit

Features: crystals tend to increase in size away from the host carbonate contact, dolomite is either grey or white

Photo A shows the main dolomite replacing the host carbonate with grey dolomite near the contact with the host and white dolomite further out. Photomicrograph B shows dolomite crystals which are elongated perpendicular to the host rock contact. Photomicrograph C shows the main dolomite contact with the main sphalerite. Grain faces are most often curved, displaying saddle dolomite morphology.

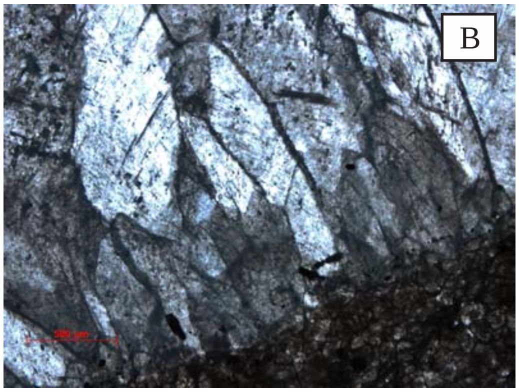

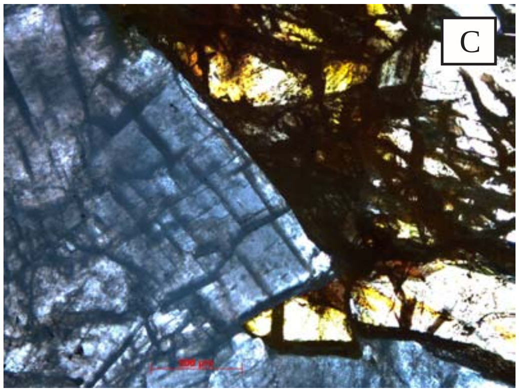

Ore Stage: Main

Paragenetic Phase: main pyrite

Distribution: minor

Features: usually subhedral to euhedral form

Photomicrograph D shows the main pyrite (P) in relation to main sphalerite (S) and main dolomite (D)

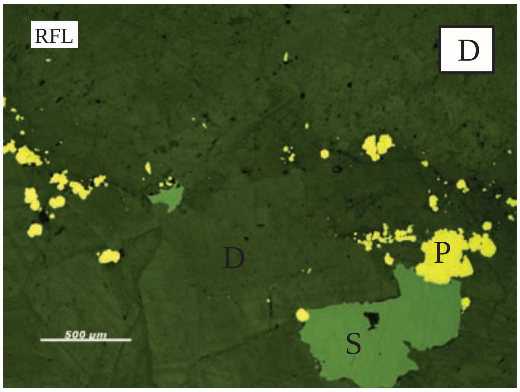

Ore Stage: Main

Paragenetic Phases: main quartz and main sphalerite

Distribution: both somewhat abundant, sphalerite more abundant than quartz

Features: quartz can be intergrown with sphalerite, sphalerite occurs in many bright colours, sphalerite often destroys host carbonate

Photo A shows the most common occurance of main sphalerite, infilling space around main dolomite. Photomicrograph B show main quartz increasing in grain size away from the host carbonate, similar in occurance to the main dolomite. Photomicrograph C is a transmitted and reflected light veiw of main sphalerite (S) destroying the host carbonate (H). Photomicrograph D shows bright orange sphalerite occuring between main dolomite grains.

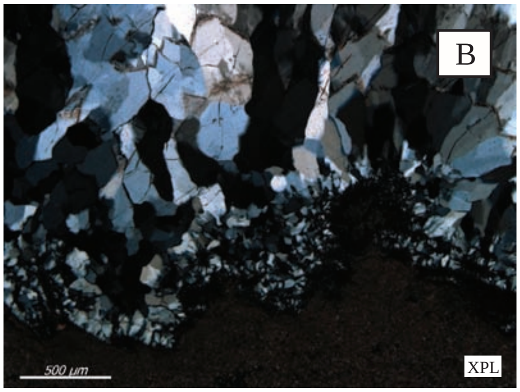

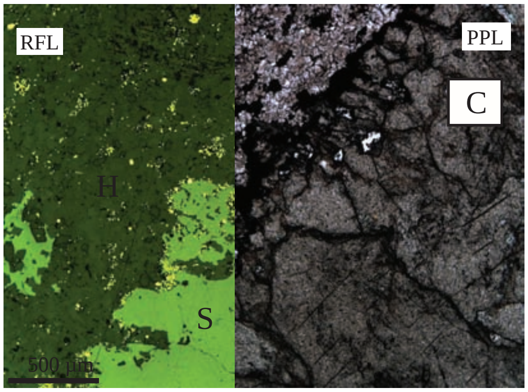

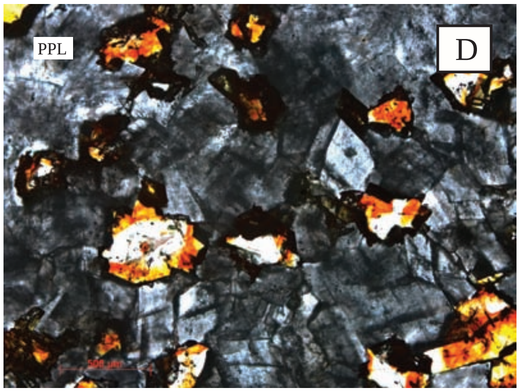

Ore Stage: Main

Paragenetic Phase: main galena

Distribution: minor

Features: commonly found with main sphalerite

Photomicrographs A and B show a transmitted and reflected light view of main galena (G) growing adjacent to main sphalerite (S) and corroding main dolomite (D).

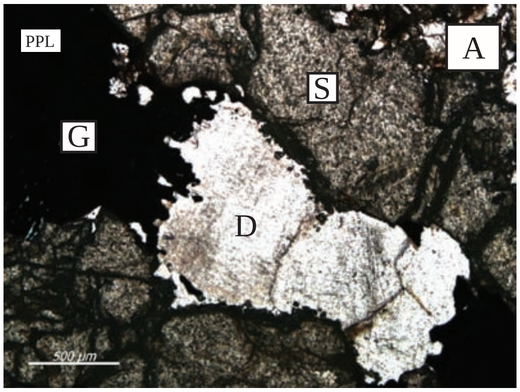

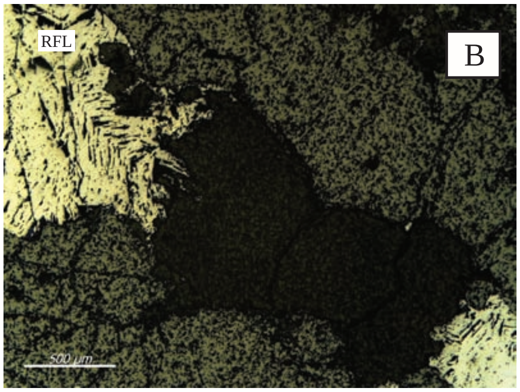

Ore Stage: Late

Paragenetic Phase: late calcite

Distribution: major

Features: crystals can be up to several centimeters in size, occurs filling remaining porosity after main ore stage, also occurs as cross-cutting veins

Photomicrograph C shows late calcite (C) filling space around main sphalerite.

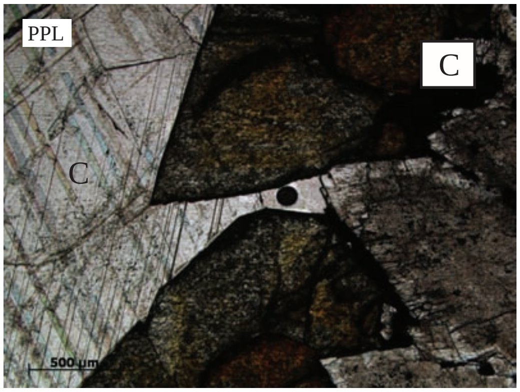

Ore Stage: Late

Paragenetic Phase: pyrobitumen

Distribution: minor

Features: filling last porosity, flecks and chunks

Photo D shows pyrobitumen in a vug.

Appendix 4

Microprobe Data

Please see additional file “Appendix 4”

Appendix 5

Microthermometry Data

Appendix 5. Microthermometric measurements of carbonates, quartz and sphalerite from the Gayna River deposit.

Sample	Chip	#	Mineral	Stage	Origin	Tfm	Tm (ice)	NaCl Eq.	Th (Deg. C)
A33 250	4	1	calcite	late	P	-55	-14.4	18.1	
A33 250	4	2	calcite	late	P		-14.4	18.1	85
A33 250	4	3	calcite	late	P	-55	-12.8	16.7	101
A33 250	4	4	calcite	late	P	-55	-11.9	15.9	95
A33 250	4	5	calcite	late	P				71
A33 250	4	6	calcite	late	P				69
A33 250	4	7	calcite	late	P	-55	-14.2	18.0	62
A33 250	7	1	calcite	late	P	-45	-22	23.7	91
A33 250	7	2	calcite	late	P	-47	-20.1	22.4	90
A33 250	2	1	calcite	late	P	-55	-15.6	19.1	69
A33 250	2	2	calcite	late	P	-55	-9.8	13.7	67
A33 250	2	3	calcite	late	P	-55	-17.5	20.4	56
A33 250	3	1	calcite	late	P	-45	-13.9	17.7	68
A33 250	3	2	calcite	late	P	-45	-9.7	13.6	67
A33 250	6	1	calcite	late	P	-55	-15.5	19.0	105
A33 250	6	2	calcite	late	P	-55	-15.1	18.7	123
A33 250	6	3	calcite	late	P	-55			121
A33 250	6	4	calcite	late	P	-55	-11.1	15.1	59
A33 250	6	5	calcite	late	P	-55	-15.5	19.0	107
A33 250	6	6	calcite	late	P	-55	-15.1	18.7	121
A33 250	7	1	calcite	late	P	-70	-21.5	23.4	
A33 250	7	2	calcite	late	P	-70			
A33 250	7	3	calcite	late	P	-70	-13.4	17.3	
A33 250	7	4	calcite	late	P	-70	-21.5	23.4	
A33 250	7	5	calcite	late	P	-70	-13.6	17.4	
A33 250	7	6	calcite	late	P	-70	-11.8	15.8	
A33 250	5	1	calcite	late	P	-75	-16.3	19.7	66
BWGRR008	A	1	calcite	late	P	-72	-16.1	19.5	169
BWGRR008	A	2	calcite	late	P				164
BWGRR008	A	3	calcite	late	P				83
BWGRR008	A	4	calcite	late	P		-16.2	19.6	168
BWGRR008	A	5	calcite	late	P	-72	-16.1	19.5	172
BWGRR008	A	6	calcite	late	P		-16.1	19.5	168
BWGRR008	A	7	calcite	late	P		-16.4	19.8	172
BWGRR008	A	8	calcite	late	P		-13.7	17.5	175
BWGRR008	A	9	calcite	late	P		-13.7	17.5	176
BWGRR008	A	10	calcite	late	P		-16.4	19.8	162
BWGRR008	A	11	calcite	late	P		-16.4	19.8	162
A35 346.2	A	1	calcite	late	P	-78			113
A35 346.2	A	2	calcite	late	P				
A35 346.2	A	3	calcite	late	P	-78	-18.3	21.2	74
A35 346.2	A	4	calcite	late	P				118
A35 346.2	A	5	calcite	late	P	-78			100
MBGRR013	C	1	calcite	late	P	-72			149
MBGRR013	C	2	calcite	late	P	-72	-21.5	23.4	150

Appendix 5 (con't). Microthermometric measurements of carbonates, quartz and sphalerite from the Gayna River deposit.

Sample	Chip	#	Mineral	Stage	Origin	Tfm	Tm (ice)	NaCl Eq.	Th (Deg. C)
MBGRR013	C	3	calcite	late	P	-72	-22.1	23.8	117
MBGRR013	C	4	calcite	late	P	-72	-21	23.0	131
MBGRR013	C	5	calcite	late	P	-72	-26.5	26.5	102
MBGRR013	C	6	calcite	late	P	-72	-21	23.0	111
MBGRR013	C	7	calcite	late	P	-72	-18	21.0	124
MBGRR013	C	8	calcite	late	P	-72	-20.1	22.4	128
MBGRR013	C	9	calcite	late	P	-72	-18.5	21.3	103
MBGRR013	C	10	calcite	late	P	-72	-25.1	25.6	137
MBGRR013	C	11	calcite	late	P	-72	-31.8	29.8	109
A30 120	1	1	calcite	late	P				170
A30 120	1	2	calcite	late	P				163
A30 120	1	3	calcite	late	P				105
A30 120	1	4	calcite	late	P				109
A30 120	1	5	calcite	late	P				181
A30 400	F	1	calcite	late	P	-51.2	-21.2	23.2	
SG7	2	1	dolomite	main	P				136
SG7	2	2	dolomite	main	P				126
SG7	2	3	dolomite	main	P				213
SG7	2	4	dolomite	main	P				154
A30 400	C1	1	dolomite	main	P				159
A30 400	C2	1	dolomite	main	P				153
A30 322.5	1	1	dolomite	main	P	-76	-23.8	24.8	151
A30 322.5	1	2	dolomite	main	P	-76	-24.4	25.2	157
A30 322.5	1	3	dolomite	main	P	-76	-29.6	28.4	158
A30 322.5	2	1	dolomite	main	P	-70	-26.9	26.7	179
A30 322.5	2	2	dolomite	main	P	-70	-31.1	29.4	179
A30 322.5	2	3	dolomite	main	P	-70	-33.2	30.8	198
A30 322.5	2	4	dolomite	main	P	-70	-18.5	21.3	166
A30 322.5	2	5	dolomite	main	P	-70	-26.7	26.6	198
A30 322.5	2	7	dolomite	main	P	-70	-30.5	29.0	189
A30 322.5	3	1	dolomite	main	P	-65	-21.5	23.4	196
A30 322.5	3	2	dolomite	main	P	-65	-27.5	27.1	174
BWGRR014B	1	1	dolomite	main	P		-2.2	3.7	163
BWGRR014B	1	2	dolomite	main	P		-2.1	3.5	146
BWGRR014B	1	3	dolomite	main	P				157
BWGRR014B	1	4	dolomite	main	P	-75	-15.3	18.9	146
BWGRR014B	1	5	dolomite	main	P				173
BWGRR014B	1	6	dolomite	main	P				182
BWGRR012	F	1	dolomite	main	P	-74	-2.1	27.0	172
BWGRR012	E	1	dolomite	main	P	-65	-34.3	31.5	134
BWGRR012	E	2	dolomite	main	P	-77	-7.6	11.2	157
BWGRR012	E	3	dolomite	main	P	-77			142
BWGRR012	E	4	dolomite	main	P				137
BWGRR012	E	5	dolomite	main	P				132
B28 212.2	B	1	dolomite	main	P		-22	23.7	231
B28 212.2	B	4	dolomite	main	P				215

Appendix 5 (con't). Microthermometric measurements of carbonates, quartz and sphalerite from the Gayna River deposit.

Sample	Chip	#	Mineral	Stage	Origin	Tfm	Tm (ice)	NaCl Eq.	Th (Deg. C)
B28 194.5	A	1	dolomite	main	P	-77			178
B28 194.5	A	2	dolomite	main	P	-77			178
B28 194.5	A	3	dolomite	main	P	-75	-24	25.0	207
B28 194.5	A	4	dolomite	main	P		-17.3	20.4	217
B28 194.5	A	5	dolomite	main	P				>225
B28 194.5	A	6	dolomite	main	P		-24.3	25.1	185
B28 194.5	A	7	dolomite	main	P	-77	-28.5	27.7	164
B28 194.5	A	8	dolomite	main	P		-27.1	26.9	154
B28 194.5	A	9	dolomite	main	P	-77	-18.5	21.3	225
B28 194.5	A	10	dolomite	main	P		-22.1	23.8	215
MBGRR013	B	1	dolomite	main	P		-12	16.0	178
MBGRR013	B	2	dolomite	main	P	-48	-13.9	17.7	178
MBGRR013	B	3	dolomite	main	P	-47	-11	15.0	167
MBGRR013	B	4	dolomite	main	P	-47	-11	15.0	167
MBGRR013	B	5	dolomite	main	P	-47			162
BWGRR008	B	1	dolomite	main	P		-17.8	20.8	110
BWGRR008	B	2	dolomite	main	P				
BWGRR008	B	3	dolomite	main	P				65
BWGRR008	B	4	dolomite	main	P		-10	13.9	
BWGRR008	B	5	dolomite	main	P		-0.8	1.4	74
A30 120	1	1	dolomite	main	P				192
A30 120	1	2	dolomite	main	P				202
A30 120	1	3	dolomite	main	P				174
A30 120	1	4	dolomite	main	P				171
A30 120	1	5	dolomite	main	P				198
A30 120	1	6	dolomite	main	P				152
A30 120	1	7	dolomite	main	P				154
A30 347	2	1	dolomite	main	P				155
A30 347	2	2	dolomite	main	P				
A30 347	2	3	dolomite	main	P				
A30 347	2	4	dolomite	main	P				
75C001	1	1	quartz	late	P	-65	-12.2	16.1	223
75C001	1	3	quartz	late	P	-62	-11.8	15.8	175
75C001	1	4	quartz	late	P		-14.7	18.4	148
75C001	1	5	quartz	late	P		-15.5	19.0	148
75C001	1	6	quartz	late	P		-12.9	16.8	171
CAGRR001	4	1	quartz	main	P	-60.1	-19.8	22.2	152
CAGRR001	5	1	quartz	main	P	-60.6	-34.8	31.9	153
CAGRR001	5	2	quartz	main	P	-40.5	-9.8	13.7	179
CAGRR001	5	3	quartz	main	P	-61.3	-28.7	27.8	158
CAGRR001	5	4	quartz	main	P	-60.1	-36.1	32.9	120
CAGRR001	1	1	quartz	main	P	<-73	-23.7	24.8	
CAGRR001	1	2	quartz	main	P	<-73	-20.2	22.5	185
CAGRR001	1	3	quartz	main	P	<-73	-19.8	22.2	
CAGRR001	1	4	quartz	main	P	<-73	-21.8	23.6	180
CAGRR001	1	5	quartz	main	P	<-73	-22.5	24.0	196

Appendix 5 (con't). Microthermometric measurements of carbonates, quartz and sphalerite from the Gayna River deposit.

Sample	Chip	#	Mineral	Stage	Origin	Tfm	Tm (ice)	NaCl Eq.	Th (Deg. C)
CAGRR001	1	6	quartz	main	P	<-73	-22.2	23.8	
CAGRR001	1	7	quartz	main	P	<-73	-22.2	23.8	210
CAGRR001	1	8	quartz	main	P	<-73	-23.7	24.8	
CAGRR001	1	9	quartz	main	P	<-73	-20	22.4	233
CAGRR001	1	10	quartz	main	P	<-73	-22.5	24.0	
CAGRR001	3	1	quartz	main	P	-30	-21	23.0	178
CAGRR001	3	2	quartz	main	P	-77	-24.6	25.3	159
CAGRR001	6	1	quartz	main	P	-79	-20.7	22.8	183
CAGRR001	6	3	quartz	main	P	-79	-20.7	22.8	184
CAGRR001	6	4	quartz	main	P	-79	-20.7	22.8	184
CAGRR001	6	7	quartz	main	P	-79	-20.7	22.8	181
CAGRR001	6	8	quartz	main	P	-79	-20.6	22.8	168
BWGRR022A	A	1	quartz	main	P	-75			222
BWGRR022A	A	2	quartz	main	P	-75	-15.8	19.3	197
BWGRR022A	A	3	quartz	main	P	-75	-23.8	24.8	137
BWGRR022A	A	4	quartz	main	P	-75	-23.4	24.6	154
BWGRR022A	A	5	quartz	main	P	-75	-23.4	24.6	170
BWGRR022A	A	6	quartz	main	P	-75	-22.9	24.3	154
BWGRR022A	A	7	quartz	main	P	-75	-17.1	20.3	132
BWGRR022A	A	8	quartz	main	P	-75	-16.2	19.6	135
BWGRR023B	J	1	quartz	late	P	-28.5	-15.1	18.7	173
BWGRR023B	J	2	quartz	late	P		-17.1	20.3	
BWGRR023B	H1	1	quartz	late	P	<-35?	-14.6	18.3	134
BWGRR023B	H1	2	quartz	late	P	<-35?	-14.9	18.6	148
BWGRR023B	H1	3	quartz	late	P	<-35?	-12.2	16.1	134
BWGRR023B	H1	4	quartz	late	P	<-35?	-12.1	16.1	175
BWGRR023B	H1	5	quartz	late	P	<-35?	-15.7	19.2	171
BWGRR023B	H1	6	quartz	late	P	<-35?	-12	16.0	117
BWGRR023B	H1	7	quartz	late	P	<-35?	-14.5	18.2	140
BWGRR023B	H1	8	quartz	late	P	<-35?			152
BWGRR023B	H1	9	quartz	late	P	<-35?	-12.7	16.6	154
BWGRR023B	H1	10	quartz	late	P	<-35?	-12.2	16.1	150
BWGRR023B	H1	11	quartz	late	P	<-35?	-16	19.4	140
BWGRR023B	H1	12	quartz	late	P	<-35?	-16.3	19.7	130
BWGRR023B	H2	6	quartz	late	P	-68			133
BWGRR023B	H2	7	quartz	late	P	-69	-12.3	16.2	155
BWGRR023B	H2	8	quartz	late	P	-67	-11.8	15.8	99
BWGRR023B	H2	9	quartz	late	P	-67	-17.1	20.3	84
BWGRR023B	H2	10	quartz	late	P	-67	-11.8	15.8	99
BWGRR023B	H2	11	quartz	late	P	-67	-11.6	15.6	107
BWGRR023B	H2	12	quartz	late	P	-67	-11.5	15.5	144
BWGRR023B	I	1	quartz	late	P	-72	-10.7	14.7	134
BWGRR023B	I	2	quartz	late	P	-72	-11.8	15.8	171
BWGRR023B	I	3	quartz	late	P	-72	-11.6	15.6	136
BWGRR023B	I	4	quartz	late	P	-72	-11.2	15.2	151
BWGRR023B	I	5	quartz	late	P	-72	-11.8	15.8	148

Appendix 5 (con't). Microthermometric measurements of carbonates, quartz and sphalerite from the Gayna River deposit.

Sample	Chip	#	Mineral	Stage	Origin	Tfm	Tm (ice)	NaCl Eq.	Th (Deg. C)
BWGRR023B	G	1	quartz	late	P	-75	-20.2	22.5	152
BWGRR023B	G	2	quartz	late	P	-75	-12.7	16.6	143
BWGRR023B	G	3	quartz	late	P	-75	-15.8	19.3	138
BWGRR023B	G	4	quartz	late	P	-75	-15.5	19.0	142
BWGRR023B	G	5	quartz	late	P	-75	-15.2	18.8	140
BWGRR023B	G	6	quartz	late	P	-75	-12	16.0	155
SG7	5	1	sphalerite	main	P		-21	23.0	
A30 400	1A	1	sphalerite	main	P	-74	-38	34.4	208
A30 400	1A	2	sphalerite	main	P	-75	-35	32.0	207
A30 400	1A	3	sphalerite	main	P				202
A30 400	1A	4	sphalerite	main	P	-75	-36	32.8	209
A30 400	1A	5	sphalerite	main	P				203
A30 400	1A	6	sphalerite	main	P	-76	-38	34.4	203
A30 400	1A	7	sphalerite	main	P				203
A30 400	1A	8	sphalerite	main	P	-75	-37	33.6	205
A30 400	1A	9	sphalerite	main	P	-75	-36	32.8	204
A30 400	1A	10	sphalerite	main	P	-76	-36	32.8	204
A30 400	B	1	sphalerite	main	P	-67.5	-31.4	29.6	212
A30 400	B	2	sphalerite	main	P	-67.3	-31	29.3	227
A30 400	C	1	sphalerite	main	P	-71	-36.7	33.3	208
A30 400	C	2	sphalerite	main	P	-71.8	-35.3	32.3	208
A30 400	C	3	sphalerite	main	P	-71.2	-36.6	33.2	192
A30 400	C	4	sphalerite	main	P	-71.4	-36.4	33.1	203
A30 400	C	5	sphalerite	main	P	-71.4	-36.4	33.1	
MBGRR013	A	1	sphalerite	main	P		-15.6	19.1	178
MBGRR013	A	2	sphalerite	main	P				177
MBGRR013	A	3	sphalerite	main	P				178
MBGRR013	A	4	sphalerite	main	P		-13.8	17.6	182
MBGRR013	A	5	sphalerite	main	P		-16.1	19.5	179
MBGRR013	A	6	sphalerite	main	P				177
MBGRR013	A	7	sphalerite	main	P		-16.1	19.5	178
MBGRR013	A	8	sphalerite	main	P				182
MBGRR013	A	9	sphalerite	main	P				178
RTS2B	1	1	sphalerite	main	P	-72	-31.5	29.6	190
RTS2B	1	2	sphalerite	main	P		-31.1	29.4	225
RTS2B	1	3	sphalerite	main	P		-16.1	19.5	225
RTS2B	1	4	sphalerite	main	P				188
RTS2B	1	5	sphalerite	main	P	-76	-26.8	26.7	178
RTS2B	1	6	sphalerite	main	P	-76	-30.1	28.7	185
RTS2B	1	7	sphalerite	main	P	-76	-32.5	30.3	268
RTS2B	1	8	sphalerite	main	P	-72			
RTS2B	1	9	sphalerite	main	P	-76			188
A30 347	1	1	sphalerite	main	P		-10.5	14.5	169
A30 347	1	2	sphalerite	main	P		-10.1	14.0	161
A30 347	1	3	sphalerite	main	P		-10.1	14.0	169
A30 347	1	4	sphalerite	main	P		-14.7	18.4	171

Appendix 5 (con't). Microthermometric measurements of carbonates, quartz and sphalerite from the Gayna River deposit.

Sample	Chip	#	Mineral	Stage	Origin	Tfm	Tm (ice)	NaCl Eq.	Th (Deg. C)
BWGRR023B	E1	1	sphalerite	early	P		-22.2	23.8	
BWGRR023B	E1	2	sphalerite	early	P				107
BWGRR014B	a	1	sphalerite	early	P	-75	-26.7	26.6	183
BWGRR023B	A	1	sphalerite	early	P	-56	-10.8	14.8	123
BWGRR023B	A	2	sphalerite	early	P	-56	-11.1	15.1	154
BWGRR023B	A	3	sphalerite	early	P	-72			107
BWGRR023B	A	4	sphalerite	early	P	-72	-10.9	14.9	135
BWGRR023B	A	5	sphalerite	early	P	-56	-12.8	16.7	154
BWGRR023B	A	6	sphalerite	early	P	-56	-15	18.6	151
BWGRR023B	A	7	sphalerite	early	P	-50	-10.7	14.7	128
BWGRR023B	A	8	sphalerite	early	P	-56	-10.8	14.8	
B28 212.2	A	3	sphalerite	early	P				178
B28 212.2	A	5	sphalerite	early	P				195
B28 212.2	A	6	sphalerite	early	P				195
BWGRR012	H	1	sphalerite	early	P	-70	-10.3	14.3	190
BWGRR012	H	2	sphalerite	early	P				186
BWGRR012	H	3	sphalerite	early	P		-12.3	16.2	214
BWGRR012	H	4	sphalerite	early	P		-12.5	16.4	179
BWGRR012	H	5	sphalerite	early	P	-70			182
BWGRR012	H	6	sphalerite	early	P	-70	-12.5	16.4	186
CAGRR001	4	2	quartz	main	S				184
CAGRR001	4	3	quartz	main	S				195
A30 322.5	2	6	dolomite	main	S	-70			185
BWGRR023B	H2	4	quartz	late	S	-68	-11.5	15.5	148
CAGRR001	4	4	quartz	main	S				83
BWGRR023B	H2	1	quartz	late	S	-68			146
BWGRR023B	H2	2	quartz	late	S	-68			152
BWGRR023B	H2	3	quartz	late	S	-68			152
BWGRR023B	H2	5	quartz	late	S	-68			156
CAGRR001	6	6	quartz	main	S	-70	-20.7	22.8	200
CAGRR001	6	9	quartz	main	S	-70	-20.6	22.8	200
B28 212.2	A	2	sphalerite	early	S				192
B28 212.2	A	4	sphalerite	early	S	-72	-23.8	24.8	192
BWGRR008	A	12	calcite	late	S				168
BWGRR008	A	13	calcite	late	S	-72	-15.9	19.4	167
BWGRR008	A	14	calcite	late	S		-15.9	19.4	164
BWGRR008	A	15	calcite	late	S				165
BWGRR008	A	16	calcite	late	S				164
CAGRR001	6	2	quartz	main	S	-70	-20.7	22.8	201
CAGRR001	6	5	quartz	main	S	-70	-20.7	22.8	201
75C001	1	2	quartz	late	S				108
BWGRR023B	E2	1	sphalerite	early	S	-41.1	-10.6	14.6	135
BWGRR023B	C1	1	sphalerite	early	S		-10.7	14.7	

Appendix 6

Strontium Isotope Data

Please see additional file “Appendix 6”